Genetics of human sleep EEG:
Analysis of EEG microstructure in twins

Dissertation

an der Fakultät für Biologie
der Ludwig-Maximilians-Universität München

vorgelegt von
Marek Adamczyk

München, 13. Februar 2014

Erstgutachter: Prof. Dr. Rainer Landgraf
Zweitgutachter: Prof. Dr. Christian Leibold

Tag der Einreichung: 13. Februar 2014
Tag der mündlichen Prüfung: 12. Mai 2015

ERKLÄRUNG

Hiermit versichere ich ehrenwörtlich, dass meine Dissertation selbständig und ohne unerlaubte Hilfsmittel angefertigt worden ist.
Die vorliegende Dissertation wurde weder ganz, noch teilweise bei einer anderen Prüfungskommission vorgelegt.
Ich habe noch zu keinem früheren Zeitpunkt versucht, eine Dissertation einzureichen oder an einer Doktorprüfung teilzunehmen.

München, 13. Februar 2014

Abstract

Sleep characteristics are candidates for predictive biological markers in patients with severe psychiatric diseases, in particular affective disorder and schizophrenia. The genetic components of sleep determination in humans remain, to a large degree, unelucidated. In particular, the heritability of rapid eye movement (REM) sleep and EEG bursts of oscillatory brain activity in Non-REM sleep, i.e. sleep spindles, are of interest. In addition, recent findings suggest a strong role of distinct sleep spindle types in memory consolidation, making it important to identify sleep spindles in slow wave sleep (SWS) and to separate slow and fast spindle localization in the frequency range. However, predictive sleep biomarker research requires large sample sizes of healthy and affected human individuals. Therefore, the present work addressed two questions. The first aim was to optimize data analysis by developing algorithms that allow an efficient and reliable identification of rapid eye movements (REMs) and sleep EEG spindles. In the second part, developed methods were applied to sleep EEG data from a classical twin study to identify genetic effects on tonic and phasic REM sleep parameters, sleep spindles, and their trait-like characteristics.

The algorithm for REM detection was developed for standard clinical two channel electrooculographic montage. The goal was to detect REMs visible above the background noise, and in the case of REM saccades to classify each movement separately. In order to achieve a high level of sensitivity, detection was based on a first derivative of electrooculogram (EOG) potentials and two detection thresholds. The developed REM detector was then validated in n=12 polysomnographic recordings from n=7 healthy subjects who had been previously scored visually by two human experts according to standard guidelines. Comparison of automatic REM detection with human scorers revealed mean correlations of 0.94 and 0.90, respectively (mean correlation between experts was 0.91).

The developed automatic sleep spindle detector assessed individualized signal amplitude for each channel as well as slow and fast spindle frequency peaks based on the spectral analysis of the EEG signal. The spindle detection was based on Continuous Wavelet Transform (CWT); it localized the exact length of

sleep spindles and was sensitive also for detection of sleep spindles intermingled in high amplitude slow wave EEG activity. The automatic spindle detector was validated in n=18 naps from n=10 subjects, where EEG data were scored both visually and by a commercial automatic algorithm (SIESTA). Comparison of our own spindle detector with results from the SIESTA algorithm and visual scoring revealed the correlations of 0.97 and 0.92, respectively (correlation between SIESTA algorithm and visual scoring was 0.90).

In the second part of the work, the similarity of given sleep EEG parameters in n=32 healthy monozygotic (MZ) twins was compared with the similarity in n=14 healthy same-gender dizygotic (DZ) twins. The author of the current work did not participate in acquisition of twin study sample. EEG sleep recordings used for the heritability study were collected and already described by Ambrosius *et al*. (2008). Investigation of REM sleep included the absolute EEG spectral power, the shape of REM power spectrum, the amount and the structural organization of REMs; parameters of Non-REM sleep included slow and fast sleep spindle characteristics as well as the shape of the Non-REM power spectrum in general. In addition to estimating genetic effects, differences in within-pair similarity and night-to-night stability of given parameters were illustrated by intraclass correlation coefficients (ICC) and cluster analysis. A substantial genetic influence on both spectral composition and phasic parameters of REM sleep was observed. A significant genetic variance in spectral power affected delta to high sigma and high beta to gamma EEG frequency bands, as well as all phasic REM parameters with the exception of the REMs occurring outside REM bursts. Furthermore, MZ and DZ twins differed significantly in their within-pair similarity of non-REM and REM EEG spectra morphology. Regarding sleep spindles, statistical analysis revealed a significant genetic influence on localization in frequency range as well as on basic spindle characteristics (amplitude, length, quantity), except in the quantity of fast spindles in stage 2 and whole Non-REM sleep. Basic spindle parameters showed trait-like characteristics and significant differences in within-pair similarity between the twin groups.

In summary, the developed algorithms for automatic REM and sleep spindle detection provide several advantages: the elimination of human scorer biases and

intra-rater variability, investigation of structural organization of REMs, exact determination of fast and slow spindle frequency for each individual. Algorithms are fully automated and therefore well suited to score REM density and sleep spindles in large patient samples. In the second part of the study, sleep EEG analysis in MZ and DZ twins revealed a substantial genetic determination of both tonic and phasic REM sleep parameters. This complements previous findings of a high genetic determination of the Non-REM sleep power spectrum. Interestingly, smaller genetic effects and lower night-to-night stability were observed for fast spindles, especially in SWS. This is in line with recent hypotheses on the differential function of sleep spindle types for memory consolidation.

The results from the presented studies strongly support the application of sleep EEG to identify clinically relevant biomarkers for psychiatric disorders.

Table of contents

Table of abbreviations

3sRA	the REM activity computed as the total number of 3-sec mini-epochs containing at least one REM
3sRD	the average REM activity per one epoch of REM sleep, computed as the total number of 3-sec mini-epochs containing at least one REM
allRA	the total number of all detected REMs
allRD	the average REM activity per one epoch of REM sleep, computed as the total number of all detected REMs
ATR	antidepressant treatment response
BMS	between-group mean square
CODIS	combined DNA index system
CWT	continuous wavelet transform
DFT	discrete Fourier transform
DR	the derivative
Dr2σR	the 2nd derivative of σR
DZ	dizygotic
EEG	electroencephalography
EMG	electromyography
EOG	electrooculography
FFT	fast Fourier transform
FIR	finite input response
GABA	gamma-aminobutyric acid
GCT	combined among- and within-twin pair genetic variance estimate
GVA	genetic variance analysis
GWT	within-pair genetic variance estimate
HRP	high risk subjects
ICC	intraclass correlation coefficient
IEG	immediate early gene activity
LORETA	low-resolution electromagnetic tomography
MANCOVA	multivariate analysis of covariance
MnPN	median preoptic nucleus
MSP	mean signal power
MZ	monozygotic
NREM	non-rapid eye movement
PFR	pontine reticular formation
PGO	ponto-geniculo-occipital
PSG	polysomnography
rANOVA	repeated measures analysis of variance
RE	thalamic reticular
REM	rapid eye movement

RinB	the number of all detected REMs inside REM bursts
RinB%	percentage of rapid eye movements in burst state
RMS	root mean square
RoutB	the number of all detected REMs outside REM bursts
RSL	REM sleep latency
SA	sigma activity
SO	slow oscillations
SEI	sleep efficiency index
SEM	standard error of the mean
SOL	sleep onset latency
SPT	sleep period time
SWA	slow wave activity
SWR	sharp wave-ripples
SWS	slow wave sleep
TC	thalamocortical
TST	total sleep time
VLPO	ventrolateral preoptic
WMS	within-group mean square
σR	the EEG amplitude spectrum in 10–16 Hz frequency range
σDf	the difference between two EEG amplitude spectra in 10–16 Hz frequency range

Introduction

Sleep is a highly complex global state of reduced activity and responsiveness, regulated by a circadian clock and characterized by its rapid reversibility. It is manifested at every level of biological organization: from the genetic and cellular levels to networks of cell populations and central neuronal systems (Pace-Schott and Hobson, 2002). An average human spends one-third of his life sleeping, with sleep time in mammals varying between 3 to 20 hours per day (Siegel, 2005). In mammals and birds, sleep can be divided into rapid eye movement (REM) sleep and non-REM (NREM) sleep. Functions of neuronal systems during sleep are monitored with electrophysiological techniques collectively termed polysomnography (PSG). A polysomnographic recording consists of electroencephalography (EEG), which records synchronized excitatory and inhibitory postsynaptic potentials in cortical neurons, electrooculography (EOG), which records eye movements and electromyography (EMG) which measures muscle activity.

1.1 *The physiology of human sleep*

The amount and architecture of sleep are age dependent. Neonates sleep around 18 hours per day and 50% of their sleeping time is REM sleep. REM sleep preponderance decreases progressively as waking time increases until around 1.5 hour during adulthood (see Figure 1.1).

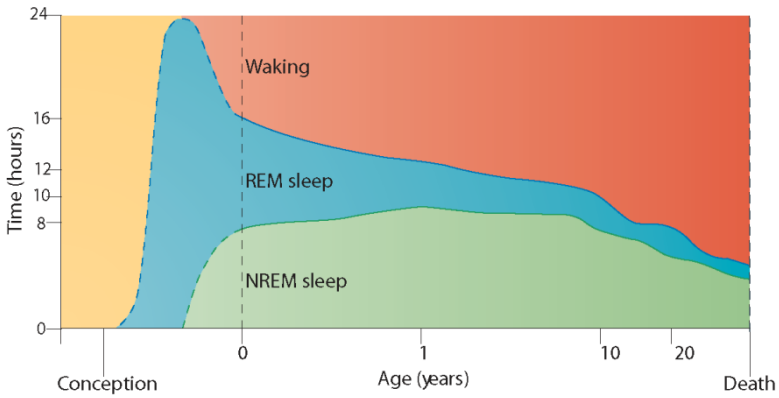

Figure 1.1: The pattern of human vigilance states in a life span (Reprinted by permission from Macmillan Publishers Ltd: Nature. Hobson, Nat Rev Neurosci; 10:803–862, copyright 2009).

1.1.1 *Sleep regulation*

The sleep-wake cycle is modulated by two independent processes, the sleep homeostasis and the circadian rhythm. The characteristic aspect of the homeostatic process is its sleep/wake dependence. Homeostatic mechanisms counteract deviations from an average "reference level of sleep" (Borbély, 1981). Sleep pressure is at minimum after waking, increases during the wake period, reaches its maximum at bedtime and declines during sleep. The EEG correlate of sleep homeostasis is slow wave activity (SWA), which is defined as a signal power in the frequency range of 0.5 to 4.5 Hz. (Borbély, 1980). The second process, the circadian rhythm controlled by the endogenous circadian pacemaker, is located in the suprachiasmatic nuclei and is influenced by daylight. The intrinsic period of the human circadian pacemaker averages 24.2 hours (Czeisler *et al.*, 1999).

It has been shown that sleep homeostasis does not dependent on circadian rhythm. Shifting the circadian rhythm with bright morning light did not affect the time course of SWA (Dijk *et al.*, 1989). It has also been shown that circadian rhythm does not dependent on sleep homeostasis. Subjective alertness of sleep deprived subjects showed a prominent circadian rhythm (Åkerstedt and Fröberg, 1977).

The circadian rhythm and sleep homeostasis interact, thus forming the pattern of daily activity. The two-process model of sleep regulation which simulates the interaction between circadian rhythm and sleep homeostasis was first proposed by Borbély (1982) and later extended, forming also the basis for other models addressing the regulation of fatigue and performance (for example Åkerstedt *et al.*, 2004). In this model the homeostatic process (Process S) rises during waking and declines during sleep, whereas the circadian process (Process C) modulates two thresholds determining sleep onset (threshold H) and sleep termination (threshold L). A schematic representation of this model is illustrated in Figure 1.2.

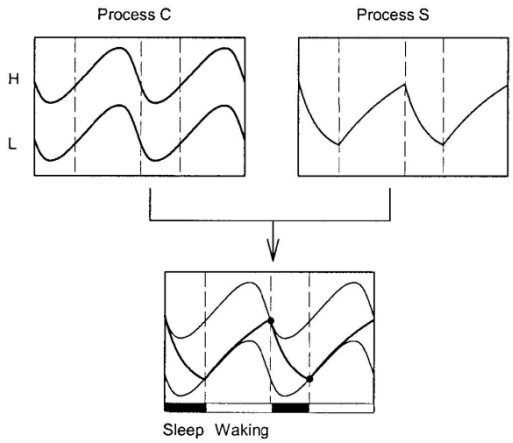

Figure 1.2: The two-process model of sleep regulation. Process S) rises during waking and declines during sleep. Process C modulates two thresholds determining sleep onset (threshold H) and sleep termination (threshold L). Interaction of S, H and L determines sleep onset and sleep termination (Statement of Use: These materials are included under the fair use exemption and are restricted from further use. Achermann, Aviat Space Environ Med; 75(3):A37–43 copyright 2004).

1.1.2 *Wake-sleep transition*

NREM sleep is regulated by the hypothalamus (as detailed in Szymusiak and McGinnty, 2008). Brain lesions in the anterior regions of the hypothalamus cause insomnia, whereas lesions in the posterior hypothalamus cause sleepiness (Von Economo, 1930). Furthermore, the anterior thalamus, the median preoptic nucleus (MnPN) and the ventrolateral preoptic (VLPO) region seem to play an important role

in promoting sleep. It has been shown that cells in these regions are mainly active during sleep (Sherin *et al.*, 1996; Gong *et al.*, 2000). Neurons in the VLPO are inactive during waking, whereas neurons in the MnPN are active in sleep-deprived animals. Therefore has been suggested that the VLPO is important for maintaining sleep stability and the MnPN controls the transition from wake to NREM sleep and mediates sleepiness (Szymusiak *et al.*, 2007). Neurons in these regions contain the inhibitory neurotransmitter gamma-aminobutyric acid (GABA) (Gvilia *et al.*, 2006). The preoptic area inhibits multiple arousal systems located in the brainstem and posterior hypothalamus (Sherin *et al.*, 1996; Zardetto-Smith and Johnson, 1995) and conversely, the VLPO is inhibited by monoaminergic arousal systems (Chou *et al.*, 2002). This circuit contains mutually inhibitory elements which set up a self-reinforcing loop, where the activity in one of the competing sites shuts down the other side. It is called the "flip-flop switch" (Figure 1.3) and can be compared to flip-flop circuits in engineering, since it creates fast changes, avoiding transitional states between sleep and wake (Saper *et al.*, 2005).

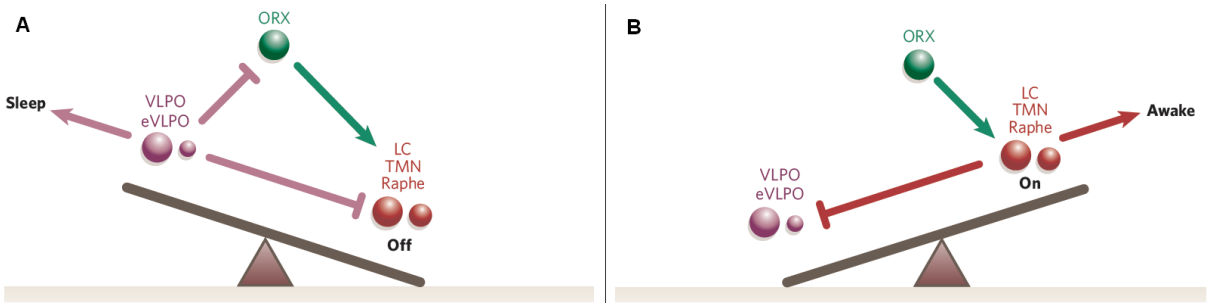

Figure 1.3: The flip-flop switch model of sleep / wake transitions. During sleep (**A**), the ventrolateral preoptic nucleus (VLPO) inhibits monoaminergic arousal systems, thereby relieving its own inhibition. This also allows it to inhibit the orexin (ORX) neurons, to further prevent monoaminergic activation. During waking (**B**) monoaminergic arousal systems inhibit VLPO. Orexin neurons stabilize the switch. eVLPO: extended ventrolateral preoptic nucleus, LC: *locus coeruleus*, TMN: tuberomammillary nucleus (Adapted by permission from Macmillan Publishers Ltd: Nature. Saper *et al.*, Nature; 437(7063):1257–1264, copyright 2005).

1.1.3 *Sleep spindles generation*

In EEG recordings, sleep onset is identified by a first localized sleep spindle. Sleep spindles are bursts of rhythmical activity in the 10–16 Hz frequency range, with waxing and waning shapes lasting from 0.5 to 2.5 sec (Figure 1.4).

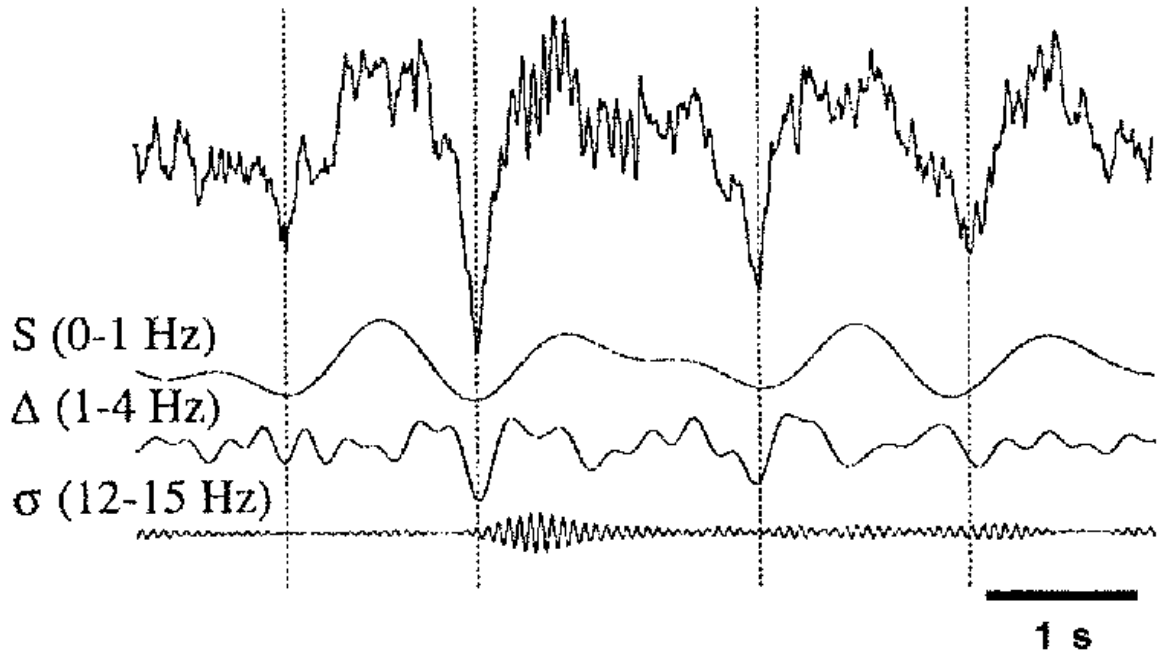

Figure 1.4: Sleep spindle in human EEG (upper signal), the same signal in 0–1, 1–4 and 12–15 Hz frequency, respectively. Spindle is located at the point where increased activity in the 12–15 Hz frequency is visible (Steriade, 2000, Neuroscience by International Brain Research Organization reproduced with permission of Elsevier BV in the format reuse in a thesis/dissertation via Copyright Clearance Center).

The mechanism of spindle generation was described by Steriade and colleagues based on observations in cats (as detailed in Steriade, 2000). The inhibition of brainstem neurons (glutamatergic, cholinergic and monoaminergic) with sleep onset starts a sequence of events leading to sleep spindles. Brainstem cholinergic neurons, when active, depolarize thalamocortical (TC) neurons and hyperpolarize thalamic reticular (RE) neurons (Curró Dossi *et al.*, 1991; Hu *et al.*, 1989). The decreased activity of brainstem neurons leads to hyperpolarization of TC and depolarization of

RE neurons. As a result, RE GABAergic cells fire and inhibit TC neurons. Inhibitory postsynaptic potentials in TC neurons result in rebound depolarizations. This process creates a loop and produces synchronized oscillations distributed to cortical areas, which are recorded as sleep spindles. The mechanism of spindle oscillations generation is illustrated in Figure 1.5. A similar process, but with higher levels of hyperpolarization, leads to slow oscillations (delta waves: 0.5–4 Hz) (Steriade *et al.*, 1991).

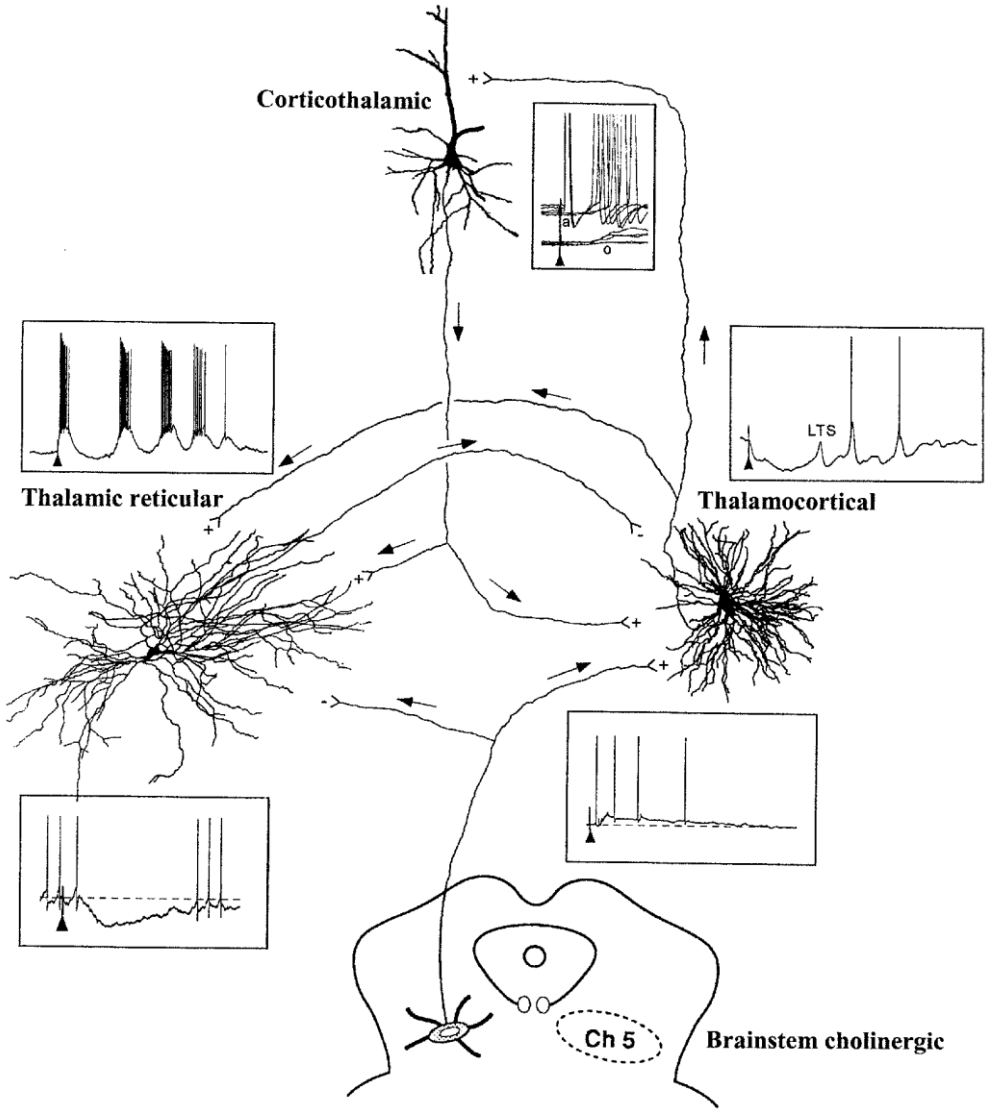

Figure 1.5: The electrophysiological scheme of sleep spindle and delta waves creation (Steriade, 2000, Neuroscience by International Brain Research Organization reproduced with permission of Elsevier BV in the format reuse in a thesis/dissertation via Copyright Clearance Center).

According to EEG studies there are two types of sleep spindles. The so-called fast spindles are mainly present in parietal regions, whereas slow spindles predominate in frontal brain areas. The average spindle peak in frontal areas is 11.5 Hz and in parietal areas 13 Hz (Werth *et al.*, 1997). Interestingly, previous studies suggest that sleep spindles observed in animals correspond to fast spindles in humans (Contreras *et al.*, 1997). There is growing evidence that the two types of spindles in humans have their sources in different regions of the brain. Low-resolution electromagnetic tomography (LORETA) demonstrated a distributed slow spindle source in the prefrontal cortex and a fast spindle source in the precuneus (Anderer *et al.*, 2001), as illustrated in Figure 1.6. The localized cortical brain regions are directly connected with adjacent parts of the dorsal thalamus (Talairach and Tournoux, 1988), where sleep spindles are generated.

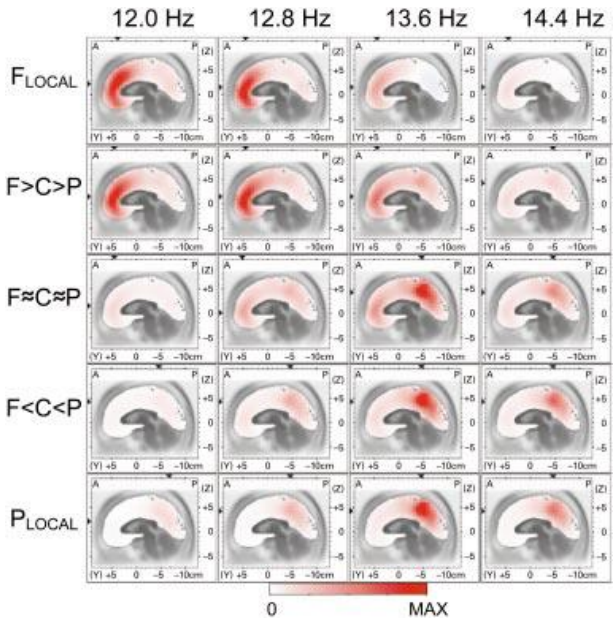

Figure 1.6: LORETA images of spindle power at discrete frequencies for spindles with different scalp topography. FLOCAL: spindle visible only on frontal areas, PLOCAL: spindle visible only in parietal areas, F>C>P: spindle most visible in frontal and least visible in parietal area, F<C<P: spindle most visible in parietal area, F≈C≈P: equal distribution over the scalp (Anderer *et al.*, 2001, Neuroscience by International Brain Research Organization reproduced with permission of Elsevier BV in the format reuse in a thesis/dissertation via Copyright Clearance Center).

High resolution EEG studies revealed that slow spindles show a dynamic topography primarily over the frontal cortex as well as variability between and within spindles. In contrast, fast spindles are topographically limited to the superior central and parietal cortex as well as consistent in amplitude and voltage propagation. Therefore, it has been proposed that slow spindles result from cortico-cortical activation following spindle initiation, while fast spindles reflect only cortico-thalamic activation (Doran, 2003). In slow wave sleep, fast spindles are synchronized to the depolarizing slow oscillations up-state, whereas slow spindles occur mostly at the transition to the slow oscillations down-state and reveal a higher probability to follow fast spindles, rather than precede them (Mölle *et al.*, 2011). Zygierewicz *et al.* (1999) also observed a fixed time delay between fast and slow spindles, with slow spindles following fast ones, and suggested that there might be some weak coupling between them, where the fast spindle "generator" occasionally drives the slow spindle "generator".

1.1.4 *REM sleep*

REM sleep (as detailed in Siegel, 2009a) is regulated by the pontine brainstem and is characterized by tonic and phasic parameters. Tonic parameters include high brain activation comparable to the wake state, theta waves produced in the hippocampus (John *et al.*, 2004), and muscle atonia together with impaired thermo-regulation (Parmeggiani, 2003). Phasic REM parameters include ponto-geniculo-occipital (PGO) waves and rapid eye movements (REMs).

Large parts of the brain, which are active during wake and inactive during NREM sleep, are again activated during REM sleep. It has been proposed that the difference between sleep and wake comes from a reciprocal discharge by two brainstem neuronal groups called REM-on and REM-off cells (Hobson *et al.*, 1975).

REM-on cells are active during REM sleep and inactive during wake, whereas REM-off cells are active during wake and inactive during REM sleep. REM-on cells are cholinergic neurons located in the pedunculopontine tegmental, and REM-off cells are serotonergic neurons of the dorsal raphe nucleus and noradrenergic neurons of the *locus coeruleus* (Datta *et al.*, 2009). Therefore it is accepted that REM sleep is potentiated by a cholinergic mechanism and suppressed by an aminergic mechanism (Hobson, 2009). Presumably REM-on cells activate the pontine reticular formation (PFR), since it has been shown that microinjection of cholinergic compounds into PFR produces a state that resembles REM sleep (Greene *et al.*, 1989).

PGO waves are isolated electrical potentials with large amplitude. They originate in the pons, and it has been shown that the pons itself is sufficient to produce them (Matsuzaki, 1969). PGO waves propagate from the pons to the lateral geniculate nucleus and afterwards to the primary visual cortex located in the occipital lobe (Jouvet, 1962). PGO waves in the visual system trigger rapid eye movements (Nelson *et al.*, 1983), but can also lead or follow the contraction of any muscle (Siegel and Tomaszewski, 1983), briefly disrupting muscle atonia. Events correlated with PGO waves are episodical and are therefore called phasic REM parameters.

It seems that muscle atonia during REM sleep is achieved by activation of inhibitory regions in pons and medulla, which inhibit the *locus coeruleus* and the midbrain locomotor region (Mileykovskiy *et al.*, 2000).

1.2 *Sleep in the EEG*

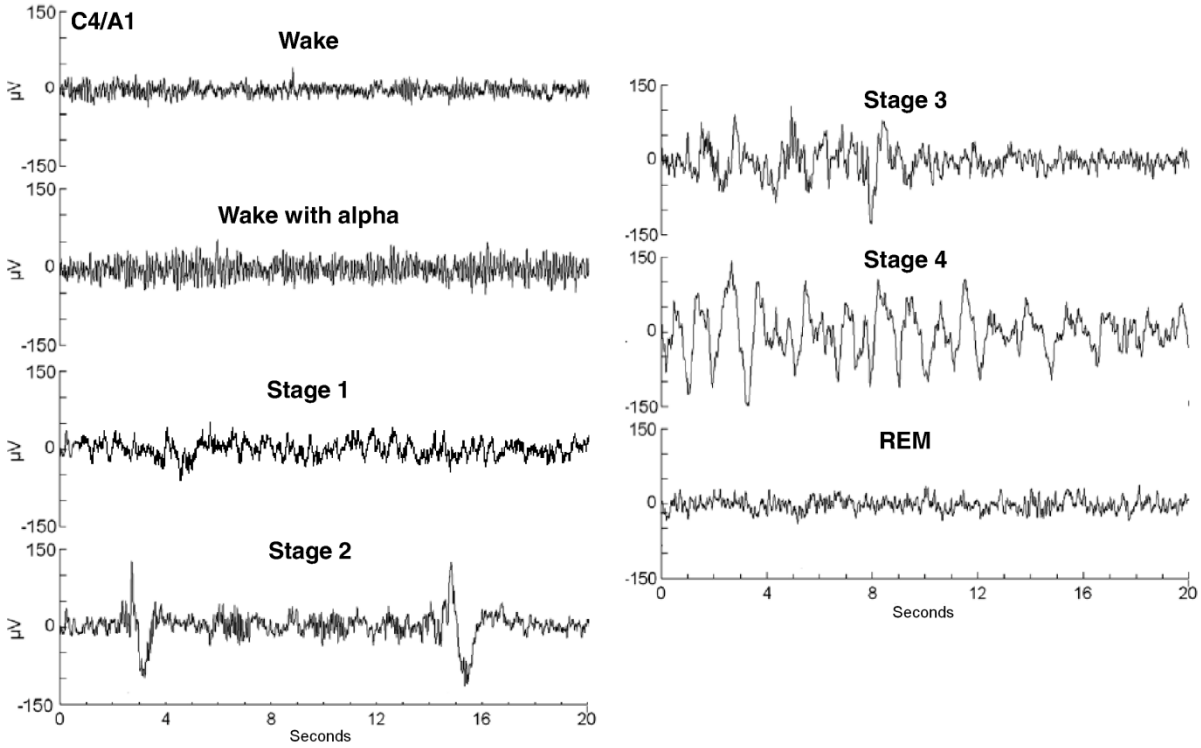

Figure 1.7: Examples of various EEG states recorded from C4A1 derivation placed in the central brain area (Adapted by permission from Dr. Elisabeth Friess (Max Planck Institute of Psychiatry) copyright 2007).

1.2.1 *Characteristics of EEG states*

The wake EEG (as detailed in Niedermeyer and DaSilva, 1999 and The American Academy of Sleep Medicine Manual, 2007) is characterized by desynchronized, high frequency and low amplitude (voltage) signal (Figure 1.7). The EEG is dominated by the beta rhythm (18–30 Hz), and high to medium levels of muscle tone are present in the electromyogram (EMG). When the eyes are closed, the subject is relatively inactive and relaxed (sleepy), synchronized alpha rhythm (8–13 Hz) occurs mostly in the posterior brain regions and muscle tone is moderate to low. Alpha waves show waxing and waning shapes (similar to sleep spindles), sinusoidal waveforms and amplitudes in a medium range of around 10 to 50 μV (Simonova *et al.*, 1967).

Stage 1 is a state of transition between sleep and wake (Figure 1.7). Alpha rhythm disappears and theta activity (4 to 7 Hz) emerges. The background signal has low amplitude and mixed frequencies. Vertex waves may occur in central brain areas. They are characterized by a sharp 'V' shape, last for around 0.5 sec and have amplitudes above 100 μV. Slow-rolling eye movements are the next characteristic feature of stage 1. They are visible in the electrooculogram (EOG) as sinus waves with a period of around 2 sec.

When the first sleep spindle is visible in EEG, it is interpreted as sleep onset and scored as stage 2. Muscle tone and overall EEG frequency are further decreased. Stage 2 is characterized by transient "graphoelements": sleep spindles (sleep spindles are described in section 1.1.3) and K-complexes (Cash *et al*., 2009). The K-complex has the highest amplitude in frontal EEG derivations and is characterized by a short high amplitude (above 100 μV) positive peak followed by a slower, larger surface-negative complex with a peak around 350–550 msec with sleep spindles sometimes intermingled. Examples of K-complexes are illustrated in Figure 1.7 (Stage 2).

As EEG synchronization increases, the subject enters slow wave sleep (SWS) (also called "deep sleep") (Figure 1.7). In order to score a sleep epoch (usually defined as 20 or 30 sec) as SWS, more than 20% of EEG must be occupied by delta waves (0.5–2 Hz). Delta waves have an amplitude of minimum 75 μV and predominate in frontal derivations. Sleep spindles are still present, however, due to massive occurrence of delta waves, it is harder to identify them in the EEG. SWS is still divided into stage 3 and stage 4 of NREM sleep; in stage 4 delta waves have to be present in more than 50% of the epoch. However, the AASM guidelines from 2007 have suggested collapsing stage 3 and 4 into SWS.

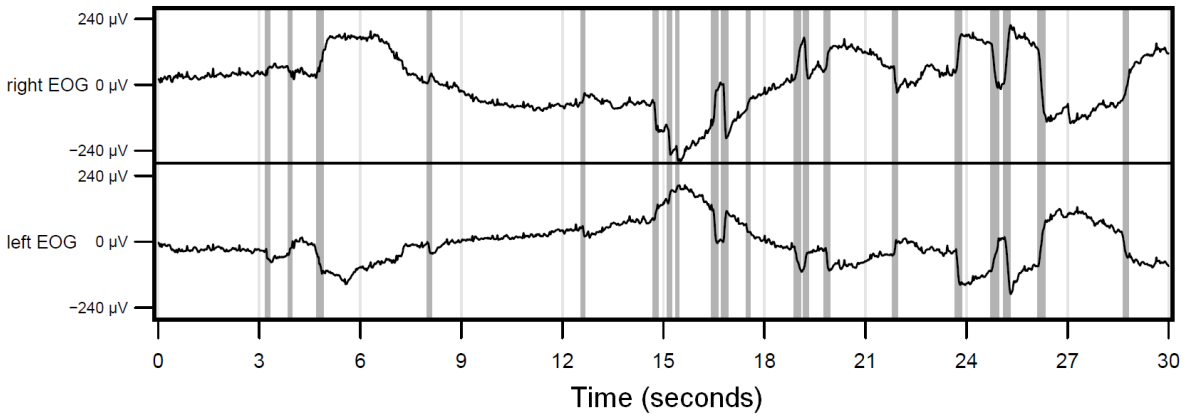

Figure 1.8: The electrooculogram (EOG) trace with rapid eye movements during REM sleep. Rapid eye movements are marked with a dark grey lines.

REM sleep is also called "paradoxical sleep", since it resembles the wake state in the EEG signal (Figure 1.7). The EEG signal is desynchronized and low-voltage with beta (18–30 Hz) rhythm, as during the wake state. Alpha waves (8–12 Hz) may occur and so-called 'sawtooth waves' are sometimes visible. Sawtooth waves are best visible in central derivations and have a frequency between 2 and 6 Hz. Muscle tone is absent during REM sleep, sometimes muscle twitches are visible in the EMG, but they are transient and last below 0.25 sec. Electrooculogram (EOG) traces show rapid eye movements, which have a rapid time course and appear simultaneously in both EOG channels (Figure 1.8).

1.2.2 *Sleep architecture*

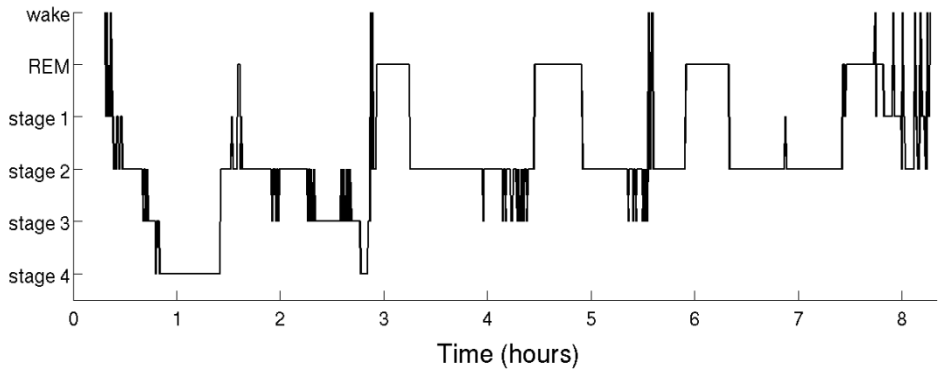

Figure 1.9: An example of sleep architecture in a young healthy adult.

According to the European Sleep Research Society, during normal sleep, around 45–55% of total sleep time consists of NREM sleep stage 2, 20–25% of REM sleep, around 20% of SWS and 5% of stage 1. Figure 1.9 shows a hypnogram exemplifying the typical sleep architecture of a young healthy person. Due to the repetitive occurrence of longer periods of NREM sleep followed by shorter periods of REM sleep we distinguish subsequent sleep cycles with an average length of approximately 90 min. Usually 4 to 5 cycles occur during the night (Billiard, 2003). The first part of the night consists mostly of NREM stage 2 and SWS with short REM sleep episodes. In the second part of the night REM sleep episodes are much longer and SWS is usually not present.

1.3 *Possible functions of sleep*

One of the obvious benefits of sleep in animals is energy conservation. Sleep increases the efficiency of behavior by reducing energy use and activity when it is not beneficial and as a result can be seen as an “adaptive state of inactivity” (Siegel, 2009b).

Sleep deprivation experiments in rats performed by Alan Rechtschaffen and colleagues (Rechtschaffen *et al.*, 1989; 1995) emphasized the importance of sleep in mammals. Chronic sleep deprivation led to temperature changes, heat seeking behavior, increased food intake, weight loss and an increased metabolic rate. All animals died with a syndrome of caloric and thermal dyscontrol. These findings show that, at least in rats, sleep is necessary for maintaining body weight and body temperature.

Sleep loss alters the immune function and sleep is disturbed during infectious diseases as well. Humans with rhinovirus infection (common cold) exhibit decreased total nocturnal sleep time and reduced sleep efficiency (Drake *et al.*, 2000). On the

other hand, 64 hours of sleep deprivation in humans resulted in leukocytosis, i.e. increased natural killer cell activity and increased counts of white blood cells (Dinges *et al.*, 1994). It has been proposed that the alterations in sleep architecture during infection facilitate the generation of fever, which promotes recovery (Imeri and Opp, 2009).

Very high levels of REM sleep until the first year of human life (see Figure 1.1) together with intense brain activation suggest that REM sleep strongly contributes to early brain-mind development. REM sleep may permit neuronal development according to the genetic program (Jouvet, 1978). It has been proposed (Hobson, 2009) that the fundamental role of REM sleep is to provide a virtual reality model that is of functional use to the development and maintenance of waking consciousness.

Sleep deprivation in humans influences a number of cognitive processes. Neuroimaging studies showed reduced metabolic activity after sleep loss in the prefrontal cortex, the anterior cingulate, the thalamus, the basal ganglia and the cerebellum. These brain regions are important for attention, information processing and executive control (Killgore, 2010). It is well documented that insufficient sleep leads to a decline in general vigilance and attention (Lim and Dinges, 2010) as well as to altered emotional processing, such as emotional perception, control, comprehension and expression (Walker and Van der Helm, 2009).

There is good evidence from animal and human sleep studies that one function of sleep is to optimize memory consolidation (as detailed in Diekelmann and Born, 2010). Significant benefits of sleep on memory are observed after night sleep as well as after shorter (60–90 min) naps (Mednick *et al.*, 2003). In this context slow wave sleep (SWS) seems to consolidate primarily declarative memory processes (system consolidation), whereas REM sleep mainly supports procedural memory contents (synaptic consolidation) (Plihal and Born, 1997; Diekelmann and Born, 2010). It was

first found in rats that the spatio-temporal patterns of neuronal firing in the hippocampus during exploratory behavior or spatial tasks were reactivated in the same order during SWS (Wilson and McNaughton, 1994). Human brain imaging studies suggest that these sleep dependent reactivations lead to redistribution of hippocampal memory traces to the neocortex for long term storage (Gais *et al*., 2007). It seems that the transfer of re-activated information between hippocampus and neocortex is supported by slow oscillations (SO), which synchronize thalamo-cortical spindles and hippocampal sharp wave-ripples (SWR) (Diekelmann and Born, 2010).

A reactivation of hippocampal neural patterns occurs mostly during SWR (O'Neill *et al.*, 2010). It was observed in rats that the suppression of SWR by electrical stimulation during the post-learning rest impaired formation of long-lasting spatial memories (Girardeau *et al.*, 2009), suggesting a promoting role of hippocampal SWR in the memory 'replay'. Studies in human epilepsy patients show that, during sleep, that SWR activity is tightly (within msec) phase-locked to the troughs of parietal and parahippocampal spindles. On a timescale of seconds, ripple activity showed a continuous increase before the peak of these spindles and decreased thereafter, whereas slow spindles showed a less close relationship to SWR, following parietal and parahippocampal spindles at a variable delay of up to 0.5 sec (Clemens *et al.*, 2011).

Increased spindle density and activity has been observed in humans during NREM sleep and SWS after both declarative and procedural learning (Gais *et al.*, 2002; Morin *et al.*, 2008). In some studies these increases were positively correlated with retention (Nishida and Walker, 2007), especially concerning sleep spindles in SWS (Cox *et al.*, 2012). Thalamo-cortical spindles were shown to be relevant for

information transfer to the neocortex. They induce long-term potentiation (Rosanova and Ulrich, 2005), which is important for synaptic plastic processes (this relates to fast spindles occurring during the depolarizing SO up-state as a phase of neuronal excitability). Interestingly, Mölle *et al.* (2009) observed that spindle activity occurs more in the depolarizing SO up-state after a learning episode. These spindles were later recognized as fast spindles (Mölle *et al.*, 2011). Taken together, fast spindles together with sharp wave-ripples might facilitate the memory-related information transfer from the hippocampus to the neocortex, while slow spindles might be related to a cortico-cortical cross-linking of transferred information with the prefrontal circuitry (Mölle *et al.*, 2011).

It is assumed that after integration of newly encoded memories into the existing networks in NREM sleep, REM sleep promotes strengthening and stabilization of memory traces, supporting synaptic consolidation (Diekelmann and Born, 2010). Local processes of synaptic consolidation in REM sleep might be facilitated due to disengagement of memory systems (Robertson, 2009) and overall desynchronization, reduction of coherence between different brain regions and increase of noise. In addition, plasticity-related immediate early gene activity (IEG) is upregulated in REM (Ribeiro *et al.*, 2002). Putatively, the high cholinergic activity during REM sleep (Teber *et al.*, 2004) also supports the maintenance of long-term potentiation in the hippocampus-medial prefrontal cortex pathway (Lopes Aguiar *et al.*, 2008), a main route for memory transfer between hippocampus and neocortex in SWS (Gais *et al.*, 2007).

1.4 *Fingerprint characteristics of the sleep EEG*

1.4.1 *Sleep structure*

A trait can be established by demonstrating that the inter-individual differences are significant, stable over time and robust when manipulated experimentally (Van Dongen *et al.*, 2005). It has been shown that many features of human EEG sleep recordings have trait-like characteristics. Tucker *et al.* (2007) investigated inter-individual variability and stability of standard sleep structure parameters, including multiple baseline and recovery nights after sleep deprivation. The variables included sleep latency, efficiency, total sleep time, SWS and REM latency, durations of all sleep states and number of sleep cycles. Inter-individual differences quantified by means of intraclass correlation coefficients (ICC) were considerable for all variables except SWS latency.

1.4.2 *EEG spectral power topography*

Finelli *et al.* (2001) compared baseline night to recovery night after sleep deprivation and showed that topographical distribution maps of EEG power over scalp have “fingerprint” characteristics. NREM sleep power distributions were derived from 27 EEG derivations and five distinct frequency bands in the range from 2 to 25 Hz. For each band, a power map was represented by a vector with 27 power values and was normalized by its mean. The authors observed the response to sleep deprivation in enhanced low frequency EEG power (up to 11 Hz) and decreased power in higher frequencies with the strongest drop in 11–16 Hz sigma activity. However, the comparison of individual maps for baseline and recovery sleep revealed very similar patterns within each frequency band. Differences between the subjects were much higher than intra-individual differences due to sleep deprivation. The authors

suggested that highly individual topographic patterns may be related to anatomical differences in the human cerebral cortex.

1.4.3 *EEG spectral pattern*

In addition to the EEG spectral power topography, the frequency spectrum also has individual patterns. First, De Gennaro *et al.* (2005) focused on a range of 8.0–15.5 Hz (sigma range) EEG frequencies in NREM sleep, which includes sleep spindles. Participants spent 6 nights in the sleep laboratory under diverse experimental conditions, including awakenings, nights with SWS deprivation and, at the end, a recovery night. It was found that each individual is characterized by an individual shape of the sleep EEG power spectra in the sigma range and that this shape remains robust across nights under varying experimental conditions. This finding was further extended by Buckelmüller *et al.* (2006) who investigated two pairs of baseline nights separated by 1 month. 8 subjects participated in the experiment and the analyzed EEG signal was recorded in the central area of the brain. The hierarchical cluster analysis performed on the EEG power spectrum within 0.75–20 Hz range grouped the nights of each subject into a distinct cluster when analyzing REM as well as NREM sleep. Though a stronger separation between the subjects was observed for NREM sleep, the EEG power spectrum of both sleep phases showed strong trait-like individual differences.

A similar experiment was performed in order to investigate the EEG changes during adolescent development (Tarokh *et al.*, 2011). EEG was recorded during two consecutive nights in 9–10 year-old children as well as in 15–16 year-old teens. EEG recordings were repeated in the same subjects 1.5–3 years later. EEG frequencies in 0.6–16 Hz range were investigated and the stability of the EEG across development was assessed. Both children and teens showed high stability when considering

absolute EEG power in separate frequency bins. However, the hierarchical cluster analysis failed to separate properly recordings that were several years apart. Only 53% to 77% subjects clustered depending on the sleep state (NREM or REM sleep) and the cohort (children and teens). The authors suggested multiple explanations for this observation. First, the number of participants was increased (19 children, 26 teens) when compared to Buckelmüller *et al.* (2006), making clustering more difficult. Second, REM sleep spectra may be more difficult to cluster since the REM sleep spectral pattern is less characteristic. Finally, REM sleep lasts for a shorter period of time than NREM, providing less signal for spectral analysis and consequently a less stable measure. In NREM sleep the peak frequency in the sigma band (10–16 Hz frequency range in which sleep spindles are visible) was found to be increased between assessments in a majority of participants in both groups.

1.5 *EEG in twin studies*

1.5.1 *Sleep structure*

Twin studies compare the differences in the phenotypic resemblance in monozygotic (MZ) and dizygotic (DZ) twins and help to provide an estimate on the heritability of a certain phenotype. Already Geyer (1937) observed that a number of sleep parameters in MZ twins is more similar than in DZ twins. A possible genetic trait of sleep structure was suggested by Hori (1986), who studied adolescent twin pairs and found that measures related to the REM sleep correlated in MZ twins. However, the study sample was very small (4 MZ, 3 DZ pairs). Further evidence of possible genetic influence on sleep was shown by Webb and Campbell (1983) in young adult twins, where awakening measures, stage changes, and REM sleep duration were significantly correlated in MZ twins, but not in DZ twins. Linkowski performed two studies on the heritability of sleep EEG in adult male twins (Linkowski *et al.*, 1989;

1991). In the first study cohabitation was found to be a confounding factor that may have a synchronizing effect on sleep architecture, therefore the second study focused on twins living apart. In addition to standard sleep architecture parameters, rapid eye movement (REM) density (the average number of rapid eye movements per REM sleep epoch) was investigated. Both studies found a significant genetic effect on the duration of stage 2, slow wave sleep (SWS) as well as on REM density. Interestingly, the authors were not able to confirm the genetic effect on REM sleep suggested in the previously mentioned studies (the effect was positive in the first study but confounded by cohabitation). The sleep parameters showing the best night-to-night stability (in this case SWS duration) were reported to have the strongest genetic component.

1.5.2 *Spectral composition in wake EEG*

Spectral composition of the background wake EEG has been shown to be one of the most heritable human traits. Heritability of absolute power in the traditional frequency bands (from delta to beta) ranges from 55% to 90% in young twins (Van Baal *et al.*, 1996; 209 investigated twin pairs) and from 70% to 90% in adolescent twins (Van Beijsterveldt *et al.*, 1996; 213 investigated pairs). Smit *et al.* (2005) performed large studies (n=142 MZ, n=167 DZ pairs) in adult twins which confirmed this finding and suggested an additive genetic effect in all analyzed EEG frequencies (1–25 Hz). The results of genetic correlations performed between the EEG frequency bands suggested that a significant proportion of the heritable variance in all frequency bands may be attributed to a common genetic source.

1.5.3 *Spectral composition in NREM sleep EEG*

The twin study of our own laboratory on heritability of NREM sleep EEG (Ambrosius *et al*., 2008, n=35 MZ and n=14 DZ twin pairs) showed significant genetic effects in 2 to 13 Hz frequency and up to 18 Hz when DZ twins were compared only to a subgroup of 14 MZ twin pairs matched for age and gender. Regarding sleep architecture, the study identified significant genetic influences on the duration of stage 3 and REM sleep. In addition, marginal genetic effects were observed for the duration of stage 4. The authors suggested that the significant genetic effect on the common EEG frequency range during both wakefulness and NREM sleep could be the consequence of a common genetically driven neuronal mechanism which generates these EEG oscillations irrespective of the vigilance state. In another twin study performed on young adults, De Gennaro *et al.* (2008) compared n=10 MZ and n=10 DZ twins. The authors focused on background NREM EEG in the 8–15.75 Hz frequency range and analyzed baseline and recovery night after sleep deprivation. No genetic effects were observed in any of the sleep architecture parameters, since sleep architecture was strongly affected by sleep deprivation during the recovery night. However, sleep deprivation did not affect the overall very strong genetic effect on the investigated EEG frequency spectrum, resulting in 96% heritability estimation of NREM sleep background EEG power.

1.6 *Genetic effects on sleep and EEG*

In summary, results of twin studies show significant genetic effects on only some parameters describing sleep organization and very strong heritability estimates on wake and NREM sleep background EEG. The genetic components of sleep EEG patterns is further supported by the identification of genes which influence sleep and EEG. Certain gene polymorphisms and genomic loci have been suggested to

influence circadian rhythm and a number of sleep disorders, e.g. narcolepsy, sleep apnea, insomnia and restless legs syndrome (as detailed in Taheri and Mignot, 2001; Dauvilliers *et al.*, 2005). An interesting finding concerning the genetics of sleep EEG was reported by Tafti *et al.* (2003) who found that, in mice, only one gene, *Acads* (coding for short-chain acylcoenzyme-A dehydrogenase), controls the peak frequency of theta oscillations (5–9 Hz) during REM sleep. Deficiency in short-chain acylcoenzyme-A dehydrogenase in mice caused slowing in theta frequency. *Acads* was highly expressed in the hippocampus and slow-theta mice showed poor memory performance. In humans, Vogel and colleagues (Anokhin *et al.*, 1992; Steinlein *et al.*, 1992) studied a rare variant (around 5% of population) of wake EEG, so called low voltage EEG. In addition to low voltage, the EEG of these subjects is characterized by a lack of synchronized alpha activity in occipital regions during wakefulness with closed eyes. After focusing on family studies the authors localized the putative genomic region determining this phenotype to the human chromosome 20q.

1.7 *Sleep EEG and psychiatric diseases*

Associations between sleep alterations and psychiatric diseases are frequently observed phenomena, as already suggested by Emil Kraepelin (1883). 80% of patients suffering from depression or schizophrenia report sleep problems. This is not surprising, since these disorders commonly affect neurotransmitter systems regulating sleep and circadian rhythm (as detailed in Wulff *et al.*, 2010).

1.7.1 *Schizophrenia*

Sleep abnormalities in schizophrenia include shorter REM latency (minutes after sleep onset until onset of REM sleep), reduced REM density and decrease in SWS

(Cohrs, 2008). Regarding quantitative EEG analysis, Keshavan *et al.* (1998) have shown reduced delta (1–4 Hz) and theta (4–8 Hz) activity.

Regarding sleep spindle analysis, findings are inconsistent. Hiatt *et al.* (1985) reported increased spindle counts in five unmedicated schizophrenia patients. On the other hand, Van Cauter *et al.* (1991) as well as Poulin *et al.* (2003) found no differences in spindle parameters in studies of n=9 and n=11 schizophrenia patients, respectively. However, data provided by Ferrarelli *et al.* (2007) based initially on n=15 medicated schizophrenia patients and then further extended to n=49 patients (Ferrarelli *et al.*, 2010) show a strong decrease in all spindle parameters (amplitude, duration, number and integrated activity) in schizophrenia patients in both slow and fast spindles. The authors explained the differences between their own findings and previous studies by the differences in sample size, EEG assessment and spindle detection methods. Recently, Wamsley *et al.* (2012) reproduced these findings, reporting reduced spindle numbers, density and coherence in schizophrenia patients.

1.7.2 *Affective disorders*

A number of sleep EEG abnormalities have been reported in patients with depression as well as in animal models of depression (as detailed in Steiger and Kimura, 2010). The converging evidence is that elevated REM sleep is a characteristic sleep alteration in depression. Various approaches using rat and mice models for depression consistently showed increased amounts of REM sleep in the animals (Dugovic *et al.*, 1999; Touma *et al.*, 2008). Humans with depression show a reduced amount of SWS, shortened REM latency (minutes after sleep onset until onset of REM sleep) and elevated REM density (measure for the amount of REMs in REM sleep) (Armitage, 2007). REM density seems to be an especially sensitive parameter. Studies in human subjects between 18 and 65 years demonstrated that REM density

measures did not vary with age and were continuously increased in depressed patients (Lauer *et al.*, 1991). Elevated REM density was also found in healthy subjects with a high risk for affective disorders due to the positive family history for the disease. Therefore, REM density has been proposed as a vulnerability marker for affective disorders (Lauer *et al.*, 1995). The Munich Vulnerability Study on Affective Disorders in high risk subjects (HRP) showed that REM density was stable over time and significantly increased in HRPs when compared to healthy control subjects during the first examination as well as after 3.5 years (Modell *et al.*, 2002). During the follow-up period, 20 HRPs developed an affective disorder and their sleep EEG showed an increased REM density compared to the control group (Modell *et al.*, 2005). The authors concluded that REM density is predictive for the onset of an affective disorder and recommended this parameter as the endophenotype of these diseases. Interestingly, the observed variability in EEG sleep measures in depressed patients may be partly confounded by latent bipolar illness. Rao *et al.* (2002) reported a potential difference between sleep EEG measure between depressed patients with unipolar disease course and patients who converted bipolar disorder. In this study, original data from subjects who met the criteria for unipolar major depression were re-investigated after 7 years. Depressed subjects with a unipolar course showed reduced REM latency, higher REM density, and more REM sleep compared to depressed subjects who converted to bipolar disorder and controls.

Regarding the differences in sleep spindle activity between depressed patients and control subjects, the current findings are not consistent. De Maertelaer *et al.* (1987) reported significantly lower spindle activity in depressed patients than in control subjects, Lopez *et al.* (2010) also reported lower spindle activity in both young subjects with a high-risk for depression and already depressed young subjects. Conversely, Ferrarelli *et al.* (2007) found no differences in spindle parameters

between depressed and control participants. Plante *et al.* (2012) reported increased spindle density, amplitude and duration in depressed females for both frontal (slow) and parietal (fast) spindles, in contrast to a decrease or no differences in spindle parameters of depressed males.

1.8 *Aim of this study*

In view of findings reporting the importance of REM sleep abnormalities in affective disorders, growing evidence for sleep spindle reduction in schizophrenia as well as inconsistent findings regarding spindle activity in depression, the first goal of the present work was the optimization of current EEG data analysis by developing the automatic algorithms, which would robustly detect rapid eye movements and sleep spindles. In the second part of the project, the developed methods were applied to sleep EEG data from a classical twin study in order to identify genetic effects on phasic REM sleep parameters, background REM sleep EEG, sleep spindles and their trait-like characteristics. The overall aim of the present work was to significantly improve the current methods of identifying clinically relevant biomarkers in psychiatric disorders.

Methods

2.1 *Signal processing tools*

2.1.1 *Discrete Fourier transform*

Spectral analysis was applied to analyze background sleep EEG in twin data (results section 3.2). The discrete Fourier transform (DFT) converts the time series x of length N into the frequency domain (as detailed in Oppenheim, 2006) using the set of complex sinusoids: $\cos\phi + i\sin\phi = e^{i\phi}$. DFT is defined as:

$$X(k) = \sum_{n=0}^{N-1} x_n e^{-i2\pi kn/N} \qquad (1)$$

In this equation, $X(k)$ is a complex number with information on amplitude and phase of frequency, k, in the time series, x, where n is the time point in this series. The great advantage of DFT is the existence of algorithms called fast Fourier transform (FFT) for very fast DFT computation. In the current work, all analyzed EEG power spectra were computed using the FFT. In order to compute power frequency spectrum for a chosen EEG fragment, FFT was performed using a 4 sec sliding window (0.25 Hz frequency resolution) with a 1 sec shift. The resulting power spectrum was the mean power spectra over all windows.

2.1.2 *Continuous wavelet transform*

Wavelet transform was applied in the sleep spindle detector (results section 3.3.1). Discrete Fourier transform (DFT) computed over long fragments of EEG signal provides a good estimate of the frequency power spectrum. Sleep spindles (see section 1.1.3) have certain frequencies (10 to 16 Hz) and their activity is visible as a peak in the NREM sleep power spectrum. Using DFT with a short time window, it is

possible to detect such events and indeed some algorithms for sleep spindle detection using FFT already been published (Huupponen *et al*., 2007). However, DFT contains certain shortcomings, which prevent it from being successfully applied for the detection of short, specific elements in the EEG, such as sleep spindles whose length may vary between 0.5 and 2.5 sec. The shortcomings are threefold. Firstly, when computing DFT, the window of predefined length makes it difficult to localize the event exactly in time. The second drawback is the fact that DFT returns the exact estimation of frequencies distribution only when the analyzed signal consists of perfect sinusoids. However, the EEG signal is nonlinear and non-stationary. In this case the frequency spectrum obtained from DFT includes additional frequencies, which do not exist in the real signal. This is especially significant in cases of large non-stationarities in the EEG signal such as K-complexes (see section 1.2.1), where sleep spindles could be left undetected due to strong activities in other frequencies. The last important drawback is the fact that although the shape of sleep spindles is known, it is not possible to take advantage of it while using the DFT. Therefore, in order to detect sleep spindles the continuous wavelet transform (CWT) was applied (Addison, 2002). CWT is the integral of the product of the signal, $x(t)$, with a predefined function chosen from the family of wavelets called the "mother wavelet" $\psi(t)$. The mother wavelet can be dilated according to the frequency of interest using the scale parameter a and shifted across the signal using the location parameter b. CWT is defined as:

$$T(a,b) = \frac{1}{\sqrt{a}} \int_{-\infty}^{\infty} x(t)\psi\left(\frac{t-b}{a}\right) \qquad (2)$$

Where $1/\sqrt{a}$ is a normalization parameter which assures that each wavelet at each scale has the same energy. The wavelet is then shifted across the signal using the

parameter b in order to compare it with all signal fragments. As a result, CWT localizes in time and frequency the signal components, which have a structure and frequency similar to the mother-wavelet, with a scale a used in the analysis. The CWT method is more expensive computationally than the FFT. However, CWT offers high temporal and frequency resolution, and furthermore provides a number of wavelets which capture the sleep spindle characteristics. Therefore wavelet transform has been widely used in spindle detection algorithms (Latka *et al*., 2005; Wamsley *et al*., 2011) as well as in methods for very detailed analysis of within-spindle components (Zygierewicz *et al*., 1999). In the current work, the Morlet wavelet showed in Figure 2.1 was chosen for spindle detection. Morlet wavelet used in CWT follows the equation:

$$\psi\left(\frac{t-b}{a}\right) = \frac{1}{\pi^{1/4}} e^{i2\pi f_0[(t-b)/a]} e^{-1/2[(t-b)/a]^2} \qquad (3)$$

f_0 is the central frequency of the sinusoid inside the Morlet wavelet and for the sake of spindle detection its value has been set at 2, since this wavelet greatly resembles the form of expected sleep spindles.

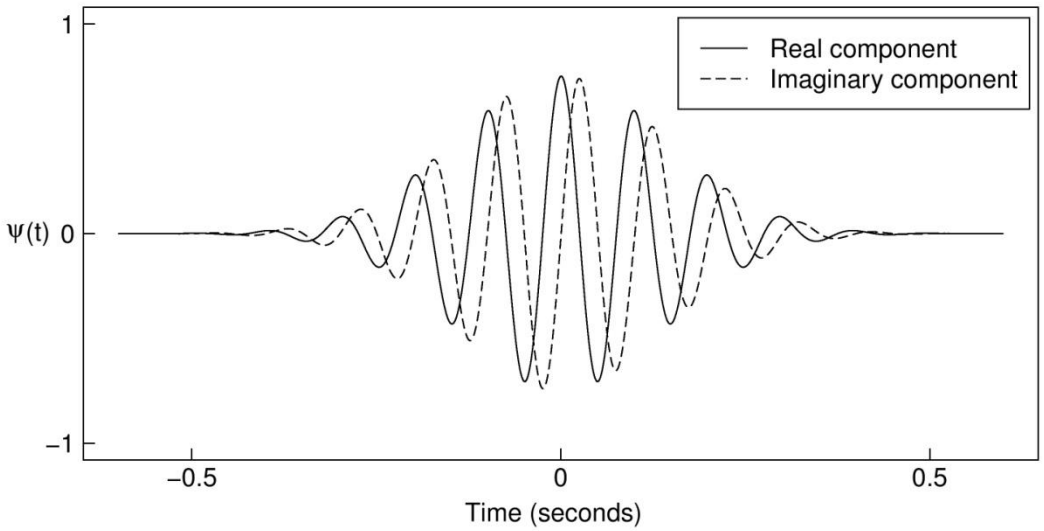

Figure 2.1: Morlet wavelet with central frequency $f_0 = 2$ used in the analysis. Presented wavelet corresponds to 10 Hz frequency.

2.2 *Twin study*

The author of the current work did not participate in acquisition of study sample. EEG sleep recordings used for the current study were collected and already described by Ambrosius *et al*. (2008). Authors of the previous study analyzed the heritability of sleep architecture and background EEG in NREM sleep. The details of the participants, study parameters, and technical details of EEG recordings have all been previously described by Ambrosius *et al*. (2008). These details are cited in parenthesis and marked in italics font.

2.2.1 *Study sample*

From Ambrosius *et al*., 2008: "*We recruited 35 pairs of MZ (mean ± SD: 24.4 ± 5.5 years; 17–43 years, 17 male pairs, 18 female pairs) and 14 pairs of DZ twins (mean ± SD: 22.5 ± 2.7 years; 18–26 years, 7 male pairs, 7 female pairs). All twin pairs were raised together; 16 of the MZ and 10 of the DZ twin pairs lived together at the time of*

the examination (cohabitation). The twins underwent extensive physical, psychiatric, and laboratory examinations including hematological, virological, clinical chemical, endocrinological, electroencephalographic, and electrocardiographic tests, to exclude acute and chronic disease. We also excluded subjects who had received any medical treatment in the 3-month period before the study and who had either a personal or a family history of psychiatric disorders, including alcohol and drug abuse, current or recent stressful life events, sleep disturbances, shift work, or a recent transmeridian flight. The subjects were asked to adhere to a regular sleep-wake schedule at least 1 week before the investigation and were not allowed to drink alcohol or caffeine containing beverages the night before and on the days of the sleep recordings. Twin zygosity was determined by using five highly polymorphic short tandem repeat loci as described by Becker et al. (1997) plus three additional markers of the Combined DNA Index System (CODIS) profiling set (D16S539, D18S51, D7S820). Genotype concordance in these markers is associated with a 99% probability that the twin pair is monozygotic."

The current analysis was performed on the second and third recording night. The first night was excluded due to a possible confounding effect of adaptation to recording conditions in the sleep laboratory. When recordings of each subject were compared night-wise, high differences in signal amplitude over whole frequency spectrum between two nights were observed in three subjects. Since this was a technical artifact (difference in EEG amplitude could result from wrong electrode placement), 3 MZ twin pairs had to be excluded. All presented results have been obtained from the remaining 32 pairs of MZ twins (23.8 ± 4.8 years (mean ± SD); range: 17–43 years, 16 males, 16 females) and 14 pairs of DZ twins (22.1 ± 2.7 years; range: 18–26

years, 7 males, 7 females). 15 of 32 MZ and 10 of 14 DZ twin pairs lived together at the time of the examination.

2.2.2 *Experimental design*

From Ambrosius *et al*., 2008: "*Psychiatry in Munich. The experimental protocol was approved by the Ethics Committee for Human Experiments of the Bayerische Landesärztekammer (Munich, Germany). Written informed consent was obtained from all participants, after the procedures had been fully explained. The subjects spent 3 consecutive nights in our sleep laboratory, where the first night served for adaptation and exclusion of sleep disturbances. In almost all cases, the twin partners were recorded at the same time.*"

2.2.3 *EEG recording*

From Ambrosius *et al*., 2008: "*Polysomnographic recordings (Schwarzer, Munich, Germany) were performed according to the international 10-20 electrode system (FP1, FP2, F3, F4, C3, C4, P3, P4, O1, O2, all referenced against the contralateral ear lobe), with an electrooculogram, a chin electromyogram, and a three-lead electrocardiogram. The sampling rate was 250 Hz, amplification 70 µV, and time constant .3 sec, filtering at .53 Hz (3dB/octave) and 70 Hz (12dB, octave), respectively. Polysomnographic recordings were visually scored in 30-sec epochs according to the guidelines of Rechtschaffen and Kales (1968) by experienced raters unaware of the study protocol. Recordings of the twin partners were scored by the same rater.*"

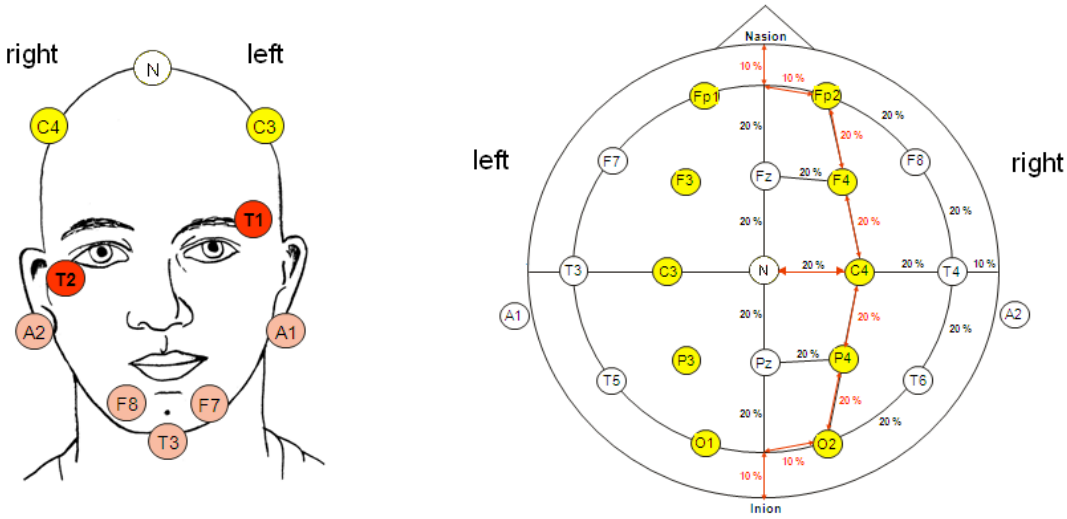

Figure 2.2: The setup used for twins EEG sleep recordings. The EEG electrodes used for the recording (FP1, FP2, F3, F4, C3, C4, P3, P4, O1, O2) are marked with a yellow color. The EEG electrodes on the left side of the scalp were referenced to right ear lobe (A2) and on the right side to the left ear lobe (A1). The EOG electrodes (T1 and T2) are marked with a red color. F7, F8 and T3 are chin electromyogram electrodes used for muscle monitoring (Adapted by permission from Luise Vogel (Max Planck Institute of Psychiatry) copyright 2007).

2.2.4 *EOG recording*

These data were acquired in the course of the study performed by Ambrosius *et al*., 2008 but were not part of the publication. Electrooculographic (EOG) montage was performed according to Rechtschaffen and Kales (1968) and is illustrated in Figure 2.2. In this two channel montage, one electrode is placed 1 cm above and slightly lateral to the outer canthus of one eye. The second is placed 1 cm below and slightly lateral to the outer canthus of the other eye. Both electrodes were referenced to the left mastoid electrode. The sampling rate for the EOG was 250 Hz and it was low- and high-pass filtered at 30 Hz and 0.095 Hz (time constant 16.75 sec, 12 dB/octave), respectively.

2.2.5 *EEG spectral composition*

From Ambrosius *et al*., 2008: "*For the present analysis we selected the EEG data from the central derivation C3/A2 of the third recording night (second night in two pairs). The EEG of non-REM sleep (stages 2, 3, 4) was submitted to Fourier transformation with an in-house software. Power spectra were derived from a 4-sec window, shifted for 1 sec, resulting in a resolution of .25 Hz. The resulting 30 spectra were averaged per epoch of 30 sec. The lowest bins (.25, .5 Hz) were excluded, owing to the filtering procedures. For analysis of frequency bands, the power was cumulated across the δ (0.75–4.5 Hz), θ (4.75–7.75 Hz), α (8.0–11.75 Hz), σ (12.0–15.75 Hz), β1 (16.0–25.0 Hz), β2 (25.25–35.0 Hz), φ (35.25–45.0 Hz), including a subdivision of the σ range into α/σ (10.0–11.75 Hz), low σ (12.0–13.75 Hz) and high σ (14.0–15.75 Hz).*"

The data from spectral analysis performed by Ambrosius *et al*. (2008) were not reused. However, the Fast Fourier Transform was performed using a sliding window of the same size and a shift resulting in the same frequency resolution. Spectral analysis for the current work was performed for both, REM and NREM sleep for the second and third recording night. Fragments with artifacts were excluded prior to spectral analysis using an automatic procedure (based on high EEG signal amplitudes as well as high activity in 0.75–3 Hz and 25–45 Hz) followed by visual inspection.

Genetic variance analysis and intraclass correlation coefficient results from the left hemisphere (derivation C3A2) are presented in the results section, whereas results from the right hemisphere (derivation C4A1) are presented in the supplementary material.

2.2.6 *Sleep spindle parameters*

The group of sleep spindle parameters chosen for heritability analysis consisted of *length*, *amplitude* and *frequency*, which describes basic spindle characteristics, and temporal parameters of spindle occurrence. The *number of spindles* in a fragment of interest was the first parameter under analysis. Thereafter the *spindle density*, defined as the average number of spindles in one sleep epoch, was assessed. It has been shown that spindle density increases after both, declarative and procedural learning (Gais *et al*., 2002 and Morin *et al*., 2008) and that overnight verbal memory retention is highly correlated with the number of sleep spindles (Clemens *et al*., 2005). Furthermore, a possible sleep spindle abnormality has been reported in depressed females by Plante *et al*. (2012), who observed increased spindle density in comparison to healthy subjects.

The last examined spindle parameter was *integrated spindle activity*. It is defined as the average sum of all detected spindle amplitudes in one sleep epoch. Integrated spindle activity was of interest since it was found that in schizophrenic patients spindle number, amplitude and length were all significantly reduced, but the strongest decrease was observed for the integrated spindle activity (Ferrarelli *et al*., 2007).

The source of slow spindles is localized in the prefrontal cortex and that of fast spindles in the precuneus (Anderer *et al*., 2001). As a consequence, slow spindles are the most prominent in frontal EEG derivations and it is the best place to measure them precisely, while the parietal EEG derivations are the most suited to measure fast spindles. The additional advantage of EEG channels distinction, when separating slow and fast spindles, is the fact that fast spindles are suppressed in the signal received by frontal derivations and slow spindles are suppressed in parietal derivations. As a result the probability of spindle misclassification is highly

decreased. Therefore slow sleep spindles were analyzed in signal from frontal EEG derivations (F3A2, F4A1) and fast spindles in parietal EEG derivations (P3A2, P4A1). In central EEG derivations both fast and slow sleep spindles are present. Therefore central EEG derivations (C3A2, C4A1) were used to analyze general spindle activity, i.e. all spindles detected in spindle frequency range (localization of individual spindle frequency range is described in section 3.3.1.4) without distinction between slow and fast ones. Separate analysis was done for whole NREM sleep as well as stage 2 and slow wave sleep (SWS) separately.

Two-way repeated measures analysis of variance (rANOVA) for factors night and hemisphere revealed no effect of night as well as no night:hemisphere interaction. However, significantly higher amounts of spindles (number of spindles: $F(1, 91)=21.880$, $p<.001$, spindle density: $F(1, 91)=22.242$, $p<.001$) as well as significantly longer spindles in the left hemisphere were found (average spindle length: $F(1, 91)=24.591$, $p<.001$). Slow spindle amplitude was significantly higher in the right hemisphere ($F(1, 91)=19.998$, $p<.001$) and fast spindle amplitude was significantly higher in the left hemisphere ($F(1, 91)=7.388$, $p<.008$). Therefore, the mean of two nights were used for heritability estimations, but each hemisphere was analyzed separately. Genetic Variance Analysis and Intraclass Correlation Coefficient results from left hemisphere are presented in the results section, whereas results from right hemisphere are presented in the supplementary material.

2.2.7 *Phasic REM sleep parameters*

REM sleep parameters designated “phasic parameters” were chosen for heritability analysis, and include all parameters connected with rapid eye movement activity during REM sleep. Rapid eye movements (REM) were of special interest because

increased REM density was proposed as an endophenotype (Lauer *et al*., 1995) and was shown to be a vulnerability marker for affective disorders (Modell *et al*., 2005). To-date, assessment of REM activity at the Max Planck Institute of Psychiatry has been based on visual scoring. This is a very tedious task, time-consuming task. Therefore, instead of counting all observed REMs, REM activity was always assessed by visual scorers as the number of 3-sec mini-epochs containing at least one REM. Visual scoring using with this method is faster and it was sufficient to observe elevated REM density in depressed patients. However, with the new REM detector presented here it is possible to add REM activity measures with all detected REMs considered. Counting each REM separately could provide more information about REM activity and could influence the estimations of heritability. Therefore, in order to compare the REM activity assessed using the "standard" REM assessment method to the REM activity assessed using each REM count, the estimates of genetic regulation were computed for both REMs quantification methods. In the results section, '*3sRA*' refers to the REM activity computed as the total number of 3-sec mini-epochs containing at least one REM, whereas '*allRA*' refers to the total number of all detected REMs. REM density, the parameter of special interest, was calculated as the average REM activity per one epoch of REM sleep. REM density obtained from 3sRA is designated '*3sRD',* and that from allRA as '*allRD'*.

Generally elevated REM density is not the only abnormality of REM sleep in depressed patients. In healthy subjects, REM sleep pressure rises during the course of the night and manifests as a lengthening of REM sleep episodes within successive sleep cycles. Patients with depression show increased REM sleep pressure from the beginning of the night, which results in a decreased time between sleep onset and the first REM sleep episode (REM latency) as well as increased REM density in the first sleep cycle (Lauer *et al*., 1991). Therefore, the time course of REM density

during the night was also of interest and the heritability estimations of REM density were performed for the whole night, for each of the first three sleep cycles as well as for each third of the night.

Lastly we were interested in the organization of rapid eye movements. It has been observed that REM organization develops during the early stage of human development. Clusters of REMs were demonstrated to increase in infants across the first 4 months of life, reaching a stable level thereafter. The amount of REMs with respect to REM density was shown, however, to further increase (Ktonas *et al*., 1990). Becker and Thoman (1981) reported that number of intense rapid eye movement periods (so called REM storms) measured at 6 months of age correlated negatively with mental development at 1 year. When comparing healthy young subjects to elderly subjects, there is no difference in REM density, however, clustering properties of REMs decrease with aging (Ficca *et al*., 1999). In order to investigate the grouping of REMs into clusters, REM burst was defined as a sequence consisting of a minimum of three REMs, with a maximum time frame between consecutive REMs of two seconds. The organization of REMs into bursts was evaluated with 3 parameters: the number of all detected REMs inside REM bursts (*RinB*), all detected REMs outside REM bursts (*RoutB*) as well as the percentage REMs in burst state (*RinB%*).

2.2.8 *Genetic variance analysis*

Genetic variance analysis was applied to estimate genetic effects in twin sample (results sections 3.1, 3.2, 3,3.2, 3.4.2). The study sample of 32 MZ twin pairs and 14 DZ twin pairs was large in comparison to other EEG sleep studies. However, this size was insufficient to reliably decompose the observed inter-individual variation amongst

the studied twins into additive genetic variation, nonshared environmental variation and dominant genetic or shared environmental variation using Structural Equation Models. Therefore, we rather focused on estimating whether the observed differences in phenotypic variation between MZ and DZ twins, which in the applied classical twin model should be the result of higher genetic differences amongst DZ twins, is significant. In order to estimate genetic variance from the twin data, a method proposed by Christian *et al*. (1974; 1987) was applied. This method is based on the general model for genetic variance estimation from twin data (Haseman and Elston, 1970). In this model, assuming that there is no evidence for inequality of the total phenotype variance of MZ and DZ twins, the expected mean squares should follow the equalities:

$$E(M_{amz} - M_{adz}) = E(M_{wdz} - M_{wmz}) = 0.5\sigma_a^2 + 0.75\sigma_d^2 + f\,0.5\sigma_i^2 \qquad (4)$$

$$E(M_{amz} + M_{wmz}) = E(M_{adz} + M_{wdz}) = 2\sigma_a^2 + 2\sigma_d^2 + 2\sigma_i^2 + 2\sigma_e^2 \qquad (5)$$

Where M is a mean square, amz: among MZ pairs, wmz: within MZ pairs, adz: among DZ pairs, wdz: within DZ pairs, σ_a^2: variance component due to additive genetic effects, σ_d^2: variance component due to dominant genetic effects, σ_i^2: variance component due to epistatic genetic effects, σ_e^2: variance component due to nonshared environmental effects. f : epistatic variance in DZ twins.

The first step of a genetic variance estimate, is to test, whether the assumption (5) of the model is valid by performing a two-tailed F' test comparing $M_{amz} + M_{wmz}$ with $M_{adz} + M_{wdz}$. The degrees of freedom for each sum of mean squares should be computed according to Smith (1936) using the following equation:

$$df = \frac{(M_1 + M_2 + \ldots + M_x)^2}{\frac{M_1^2}{n_1} + \frac{M_2^2}{n_2} + \ldots + \frac{M_x^2}{n_x}} \qquad (6)$$

Where n_i are degrees of freedom computed for M_i. In this formula, the obtained degrees of freedom are weighted according to the difference in magnitude between M_i as well as according to the difference in magnitude between n_i. Obtained degrees of freedom will be the same as the sum of n_i when all M_i and all n_i are the same. In the worst case scenario, the magnitude of one of the M_i is much larger than the others, and consequently the resulting degrees of freedom will be very close to n_i.

If the sums of mean squares are significantly unequal, the environmental variance component σ_e^2 could be unequal for MZ and DZ twins. If there is a substantial genetic or environmental variance, it may be difficult to detect differences in σ_e^2. Therefore the F' test is performed at an increased level of significance, set at 20% (as suggested by Christian *et al.* (1974)). If the variances of MZ and DZ twins are not significantly different, the general model is appropriate and the genetic variance from equation (4) can be estimated using the within-twin-pair estimate $GWT = M_{wdz} - M_{wmz}$ as well as the among-twin-pair estimate $GAT = M_{amz} - M_{adz}$. The one-tailed F test is performed to test whether the genetic variance is significant using the ratio of within-twin-pair mean squares M_{wdz} / M_{wmz}. Within-twin-pair mean squares are used, because typically their values are lower than among-twin-pair mean squares, and thus testing within-twin-pair mean squares ratio results in a more sensitive test.

If the variances of MZ and DZ twins are significantly unequal, the general model (4) has to be extended with the unique environmental effects in MZ σ_{emz}^2 and DZ σ_{edz}^2 twin set:

$$E(M_{amz} - M_{adz}) = [0.5\sigma_a^2 + 0.75\sigma_d^2 + f\,0.5\sigma_i^2] + (\sigma_{emz}^2 - \sigma_{edz}^2) \qquad (7)$$

$$E(M_{wdz} - M_{wmz}) = [0.5\sigma_a^2 + 0.75\sigma_d^2 + f\,0.5\sigma_i^2] + (\sigma_{edz}^2 - \sigma_{emz}^2) \qquad (8)$$

In this case, GWT as well as GAT estimation of genetic variance would be biased in the opposite directions. Therefore, in order to obtain the unaffected genetic variance estimation, the mean of GWT and GAT estimates is used. This combined estimator is called by the authors (Christian *et al.,* 1974) GCT:

$$GCT = \frac{GAT + GWT}{2} = \frac{(M_{amz} - M_{adz}) + (M_{wdz} - M_{wmz})}{2} = \frac{(M_{amz} + M_{wdz}) - (M_{adz} + M_{wmz})}{2}$$

(9)

The one-tailed F test is performed to test, whether the genetic variance is significant using the ratio $(M_{amz} + M_{wdz})/(M_{adz} + M_{wmz})$ where the degrees of freedom are computed as in equation (6).

The GCT estimate is always appropriate, however it is much less powerful due to high possible values of among-twin-pair mean squares. Therefore the significance of GCT estimate is tested when there is evidence for unequal sums of mean squares in MZ and DZ twins, otherwise the significance of GWT estimate is tested.

As a prerequisite for the analysis, each studied variable had to fulfill the assumptions of normal distribution (measured by a non-significant goodness-of-fit by the Kolmogorov-Smirnov test) in both twin samples and equal means between the twin samples (T-test). If the data did not fulfill the normal distribution criterion, they were log transformed prior to any analysis. The significantly unequal means between MZ and DZ twin samples indicate that the investigated variable could be associated with the type of twins being studied. In this case the estimation of genetic variance would be biased. Therefore, if there was an evidence for significantly unequal means

between MZ and DZ twin samples, the genetic variance analysis was not performed. Influence of covariates was tested by multivariate analysis of covariance (MANCOVA). EEG power spectrum at different frequencies, phasic REM parameters and sleep spindle parameters were tested in separated blocks. Three covariates were considered:

1. Cohabitation (twins living together), since in former twin studies it was found to have a possible effect on REM sleep duration (Linkowski *et al*., 1989).
2. Age, since age has an effect on duration of REM sleep (Hobson, 2009; REM sleep duration decreases with age) and EEG power (Dijk *et al.*, 1989b; Tarokh *et al*., 2011; EEG power decreases with age).
3. Sex, since sex has an effect on EEG power (Dijk *et al.*, 1989c; higher EEG power in females).

Prerequisites were considered to be violated, if the appropriate test showed a significant result at the 5% level. Genetic variance analysis was performed on mean results of 2 recording nights. In order to minimize the effects of possible covariates, a subgroup of MZ twins closely matched for age, gender and cohabitation to DZ twins was selected. All genetic variance estimations as well as intraclass correlation coefficients recomputed for matched MZ and DZ samples can be found in supplementary material.

2.2.9 *Intraclass correlation coefficient analysis*

To further illustrate differences of within-pair resemblance between MZ and DZ twins, intraclass correlation coefficients (ICCs) were computed for all parameters analyzed by genetic variance analysis (results sections 3.1, 3.2, 3,3.2, 3.4.2). ICC is the ratio of between-group variance to the sum of between and within-group variances. ICC was computed according to the formula described by Shrout and Fleiss (1979) for

one-way random single measures analysis of variance, named by the authors as ICC(1, 1). In this design, the estimate of within-group variance σ_w^2 is obtained from the within-group mean square (WMS) and the estimate of between-group σ_b^2 variance is computed by subtracting WMS from the between-group mean square (BMS) and dividing the result by the size of groups (in our case 2). As an outcome, the ICC was computed according to the following formula:

$$ICC(1,1) = \frac{\sigma_b^2}{\sigma_b^2 + \sigma_w^2} = \frac{(BMS - WMS)/2}{(BMS - WMS)/2 + WMS} = \frac{(BMS - WMS)/2}{(BMS + WMS)/2} = \frac{BMS - WMS}{BMS + WMS} \quad (10)$$

The ICC outcome varies from +1, in the case of present σ_b^2 and no σ_w^2, to -1, in the case of present σ_w^2 and no σ_b^2.

ICCs were used to illustrate both similarity of the given parameter in MZ and DZ twins (each pair of twins was a separate group) and stability for consecutive nights (two nights of each individual was a separate group). To obtain levels of statistical significance for ICC results the bootstrapping analysis was performed (similar strategy was described by Tarokh et al. (2011) when analyzing EEG frequency bins). Each sample was recreated 1000 times. To recreate the sample, subjects were chosen randomly with repetitions up to the same number as in the original set. ICCs were computed for all bootstrapped samples. When a negative ICC resulted from a bootstrapped sample, an absolute value was used, because negative ICCs would make no biological sense. For each investigated parameter ICC results from original samples together with upper percentiles (responding to *p*=0.01) and median values of bootstrapped data are presented. According to Landis and Koch (1977) ICC values from 0 to 0.2 have been termed *slight*, 0.21 to 0.40 *fair*, 0.41 to 0.60

moderate, 0.61 to 0.80 *substantial*, and 0.81 to 1 as *almost perfect* agreement. ICCs estimating within-twin-pair resemblance were performed on mean results of 2 recording nights.

2.2.10 *EEG 'fingerprint' characteristics in twins: the cluster analysis*

Buckelmuller *et al*. (2006) showed that EEG frequency power spectrum in humans has 'fingerprint' characteristics, i.e. having EEG frequency spectrum of an individual from a night recording, it should be possible to identify this individuals other night recording from the set of recordings just by comparing the frequency spectra. The hierarchical cluster analysis was performed to analyze how the 'fingerprint'-like characteristics of EEG frequency power spectra with respect to their morphology were preserved in twins (results sections 3.2.1.2 and 3.2.2.1). In addition, the clustering properties of sleep spindles with respect to their basic characteristics (density, amplitude, length and frequency) were also investigated (results section 3.3.2.2).

In cluster analysis, each entity is represented as a vector of chosen features. Distance between a pair of vectors is computed according to the predefined metric. In this study, in order to measure distances between clusters, the shortest distance method was applied. It takes the minimal distance of every combination of vectors from both clusters and sets it as a distance between them.

For the similarity analysis of EEG frequency power spectra morphology, vectors consisted of log transformed EEG power spectra, where each feature was a frequency bin. REM sleep EEG power spectra were represented as 178 feature vectors (0.75 to 45 Hz, 0.25 Hz bins). In NREM sleep, due to the presence of muscle tone in the EEG signals influencing high frequencies, power spectra were restricted

to 20 Hz resulting in 78 feature vectors (0.75 to 20 Hz). The distance metric used in the analysis was one minus Pearson's correlation coefficient between vectors. Pearson's correlation assesses the linear association between two sequences and systematic shifts between the two sequences do not influence the correlation results. When performing cluster analysis the shape similarities between EEG spectra was the main focus. Correlation metric seemed to be the appropriate choice since the correlation outcome when two vectors with power spectra are compared is independent of absolute power in frequency bins. This was the goal, since the heritability of absolute EEG spectral power was analyzed using intraclass correlation coefficients and genetic variance analysis.

When investigating sleep spindles similarity, each subject was represented by a vector of 22 spindle parameters: slow spindles detected in frontal derivations, fast spindles in parietal derivations and all spindles detected in central derivations were represented with mean amplitude, length and density during both, stage 2 and slow wave sleep. The remaining four parameters were precomputed from the NREM sleep power spectrum (localization of individual spindle frequency range is described in section 3.3.1.4) and consisted of: begin of spindle frequency range, slow spindle frequency peak, fast spindle frequency peak and the end of spindle frequency range. The distance metric used in the analysis of sleep spindle parameters was the standardized euclidean distance. In this measure, distance computation between vectors is the same as in euclidean distance, but each coordinate (parameter) in the sum of squares is inversely weighted by the sample variance of that coordinate. Standardized euclidean distance was used, because there were high differences in values between different spindle parameters. Therefore, performing euclidean distance measure would result in highly unequal influence of parameters on

computed distance. The normalization of each parameter according to its variance assures similar importance of each parameter on the outcome.

2.3 *REM detection algorithm*

2.3.1 *Visual scoring of rapid eye movements*

Figure 1.8 shows a sleep epoch with rapid eye movements visible in EOG derivations mounted according to Rechtschaffen and Kales (1968). Rapid eye movements are visible in this montage as simultaneous out-of-phase rapid amplitude change in both EOG derivations. Rapid eye movement should be visible above the background noise and should be counted regardless of the amplitude of the eye movement (Aserinsky, 1971). The stepwise saccades are all counted as separate eye movements.

Rapid eye movement activity, reported by a visual scorer in our institute, is defined as the total number of 3 sec-miniepochs containing at least one rapid eye movement for each 30 sec sleep epoch. Consequently, for each sleep epoch the information available from visual scoring is a number from 0 to 10 describing rapid eye movement activity in this epoch.

The experts scoring REM density were trained sleep scorers who had extensive experience scoring sleep EEG data. The scorers were trained at regular intervals. Inter- and intra-rater variability was assessed for sleep recordings with varying degrees of sleep disturbance. Inter-rater reliability was above 80%.

2.3.2 *Study sample*

The data set consisted of a development and a validation sample. The development sample was drawn from the twin study described in section 2.2. Within this sample

rapid eye movement density was visually scored in n=59 subjects (23.1 ± 5.0 years (mean ± SD); range: 17–43 years, 25 females, 34 males) during the second recording night. The validation sample consisted of seven healthy subjects (23.7 ± 2.3 years; 21–27 years, 3 females, 4 males) possessing good sleep quality participating in a different ongoing study. The setup of EEG and EOG derivations was the same for all recordings used for development and validation of the algorithm (see section 2.2.3 and 2.2.4).

For the development of the REM detection algorithm, the development sample, scored by one of the expert scorers (scorer 1) was used. After the development of the basic algorithm two further nights were used from the validation sample which were scored by two experts (scorer 1 and scorer 2) to obtain adequate thresholds for the parameters of the algorithm (training set). These two nights were excluded from further analysis of inter-scorer and scorer vs. algorithm agreement. The algorithm was then used to analyze the validation set (12 recordings from 7 healthy subjects), which was scored by the two scorers. Epoch-wise Pearson’s correlation and Cohen's kappa coefficient was used in order to assess inter-scorer (scorer 1 vs. scorer 2) and scorer vs. automatic algorithm agreement.

2.3.3 *Inter-rater agreement: the kappa coefficient*

Cohen's kappa coefficient (Cohen, 1960) was applied to obtain the agreement between presented REM detector and visually scored REM density (results section 3.4.1.3). It is a statistical measure of inter-rater agreement for qualitative (categorical) items. Kappa takes into account chance agreement between scorers, and is therefore thought to be better measure than simple percent agreement. Kappa coefficient is defined as:

$$\kappa = \frac{p_0 - p_e}{1 - p_e} \quad (11)$$

Where p_0 is the observed agreement and p_e is the expected agreement obtained by chance. As an example let us assume that we want to compare two raters who evaluate n=100 features and put them into 3 different categories X, Y and Z.

		Rater 1		
		X	Y	Z
Rater 2	X	10	2	10
	Y	2	21	8
	Z	3	1	43

The observed agreement in the example is $p_0 = (10 + 21 + 43)/100 = 0.74$ whereas the expected agreement is:

$$p_e = (X_1 / n) \cdot (X_2 / n) + (Y_1 / n) \cdot (Y_2 / n) + (Z_1 / n) \cdot (Z_2 / n) = \frac{22 \cdot 15 + 24 \cdot 31 + 61 \cdot 47}{100 \cdot 100} = 0.39$$

Kappa coefficient returns the difference between the observed and chance agreement, which is normalized to <-1,1> range. -1 is obtained with no agreement, and +1 with a perfect agreement, between raters. Values below 0 are obtained when the observed agreement is lower than agreement expected by chance. Putting p_0 and p_e into formula (11) results in kappa coefficient of 0.57.

There are several benchmarks characterizing agreement based on Cohen's kappa values. According to Landis and Koch (1977), kappa values from 0.41 to 0.60 have been termed *moderate*, between 0.61 and 0.80 *substantial*, and between 0.81 to 1 as *almost perfect* agreement. According to Fleiss (1981), kappa values of 0.75 and higher are *excellent*.

According to the REM density scoring that was performed in the laboratory, absolute values of REM density ranged between 0 and 10 for each epoch of REM sleep (visual scoring of rapid eye movements is described in section 2.3.1). Because the kappa coefficient treats scoring results as mutually exclusive categories, comparing epoch-wise REM densities would lead to an underestimation of the agreement among raters. For example, if the first rater gave a score of 5 for REM density in one epoch of REM sleep, and the second rater gave a score of 6 for the same epoch, computation of the kappa coefficient yields an agreement of 0, even though both raters agreed in five 3 sec-segments and disagreed in only one 3 sec-segment of the epoch. Therefore, each 3 sec-segment was treated as one item and the epoch-wise REM density was transformed into the number of consecutive segments with REMs starting from the first 3 sec-segment. Thus, a REM density score of 5 would yield a vector with five consecutive scores 1 and five scores 0, and a REM density score of 6 would yield a vector of six consecutive scores 1 and four scores 0. The computation of Cohen’s kappa across these vectors would take the agreement in nine segments (5 with, 4 without REMs) into account.

Results

3.1 *Twins sleep architecture*

Sample means of averaged over-pairs measures revealed no significant night effects as well as no significant differences between the twin samples (see Table 3.1).

Table 3.1: Sleep architecture parameters averaged over pairs. Group mean ± SEM of sleep characteristics in minutes. TST: Total sleep time, SPT: Sleep period time, SEI: sleep efficiency index, SOL: sleep onset latency, REM: rapid eye movement sleep duration, NREM: Non-REM sleep duration, RSL: REM sleep latency, DZ: dizygotic twins, MZ: monozygotic twins.

	DZ n=14			MZ n=32		
	Night 2	**Night 3**	**2 nights mean**	**Night 2**	**Night 3**	**2 nights mean**
TST	419.33±6.27	423.64±5.65	421.49±5.73	420.89±4.01	417.51±3.94	419.20±3.39
SPT	462.75±4.31	466.57±3.23	464.66±3.55	469.26±2.23	469.85±1.72	469.56±1.62
SEI	0.94±0.01	0.95±0.01	0.95±0.01	0.94±0.01	0.94±0.01	0.94±0.01
SOL	30.05±4.66	27.23±3.55	28.64±3.94	23.41±2.27	23.14±1.56	23.27±1.61
NREM	324.21±6.17	324.89±4.50	324.55±5.09	321.54±3.16	318.48±3.64	320.01±2.98
REM	95.12±4.09	98.75±5.07	96.93±4.24	99.34±3.22	99.03±2.55	99.18±2.58
RSL	99.42±9.37	99.08±9.19	99.25±8.81	104.13±5.21	99.72±4.40	101.92±4.28

3.2 *Heritability of spectral composition of EEG in REM and NREM sleep*

3.2.1 *Rapid eye movement sleep*

3.2.1.1 *Genetic variance analysis and intraclass correlation coefficients*

The criterion of normal distribution was not fulfilled for many of the EEG frequency bins. Therefore all spectral data were log-transformed prior to analysis. Genetic variance analysis (GVA) was not applicable for 7 frequency bins (1 Hz, 16–21 Hz) nor for β1 frequency band since sample means of averaged over-pairs measurements revealed significant differences between the twin samples.

The results of GVA and intraclass correlation coefficients (ICC) with respect to EEG frequency bands are shown in Table 3.2. GVA results with respect to EEG frequency

bins are presented in Table 3.3 and ICC results are illustrated in Figure 3.1. The genetic influence was identified for all remaining frequency bins (2–15 Hz, 22–45 Hz) and bands (δ band to high σ band, β2 band to φ band). MANCOVA analysis showed that sex, as a covariate, had a significant effect on spectral power values. Female subjects had significantly higher EEG power in δ, θ, β2 and φ bands (1–7 Hz and 27–45 Hz bins).

Table 3.2: Genetic variance analysis and intraclass correlation coefficients on frequency bands in REM sleep. Results of genetic variance analysis, type of estimate applied (GCT: combined among- and within-twin pair component estimate, GWT: within-pair estimate) and intraclass correlation coefficients (ICCs). REM: rapid eye movement, ICC MZ: ICCs of monozygotic (MZ) twins, ICC DZ: ICCs of dizygotic (DZ) twins, ICC MZ cn: ICCs of consecutive nights for each subject in MZ group, ICC DZ cn: ICCs of consecutive nights for each subject in DZ group. ICC results include: original sample ICC (upper percentile of bootstrapped data, median of bootstrapped data).

* Analysis of variance not applicable (significant differences between the means in DZ and MZ twin set).

Variable	*p*	GWT *vs.* GCT	ICC MZ	ICC DZ	ICC MZ cn	ICC DZ cn
δ	.0008	GCT	0.92(0.44, 0.13)	0.27(0.67, 0.19)	0.89(0.31, 0.08)	0.87(0.45, 0.12)
θ	.0001	GWT	0.93(0.41, 0.12)	0.51(0.63, 0.18)	0.92(0.31, 0.08)	0.90(0.46, 0.12)
α	<.0001	GWT	0.91(0.46, 0.12)	0.40(0.68, 0.19)	0.95(0.33, 0.07)	0.95(0.43, 0.12)
σ	.0001	GWT	0.89(0.43, 0.12)	0.45(0.64, 0.18)	0.91(0.32, 0.08)	0.92(0.46, 0.11)
α/σ	.0002	GWT	0.90(0.45, 0.12)	0.52(0.66, 0.18)	0.94(0.34, 0.08)	0.95(0.42, 0.12)
low σ	<.0001	GWT	0.89(0.47, 0.12)	0.41(0.63, 0.19)	0.92(0.32, 0.08)	0.93(0.45, 0.11)
high σ	.0004	GWT	0.89(0.43, 0.11)	0.53(0.63, 0.18)	0.90(0.31, 0.08)	0.92(0.46, 0.11)
β1*	-	-	0.89(0.42, 0.11)	0.41(0.65, 0.16)	0.95(0.31, 0.08)	0.97(0.58, 0.08)
β2	.0008	GWT	0.92(0.43, 0.12)	0.62(0.68, 0.18)	0.97(0.30, 0.08)	0.96(0.56, 0.11)
φ	<.0001	GWT	0.92(0.43, 0.13)	0.40(0.62, 0.19)	0.94(0.32, 0.08)	0.87(0.49, 0.12)

Table 3.3: Genetic variance analysis on 1-Hz frequency bins in REM sleep. Results of genetic variance analysis and type of estimate applied (GCT: combined among- and within-twin pair component estimate, GWT: within-pair estimate). REM: rapid eye movement.

* Analysis of variance not applicable (significant differences between the means in monozygotic and dizygotic twins).

Variable	*p*	GWT *vs.* GCT
1 Hz*	-	-
2 Hz	.0012	GCT
3 Hz	.0012	GCT
4 Hz	.0013	GCT
5 Hz	.0006	GWT
6 Hz	.0009	GWT
7 Hz	.0055	GCT
8 Hz	.0015	GCT
9 Hz	<.0001	GWT
10 Hz	<.0001	GWT
11 Hz	.0002	GWT
12 Hz	.0001	GWT
13 Hz	<.0001	GWT
14 Hz	.0002	GWT
15 Hz	.0007	GWT
16 Hz*	-	-
17 Hz*	-	-
18 Hz*	-	-
19 Hz*	-	-
20 Hz*	-	-
21 Hz*	-	-
22 Hz	<.0001	GWT
23 Hz	<.0001	GWT
24 Hz	.0001	GWT
25 Hz	.0003	GWT
26 Hz	.0004	GWT
27 Hz	.0004	GWT
28 Hz	.0007	GWT
29 Hz	.0008	GWT
30 Hz	.0018	GWT
31 Hz	.0015	GWT
32 Hz	.0008	GWT
33 Hz	<.0001	GWT
34 Hz	<.0001	GWT
35 Hz	<.0001	GWT
36 Hz	<.0001	GWT
37 Hz	.0003	GWT
38 Hz	.0045	GCT
39 Hz	.0039	GCT
40 Hz	<.0001	GWT
41 Hz	<.0001	GWT
42 Hz	.0002	GWT
43 Hz	<.0001	GWT
44 Hz	.0001	GWT
45 Hz	.0002	GWT

The mean ICC for all EEG frequency bins was 0.91 in the MZ twins and 0.45 in the DZ twins. However, the mean ICCs for night-to-night stability were comparable (0.94 in the MZ group and 0.92 in the DZ group). ICC values classified according to Landis and Koch (1977) for each bin throughout the whole spectrum for MZ twins as well as night-to-night stability in both MZ and DZ groups were *almost perfect*. ICC results for DZ twins similarity (Figure 3.1D) were irregular throughout frequency spectrum, which was influenced by the smaller sample size. Within-pair similarity was, according to Landis and Koch (1977), at most *substantial* (β2 band and four bins: 31–34 Hz) and the significance threshold (p=0.01) was crossed for the two bins (31–32 Hz). In contrast, consecutive night stability within DZ set was *almost perfect* for all frequency bins. Therefore, it is unlikely that low similarity in DZ twins was caused by poor quality sleep recordings.

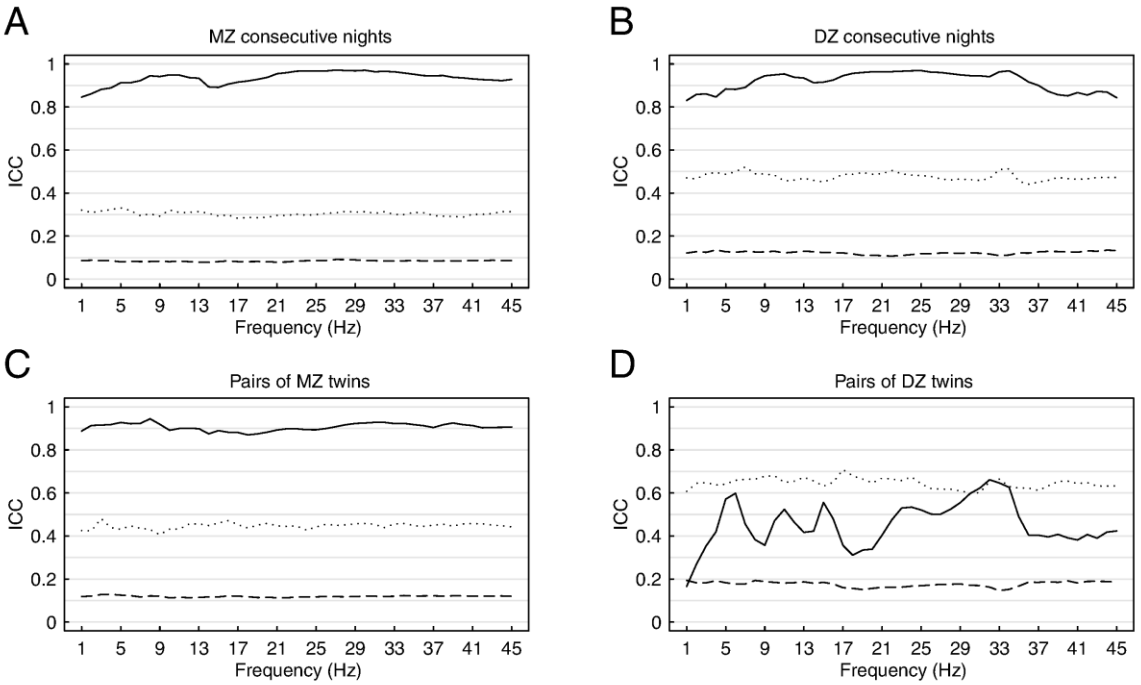

Figure 3.1: Intraclass correlation coefficients (ICCs) of rapid eye movement (REM) sleep frequency bins. On each plot solid line represents the observed real data, dotted line represents the upper percentile of bootstrapped values and dashed line represents the median of bootstrapped values. (**A**) consecutive nights of each subject in monozygotic (MZ) set (n=64); (**B**) consecutive nights of each subject in dizygotic (DZ) set (n=28); (**C**) pairs of MZ twins (each subject represented by a two nights mean, n=32); (**D**) pairs of DZ twins (each subject represented by a two nights mean, n=14). On the average, the upper percentile and the median of bootstrapped values differ between groups, which is the outcome of different sample sizes.

3.2.1.2 *Cluster analysis*

Figure 3.2 illustrates the distribution of Fisher‘s z transformed correlation values between power spectra within different groups. The mean of Fisher z transformed correlation values was 4.09 ± 0.29 (mean ± SD) between consecutive nights, 3.94 ± 0.35 between MZ twins, 3.10 ± 0.42 between DZ twins and 2.77 ± 0.39 between unrelated subjects. Pairwise comparisons of similarity distributions between these groups revealed only marginal differences between intra-individual and MZ twins similarity (p=.0821, Wilcoxon rank-sum test). The means of all other groups were significantly different when compared pairwise (p=.0015 when comparing DZ twins with inter-individual similarity and p<.0001 for all other comparisons).

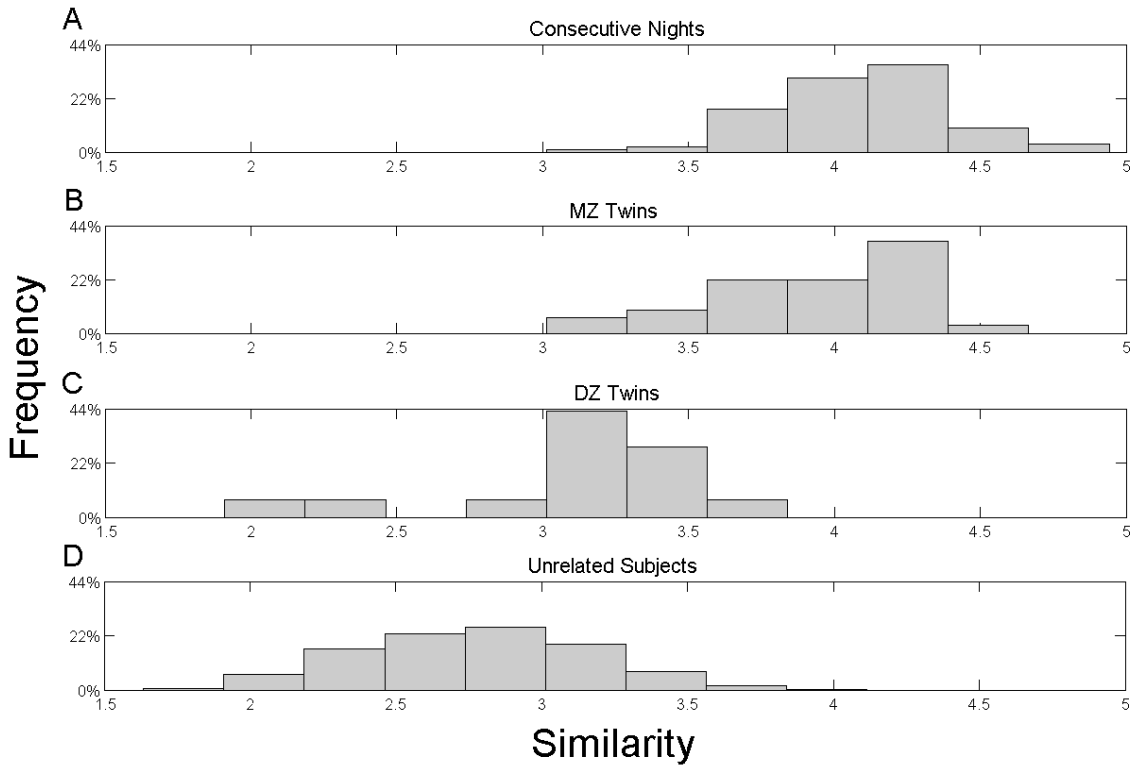

Figure 3.2: Distribution of Fisher's z transformed (*z*) Pearson's correlations for power spectra in rapid eye movement (REM) sleep. Each power spectrum was a 178 feature vector (0.75–45 Hz, 0.25 Hz bins). (**A**) Consecutive nights of each subject (n=92); (**B**) pairs of monozygotic (MZ) twins (each subject represented by two nights mean, n=32); (**C**) pairs of dizygotic (DZ) twins (each subject represented by a two nights mean, n=14); (**D**) unrelated subjects (n=16560). If there is no similarity *z*=0; if there is perfect similarity *z*=infinity.

Hierarchical clustering analysis was performed on mean EEG spectra measured from 2 recording nights as well as on each night represented separately. In the case when each night was treated separately, it was assumed that the two nights for the same subject clustered, if the distance between them was closer than to any unrelated subject. It was assumed that a twin pair clustered, if the distance between twins for any combination of their nights was closer than to any unrelated subject. Analysis of the mean spectra of two nights revealed that 27 of 32 twin pairs clustered within MZ set (Figure 3.3), whereas 4 of 14 twin pairs clustered within DZ set. Figure 3.4 illustrates the power spectra of the 2 most dissimilar twin pairs (highest correlation distance) in the MZ set (Figure 3.4 A and C) and the 2 most dissimilar twin pairs in

the DZ set (Figure 3.4B and D). Clustering performed on separated nights showed similar results. The same pairs clustered within the MZ set and one additional pair clustered within DZ set (Figure 3.5). With respect to consecutive nights, 60 of 64 subjects clustered within MZ set and 27 of 28 within DZ set.

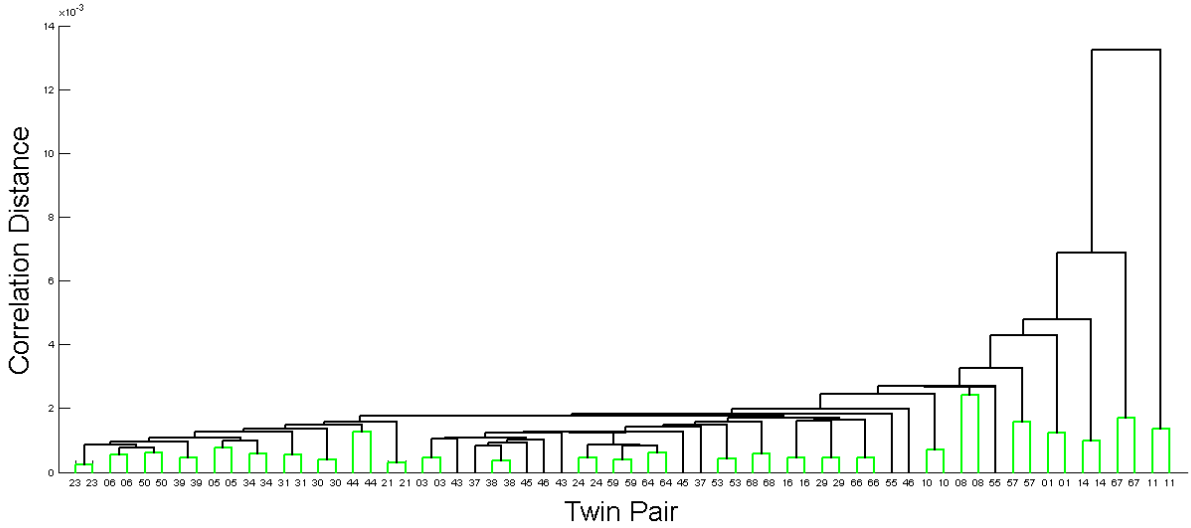

Figure 3.3: Dendrogram of cluster analysis based on distances between power spectra for rapid eye movement (REM) sleep in monozygotic (MZ) twins. Each subject is represented by a two night mean power spectrum. Each power spectrum was a 178 feature vector (0.75–45 Hz). Distance metric was one minus Pearson's correlation between vectors. Subjects with the same number represent the same MZ pair on *x* axis, distance between clusters is on *y* axis. Green clusters depict MZ pairs which clustered together.

In order to investigate whether spectrum at higher frequencies yields any additional information, the clustering experiment was repeated with separation between low and high frequencies. The increase of data size makes the clustering procedure more demanding (there is a higher probability to have a similar spectrum of unrelated subjects by chance). Therefore the analysis was performed on all 184 nights from combined MZ and DZ set. Cluster analysis performed on 0.75–45 Hz frequencies, revealed that 89.1% of consecutive nights, 81.3% of MZ pairs and 14.3% of DZ pairs clustered. When frequencies were limited to 20 Hz only 73.9% of consecutive nights

clustered. The percentage of MZ and DZ pairs which clustered did not change, although groups of MZ pairs which failed to cluster were not the same.

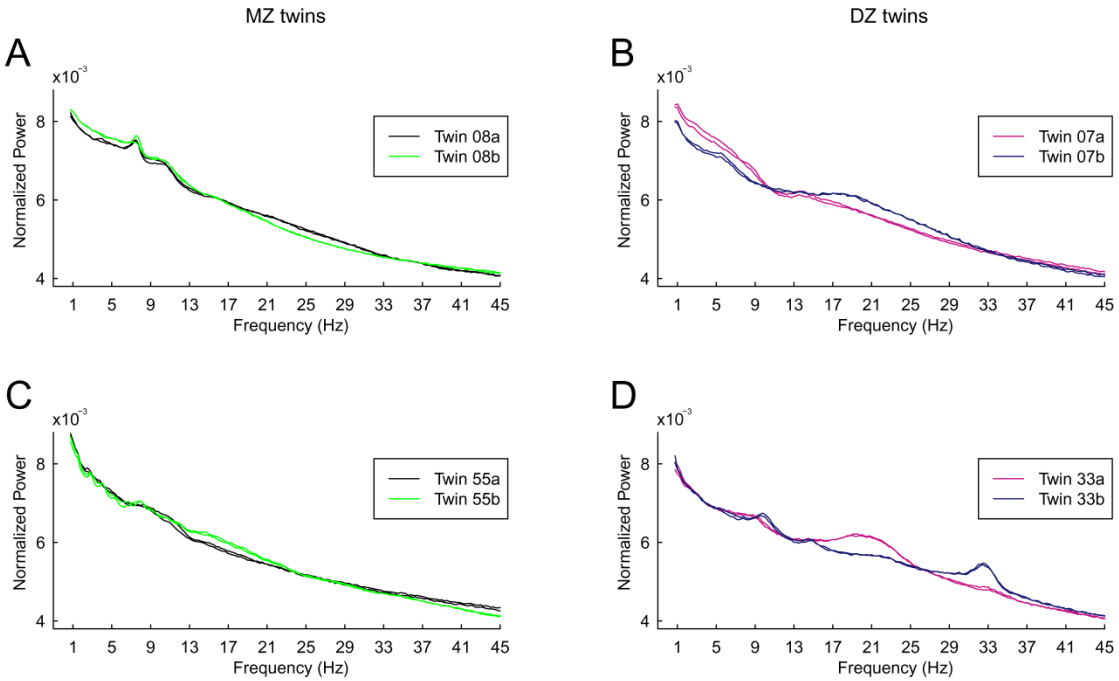

Figure 3.4: Logarithm transformed and normalized power spectra for rapid eye movement (REM) sleep of the 2 most dissimilar (according to Pearson's correlation between power spectra) monozygotic (MZ) twin pairs (**A**, **C**) and the 2 most dissimilar dizygotic (DZ) twin pairs (**B**, **D**). Consecutive nights of all presented twins clustered correctly. Each plot consists of 4 power spectra from one twin pair. 2 nights in one color from the first twin and 2 nights in different color from the second twin.

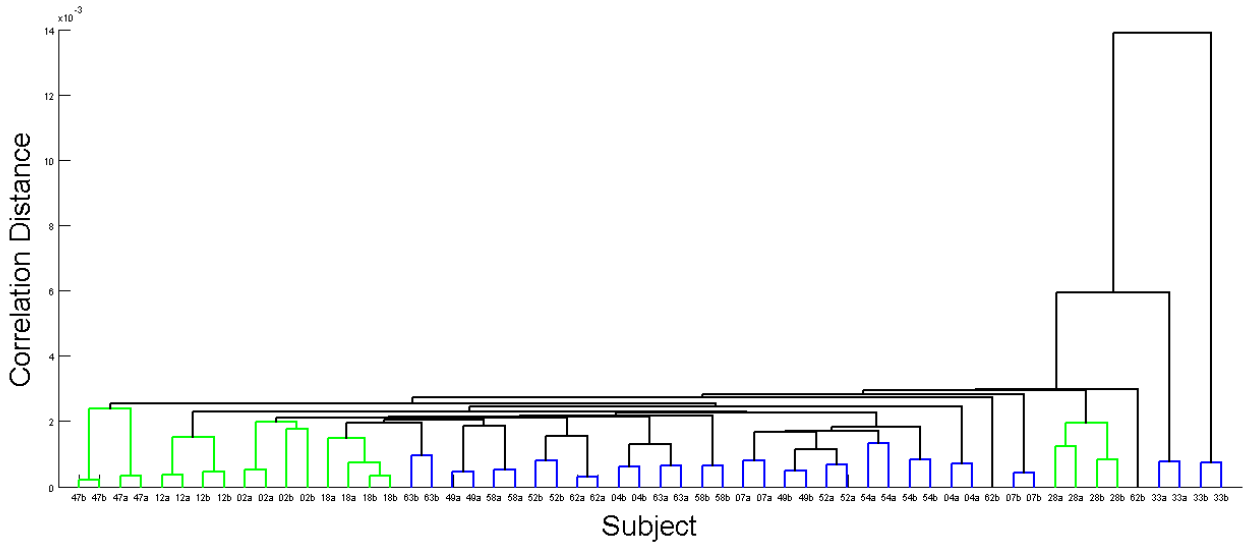

Figure 3.5: Dendrogram of cluster analysis based on distances between power spectra for rapid eye movement (REM) sleep in dizygotic (DZ) twins. Each subject is represented by two separate nights. Each power spectrum was a 178 feature vector (0.75–45 Hz). Distance metric was one minus Pearson's correlation between vectors. The subjects IDs consist of a number (defines DZ pair) and a character (defines a twin within the pair). The subjects IDs are on *x* axis, the distance between clusters is on the *y* axis. Blue clusters depict those subjects whose consecutive nights clustered together but not with related DZ twin. Green clusters depict DZ pairs which clustered together.

3.2.2 *Non-rapid eye movement sleep*

3.2.2.1 *Cluster analysis*

The investigated range of power spectrum in NREM sleep was restricted to a range of 0.75–20 Hz due to the presence of muscle activity in some of the EEG recordings, which influenced EEG spectral power at high frequencies.

Figure 3.6 illustrates the distribution of Fisher‘s z transformed correlation values between power spectra within different groups. Mean of Fisher z transformed correlation values was 3.87 ± 0.42 (mean ± SD) between consecutive nights, 3.62 ± 0.41 between MZ twins, 2.83 ± 0.34 between DZ twins and 2.31 ± 0.34 between unrelated subjects. Means of all groups were significantly different when compared

pairwise (p=.0133 when comparing MZ twins with intra-individual similarity and p<.0001 for all other comparisons, Wilcoxon rank-sum test).

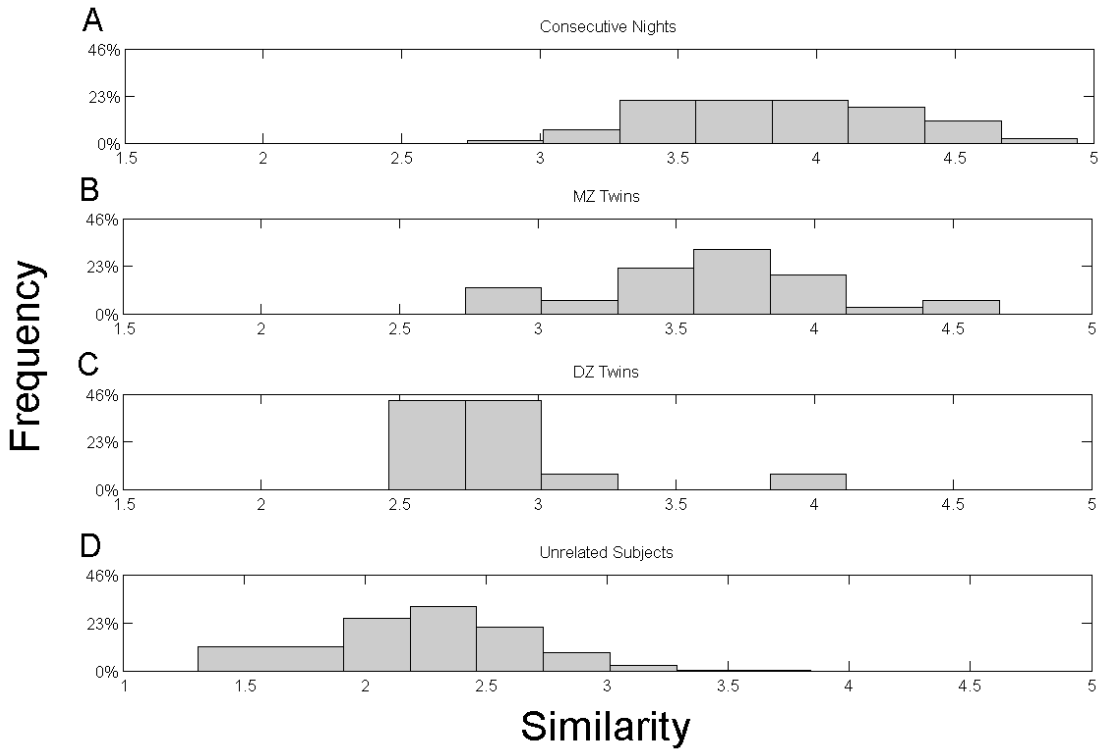

Figure 3.6: Distribution of Fisher's z transformed (z) Pearson's correlations for power spectra in non-rapid eye movement (NREM) sleep. Each power spectrum was a 78 feature vector (0.75–20 Hz, 0.25 Hz bins). (**A**) consecutive nights of each subject (n=92); (**B**) pairs of monozygotic (MZ) twins (each subject represented by two nights mean, n=32); (**C**) pairs of dizygotic (DZ) twins (each subject represented by a two nights mean, n=14); (**D**) unrelated subjects (n=16560). If there is no similarity z=0; if there is perfect similarity z=infinity.

Analysis of mean spectra of two nights revealed that 30 of 32 twin pairs clustered within the MZ set (Figure 3.7), whereas 1 of 14 twin pairs clustered within the DZ set. Figures 3.9F and 3.10B illustrate NREM power spectra of the 2 most dissimilar twin pairs (highest distance according to correlation metric) in MZ set, whereas NREM power spectra of 2 MZ twin pairs which failed to cluster are illustrated on Figure 3.10D and F. The results from the clustering experiment performed on the DZ set with separated nights are depicted in Figure 3.8. There was no difference in

clustering when it was performed on separated nights, the same pairs of twins clustered in the MZ as well as the DZ set. With respect to consecutive nights, 61 of 64 subjects clustered within the MZ set and 26 of 28 within the DZ set. The analysis performed on all 184 nights from combined MZ and DZ sets for separated nights revealed, that 90.2% of consecutive nights, 93.7% of MZ pairs and 14.3% of DZ pairs clustered.

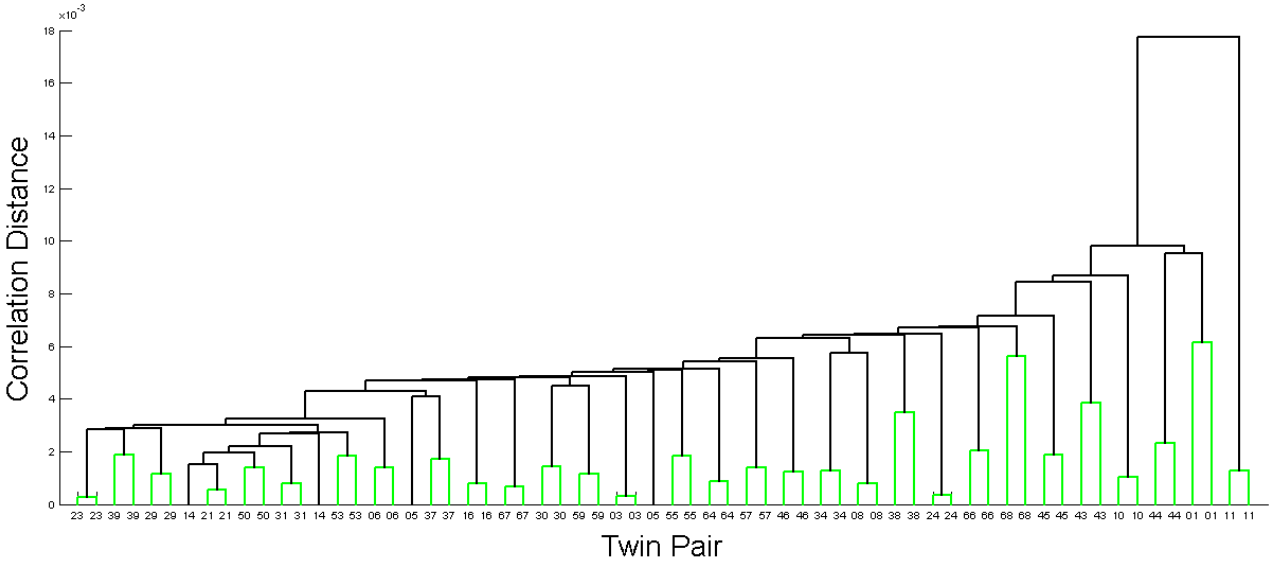

Figure 3.7: Dendrogram of cluster analysis based on distances between power spectra for non-rapid eye movement (NREM) sleep in monozygotic (MZ) twins. Each subject is represented by the two night mean power spectrum. Each power spectrum was a 78 feature vector (0.75–20 Hz). Distance metric was one minus Pearson's correlation between vectors. Subjects with the same number represent the same MZ pair on *x* axis, distance between clusters is on *y* axis. Green clusters depict MZ pairs which clustered together.

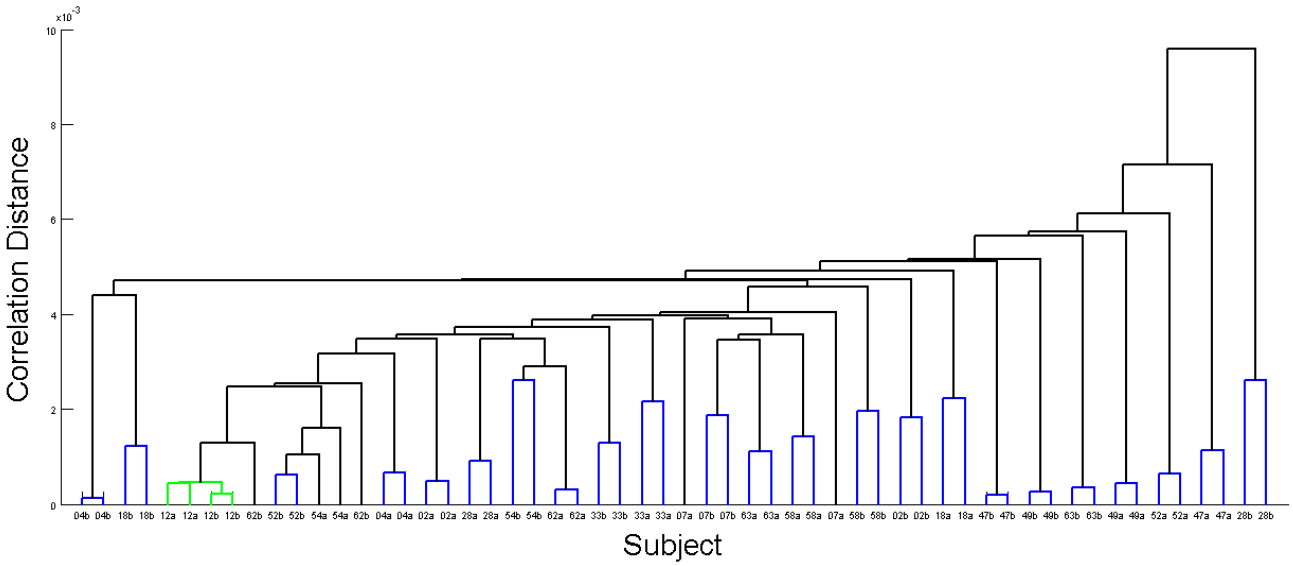

Figure 3.8: Dendrogram of cluster analysis based on distances between power spectra for non-rapid eye movement (NREM) sleep in dizygotic (DZ) twins. Each subject is represented by two separate nights. Each power spectrum was a 78 feature vector (0.75–20 Hz). Distance metric was one minus Pearson's correlation between vectors. The subject ID consists of a number (defines DZ pair) and a character (defines a twin within the pair). Subjects IDs are on the x axis; distance between clusters is on the y axis. Blue clusters depict those subjects whose consecutive nights clustered together but not with related DZ twin. Green clusters depict DZ pairs which clustered together.

3.2.3 *REM and NREM sleep: how spectral composition differences translate between sleep phases?*

Figures 3.9 and 3.10 illustrate power spectra of the 2 twin pairs which were the most dissimilar according to the Pearson's correlation metric in REM sleep (Figure 3.9A and C), the 2 most dissimilar twin pairs in NREM sleep (Figure 3.9F and 3.10B) as well as the only two pairs which did not cluster in NREM sleep (Figure 3.10D and F). In order to compare whether differences in spectral composition between MZ twins are conserved in both NREM and REM sleep, the power spectra for each twin pair are illustrated for both REM and NREM sleep. All these pairs present good night-to-night stability and constant, apparent differences in power spectrum between the twins. Twins which were classified as the most dissimilar in REM sleep (Figure 3.9A

and C) have the most prominent spectral differences in high sigma and beta range (13 to 30 Hz) background EEG activity, whereas differences within the most dissimilar twin pairs in NREM sleep power spectra are mostly due to variability in the frequency range where sleep spindles are active (10 to 16 Hz). Differences between power spectra at 10 to 16 Hz frequency during NREM sleep, suggest that the characteristics of sleep spindles could differ between the twins. Indeed, when comparing NREM power spectra within the most dissimilar twin pairs (Figure 3.9F and 3.10B, D, F) it is visible that peaks in the spindle activity range (10 to 16 Hz) differ between the twins, so the sleep spindle peak frequencies within twin pairs may be different.

All differences between the twin pairs in the background activity (occurs in all twin pairs presented in Figure 3.9, marked with a green color) seem to be preserved for both, REM as well as NREM sleep. However, differences in peak frequency and strength (twin pairs classified as dissimilar in NREM sleep, all these peaks exist in spindle activity) were preserved in both sleep phases only if an increased activity in a given frequency existed in both, REM and NREM sleep. Power spectra of twin pair 14, illustrated in Figure 3.10C and D, are an example where the faster peak in spindle range during NREM sleep in twin 14b was also visible and also faster during REM sleep.

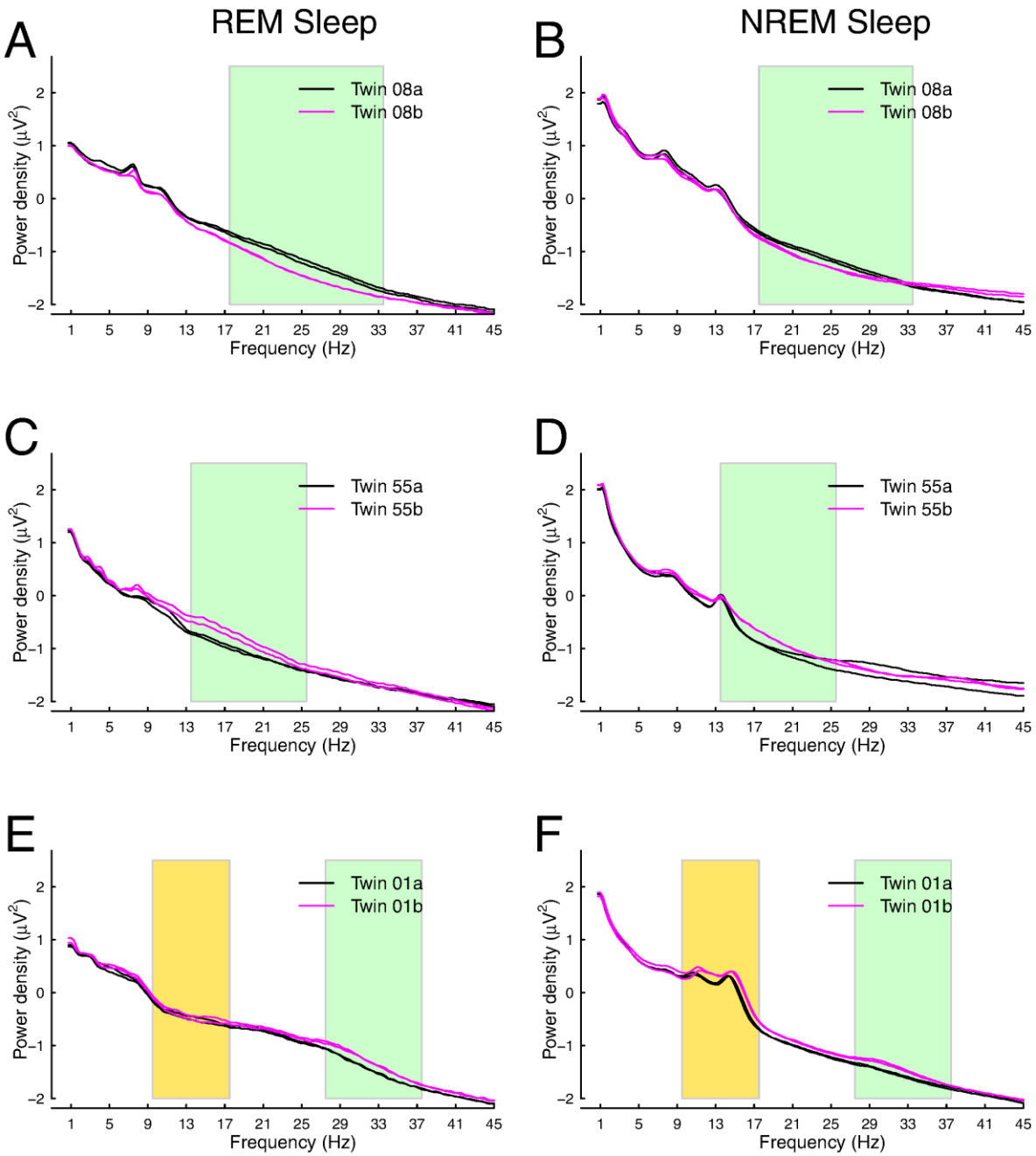

Figure 3.9: Log-10 transformed power spectra for rapid eye movement (REM) sleep and non-rapid eye movement (NREM) sleep. Two most dissimilar (according to Pearson's correlation between power spectra) monozygotic (MZ) twin pairs considering REM sleep power spectra (**A**, **C**) as well as their NREM sleep power spectra (**B**, **D**) and the most dissimilar monozygotic (MZ) twin pair considering NREM sleep power spectrum (**F**) together with REM sleep power spectrum of this pair (**E**). Consecutive nights of all presented twins clustered correctly. Each plot consists of 4 power spectra from one twin pair. 2 nights in one color from the first twin and 2 nights in different color from the second twin. Orange color background marks differences between the twins visible only in one sleep phase. Green color background marks differences between the twins visible in both, REM and NREM sleep.

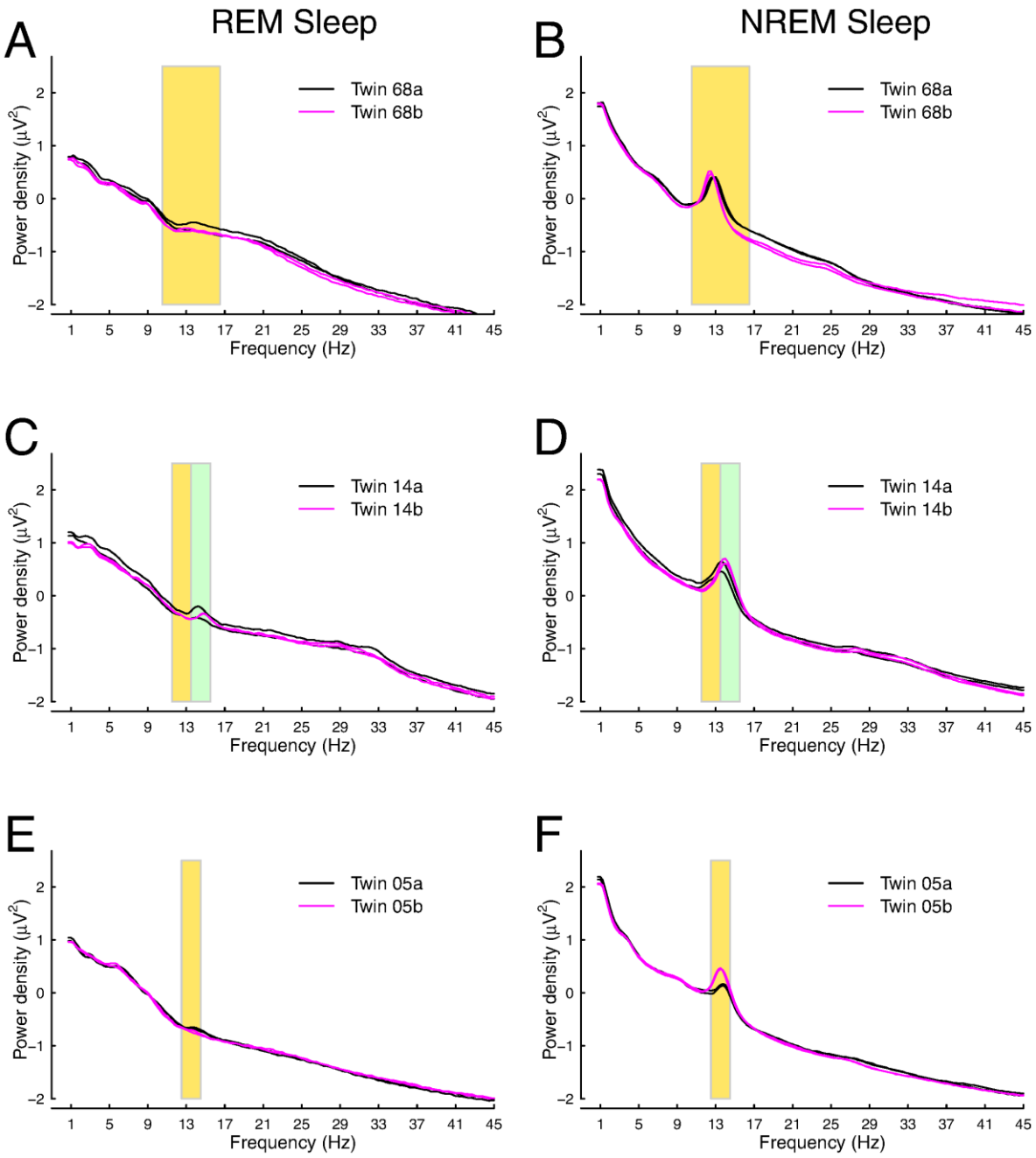

Figure 3.10: Log-10 transformed power spectra for rapid eye movement (REM) sleep and non-rapid eye movement (NREM) sleep. Second most dissimilar (according to Pearson's correlation between power spectra) monozygotic (MZ) twin pair considering NREM sleep power spectrum (**B**) together with REM sleep power spectrum of this pair (**A**) and two MZ twin pairs, which failed to cluster in NREM sleep (**D**, **F**) as well as their REM sleep power spectra (**C**, **E**). Consecutive nights of all presented twins clustered correctly. Each plot consists of 4 power spectra from one twin pair. 2 nights in one color from the first twin and 2 nights in different color from the second twin. Orange color background marks differences between the twins visible only in one sleep phase. Green color background marks differences between the twins visible in both, REM and NREM sleep.

3.2.4 *Summary of background EEG analysis*

A substantial genetic influence on the spectral composition of REM sleep was observed. Significant genetic variance in spectral power was observed in δ to high σ, and β2 to φ frequencies. All estimates of genetic variance in spectral power for derivation C3A2 were similar when the analysis was repeated for derivation C4A1 (see Supplement). The comparison of REM EEG spectral power between matched MZ and DZ twins confirmed the findings in the whole twin sample (see Supplement). In addition, significant genetic influence was found for the remaining 7 frequency bins (1 Hz, 16–21 Hz) and the β1 frequency band of the REM sleep EEG. ICC results revealed high night-to-night stability of REM spectral composition as well as within-pair similarities for MZ twins (mean ICCs for frequency bins night-to-night stability: 0.94 whereas 0.91 for MZ twins).

Significant differences between the twin groups were also observed in within-pair similarity of REM and NREM EEG spectra morphology. Slightly better clustering results were observed in NREM sleep, although performed in a narrower frequency band (REM: 0.75–45 Hz, NREM: 0.75–20 Hz). MZ twins were very close in similarity to consecutive night results in both REM and NREM sleep. MZ pairs who did not cluster in REM and NREM sleep do not overlap. In REM sleep, the mean difference between MZ twins did not differ significantly from the mean difference between consecutive nights. If prominent differences in spectral power were visible in MZ twins background EEG activity, they were preserved in REM as well as in NREM sleep.

3.3 *Sleep spindle analysis*

3.3.1 *Automatic detection of sleep spindles: description of algorithm*

3.3.1.1 *Preprocessing before spindle detection*

The algorithm analyzes the properties of the raw signal and rejects periods of signal with very high muscle contamination as well as segments dominated by alpha activity. Alpha activity is present in the EEG signal mostly during wake when the eyes are closed, but can also be present in EEG during shallow sleep, after arousals and during REM sleep. The shape of alpha waves is very similar to sleep spindles. They consist of waxing and waning bursts of activity in the range of 8–12 Hz (Figure 3.11) and can lead to false spindle detection. The problem of separating alpha waves is important especially when analyzing EEG recordings from naps, where long periods of shallow sleep are present.

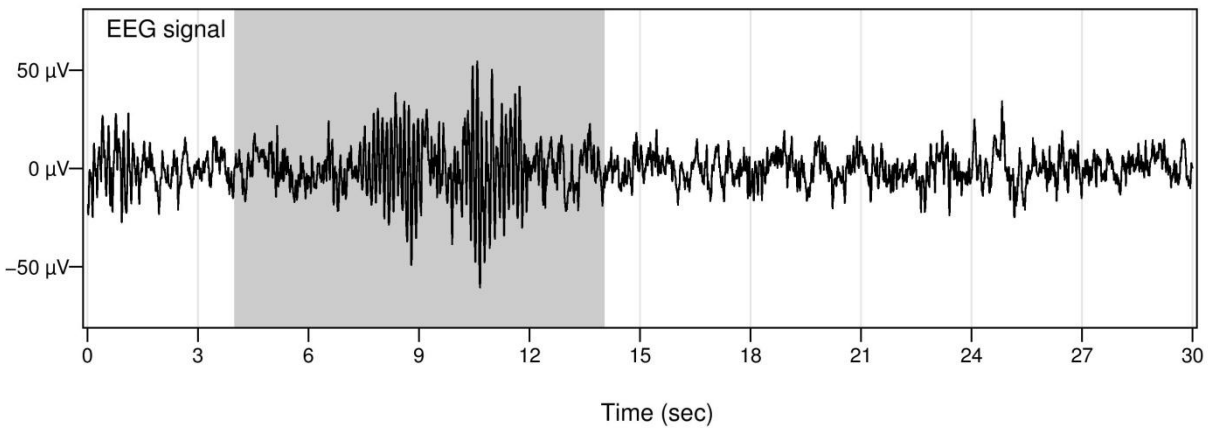

Figure 3.11: Alpha activity in derivation C3A2. Alpha activity is present in the gray area of the figure. Waxing and waning shape and overlapping frequency range makes it difficult to distinguish them from sleep spindles.

Artifact rejection: In order to identify fragments with high frequency muscle artifacts, the EEG signal was band-pass filtered (-3 dB at 19.8 and 45.5 Hz). The standard deviation of the signal was computed over a 1 sec sliding window (step: 0.5 sec) and if it exceeded 5.75 μV, a window of 6 sec (fragment in which the threshold was exceeded ± 2.5 sec) was excluded from spindle detection.

Rejection of segments with strong alpha frequency: In order to identify signal with dominant alpha frequencies, Fourier spectrum over a 5 sec sliding window (step: 1 sec) was analyzed. Mean signal power (MSP) was compared in an alpha frequency band (8–12 Hz), low frequency band (2–7 Hz) and sigma band (12–16 Hz). The low frequency band was chosen because the power in this range should be higher during deeper sleep, decreasing the chances of signal rejection, and the sigma band is the range where spindle activity is expected. The 5 sec window was excluded if the alpha activity was dominant:

$$MSP(alpha) / max[MSP(low\ band)\ MSP(sigma)] > 1.5$$

3.3.1.2 *Detection of sleep spindles*

A. Threshold setup: EEG signal amplitude can vary between subjects and channels. Reasons for this phenomenon can be of technical nature (movements during the measurement period influencing electrode placement, differences in electrode impedances and as a result in signal amplitudes) as well as physiological nature (with age, signal amplitude, including spindles, tends to decrease). Therefore the threshold for spindle detection is defined individually for each channel. In order to compute the threshold, only sleep epochs scored as stage 2 of sleep are considered. Only one stage of sleep is included in order to obtain signal

amplitude information from homogeneous source. Stage 2 was chosen as the best candidate since there are high amounts of it during each night.

EEG signal was band-pass filtered (-3 dB at 3.3 and 20.2 Hz). For every 0.25 sec of filtered signal, the root mean square (RMS) was computed. Two thresholds were defined for spindle detection: sigma activity (SA) and sigma peak (SP). SA was set as 3 times the median of all RMS values, while SP was set as 4.5 times the median of all RMS values.

B. Detection method: Spindle detection was performed using the continuous wavelet transform (CWT) with Morlet wavelet as a mother wavelet. The description of CWT as well as Morlet wavelet used in the analysis can be found in section 2.1.2. The scale of the wavelet used to analyze the sigma activity corresponded to the 12–16 Hz frequency range. A sleep spindle was identified, if the outcome of CWT exceeded SA by a period of, at least, half a second and SP at least once. The scheme of spindle detection is illustrated in Figure 3.12.

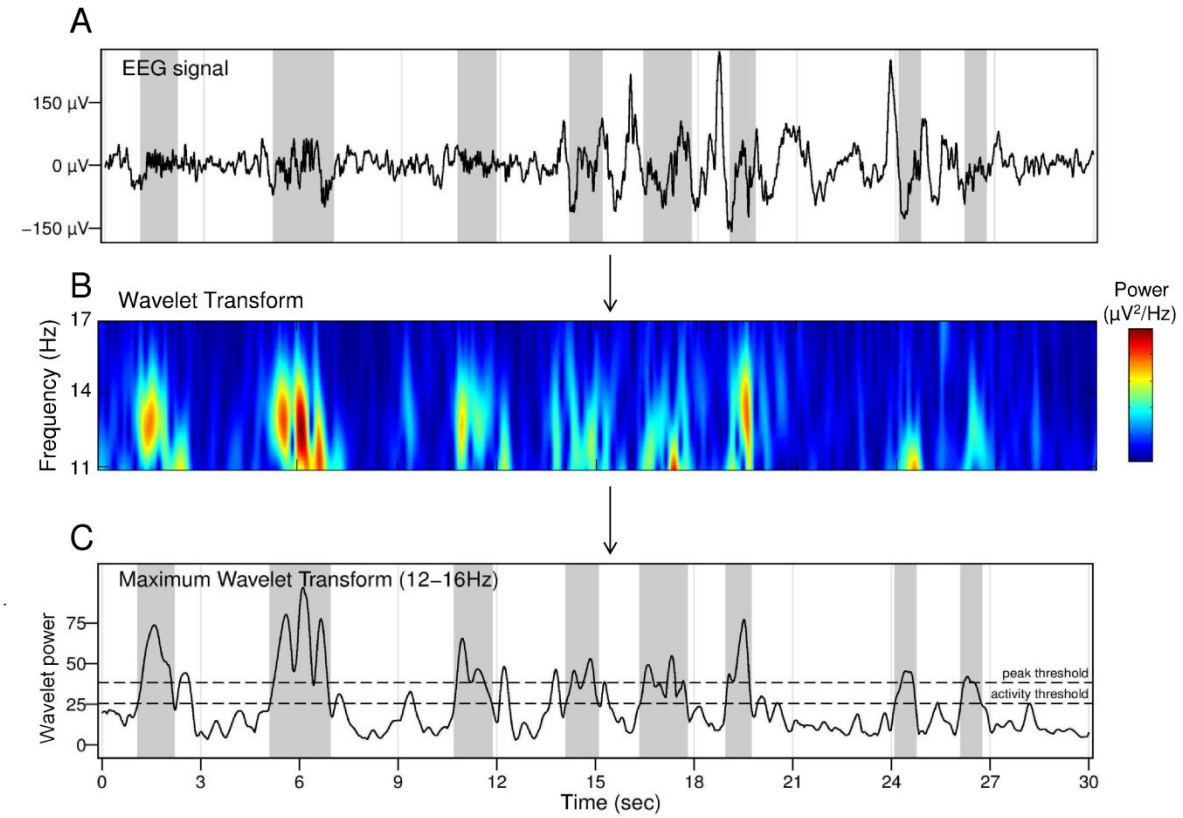

Figure 3.12: The scheme of spindle detection. (**A**) EEG signal with "typical" stage 2 activity (0 to 12 sec) as well as slow wave activity (12 to 27 sec). (**B**) The result of continuous wavelet transform in time and frequency domain. (**C**) Maximum values of wavelet transform in 12–16 Hz frequency range, which is compared with peak and activity thresholds computed before the detection for each EEG derivation separately. Gray areas are the areas where sleep spindles were detected. In this 30 sec epoch it is visible that algorithm detects spindles appropriately not only in the signal where spindle activity is dominant (0 to 12 sec), but also in fragments with strong slow wave activity (12 to 27 sec).

3.3.1.3 *Sleep spindle detector validation*

The wavelet algorithm was validated with data from an earlier study (Genzel *et al.*, in press). 18 naps from 10 subjects were randomly selected and the algorithm was compared with the SIESTA algorithm of Anderer *et al.* (2005) and with a human visual scorer. Figure 3.13 illustrates the number of sleep spindles detected in sleep stage 2 by each scorer. Considering the amount of detected sleep spindles, SIESTA algorithm and visual scorer comparisons revealed a Pearson's correlation of r=0.90. The comparison of detected spindle number between the wavelet detector and

SIESTA algorithm, revealed a correlation of *r*=0.97. Similarly, a comparison between wavelet detector and visual scorer revealed a correlation of *r*=0.92.

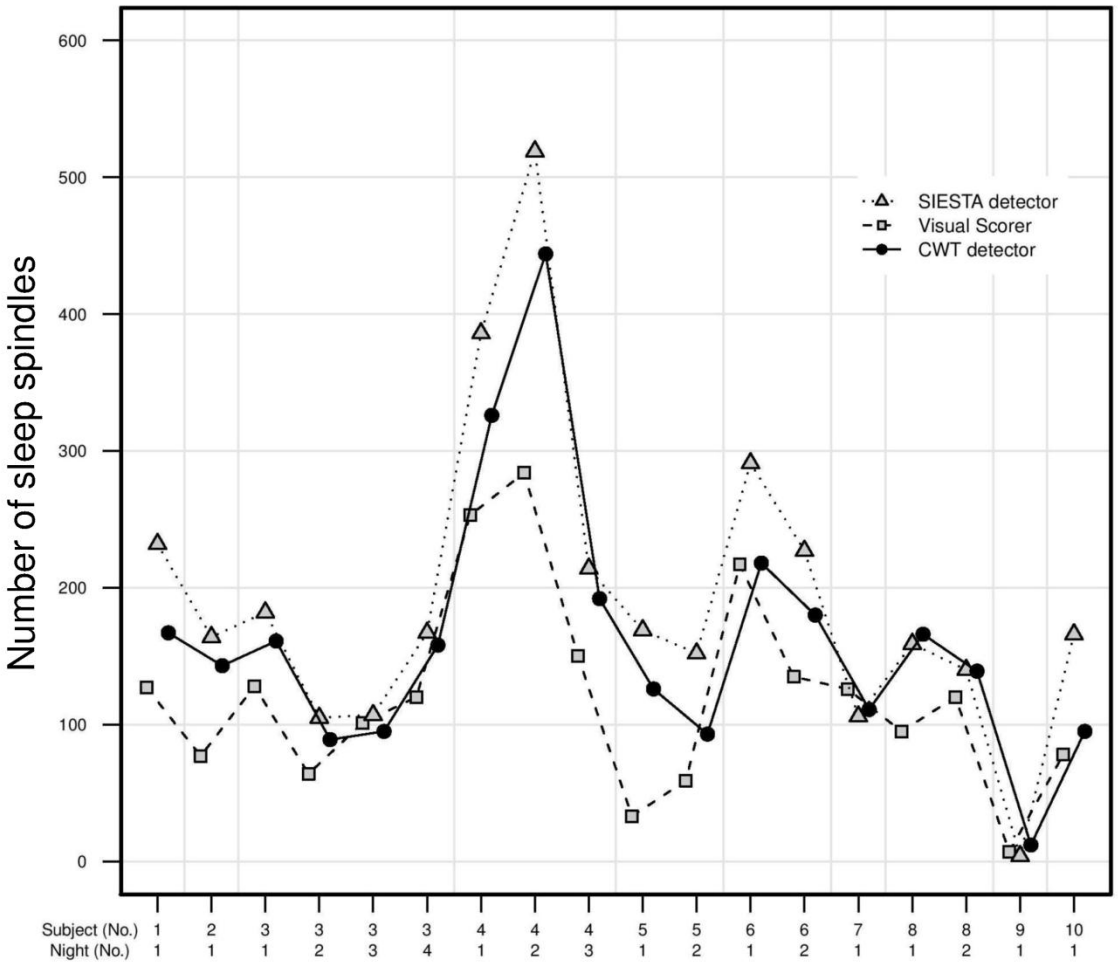

Figure 3.13: Numbers of sleep spindles in 18 nap EEG recordings detected by the new automatic algorithm called CWT detector, human visual scorer and SIESTA automatic spindle detector. Subject id and number of nap recording are presented on *x* axis. Number of detected spindles is presented on *y* axis.

In order to evaluate the agreement between the scorers in regards to the quantity of signal marked as a spindle event, the concordance measure was used. Concordance between two scorers is defined as the amount of overlapping signal recognized by both scorers as sleep spindles, multiplied by 2 and divided by the sum of all signal marked by each scorer as sleep spindles. Concordance differs between 0 (no agreement) and 1 (perfect agreement). Figure 3.14 illustrates the agreement between scorers regarding the concordance of detected sleep spindles in sleep

stage 2. The comparison of SIESTA algorithm to visual scorer revealed a mean concordance of 0.47. The comparison of wavelet detector to SIESTA algorithm revealed a mean concordance of 0.67. Similarly, the comparison between wavelet detector and visual scorer revealed a mean concordance of 0.55. Although the concordance results seem to be low, it should be noted that the validation set based on nap EEG recordings is a demanding one, since the sleep is shallower compared to regular night sleep, alpha activity is higher and sleep spindle activity is lower. A low number of spindles in the signal increase the significance of false positive discoveries in the outcome of concordance, even if there are only a few of them. A positive correlation is observed when comparing amounts of detected spindles in Figure 3.13 to concordance results in Figure 3.14. The more sleep spindles that were present during a nap, the higher the expected concordance was between the scorers. The most prominent example was the nap number 1 of subject number 9, where almost no spindles were found by any of the scorers and the outcome of concordance did not exceed 0.4 agreement for any combination of scorers.

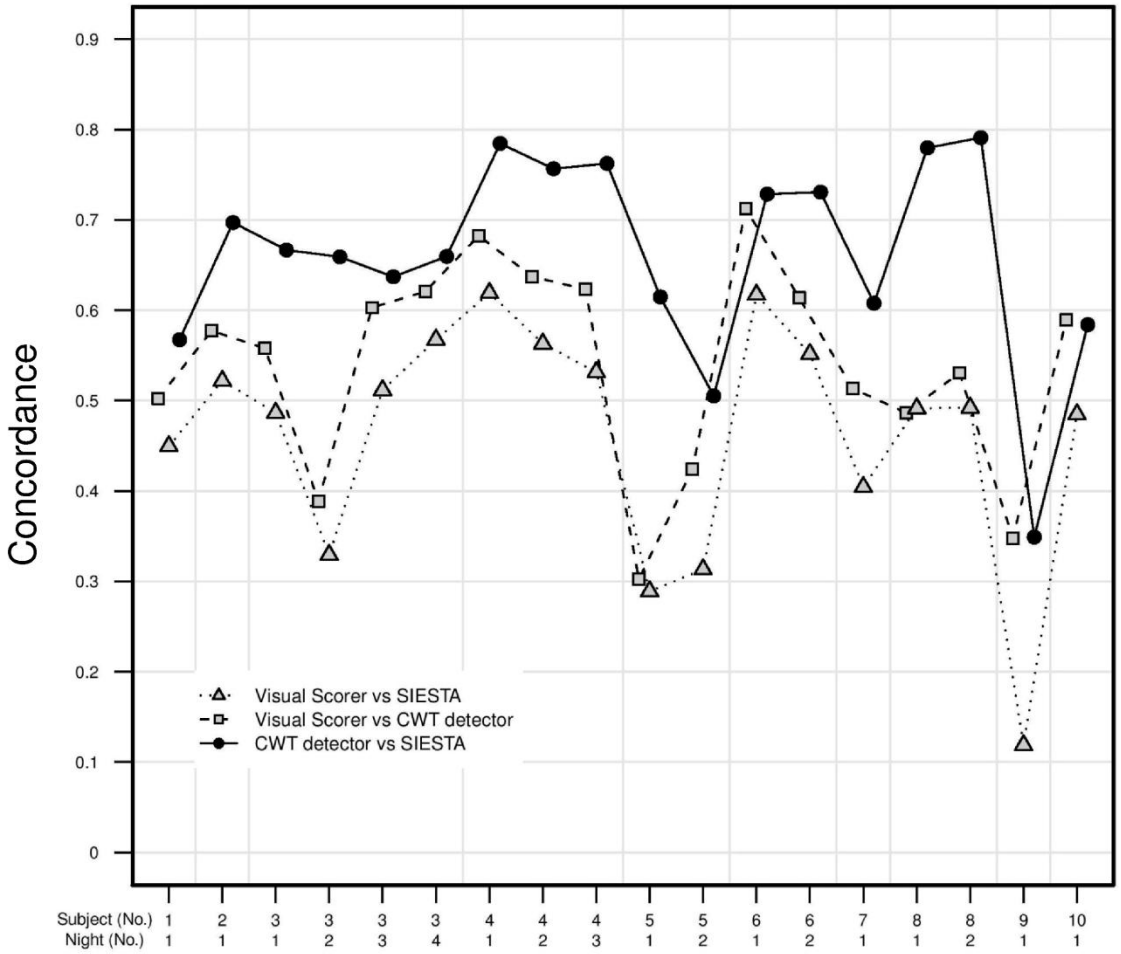

Figure 3.14: Agreement in sleep spindle detection between the new automatic algorithm called CWT detector, human visual scorer and SIESTA automatic spindle detector. Subject id and number of nap recording are presented on *x* axis. Concordance results are presented on *y* axis. Concordance between two scorers is defined as the amount of overlapping signal recognized by both scorers as sleep spindles, multiplied by 2 and divided by the sum of all signal marked by each scorer as sleep spindles. Concordance differs between 0 (no agreement) and 1 (perfect agreement).

3.3.1.4 *Algorithm extension: individual spindle frequency peak adjustment*

The frequency of sleep spindles varies between 10 and 16 Hz. When the separation between fast and slow spindles is of interest, it is done conventionally with a frequency threshold set around 13 Hz, which separates fast spindles from the slow ones. However, real frequency ranges of slow and fast spindles differ between individuals. Figure 3.15 illustrates NREM sleep power spectra of multiple subjects, which were computed using signal from frontal, central as well as parietal EEG derivations. Sleep spindle activity is visible in NREM sleep power spectra as power increases in the 10–16 Hz frequency range. Figures 3.15A and B show the power spectra with two distinct peaks in the band, which provide a clear distinction between slow and fast spindle frequency, which in this case were 11 Hz and 13 Hz, respectively. However, Figure 3.15D shows the power spectrum where the frequency of both slow and fast spindles was around 1 Hz faster. If there would be a constant threshold which separates slow spindles from fast ones at 13 Hz, slow spindle activity in subjects from Figures 3.15A and B would be overestimated and fast spindle activity would be underestimated. Therefore, more careful separation between slow and fast spindles for each EEG recording may lead to more precise evaluation of slow and fast spindle activity. To separate fast and slow spindles precisely, individual slow and fast spindle frequency peaks and ranges were localized for each subject prior to spindle detection. Slow and fast spindle frequencies were localized using the frequency amplitude spectrum computed for NREM sleep. The idea to use the amplitude spectrum for localization of slow and fast spindle frequency ranges was proposed by Bódizs *et al.* (2009) and will be described in greater detail in subsequent sections. For each EEG channel the authors computed the second derivative of NREM sleep amplitude spectrum in the 9–16 Hz range. Subsequently, second derivatives of all investigated EEG channels were averaged. In the resulting

vector, the two largest negative peaks were identified, which corresponded to two positive frequency peaks with the strongest curvatures in the amplitude spectrum. Zero-crossing points, encompassing the slower peak in the second derivative, were taken as the slow spindle range, whereas zero-crossing points, encompassing the faster peak, were taken as the fast spindle range. In the present work, this method was extended. In all subjects the fast spindle frequency peak is visible in parietal EEG channels, and in most subjects, the slow spindle peak is visible in frontal EEG channels. However, there are also problematic cases, such as presented in Figure 3.15C, in which the subject does not exhibit slow spindle frequency peak in any EEG derivation. In cases when unequivocal decision cannot be reached, slow and fast spindle ranges in Bódizs *et al.* (2009) were selected visually. The algorithm presented here took advantage of the fact that slow spindle activity is stronger in frontal EEG and fast spindle activity is stronger in parietal EEG. The parietal amplitude spectrum was compared with the frontal amplitude spectrum to localize the slow spindle frequency peak. The developed method was fully automated, and besides the information about slow and fast spindle frequency ranges, it returned the exact spindle frequency peaks.

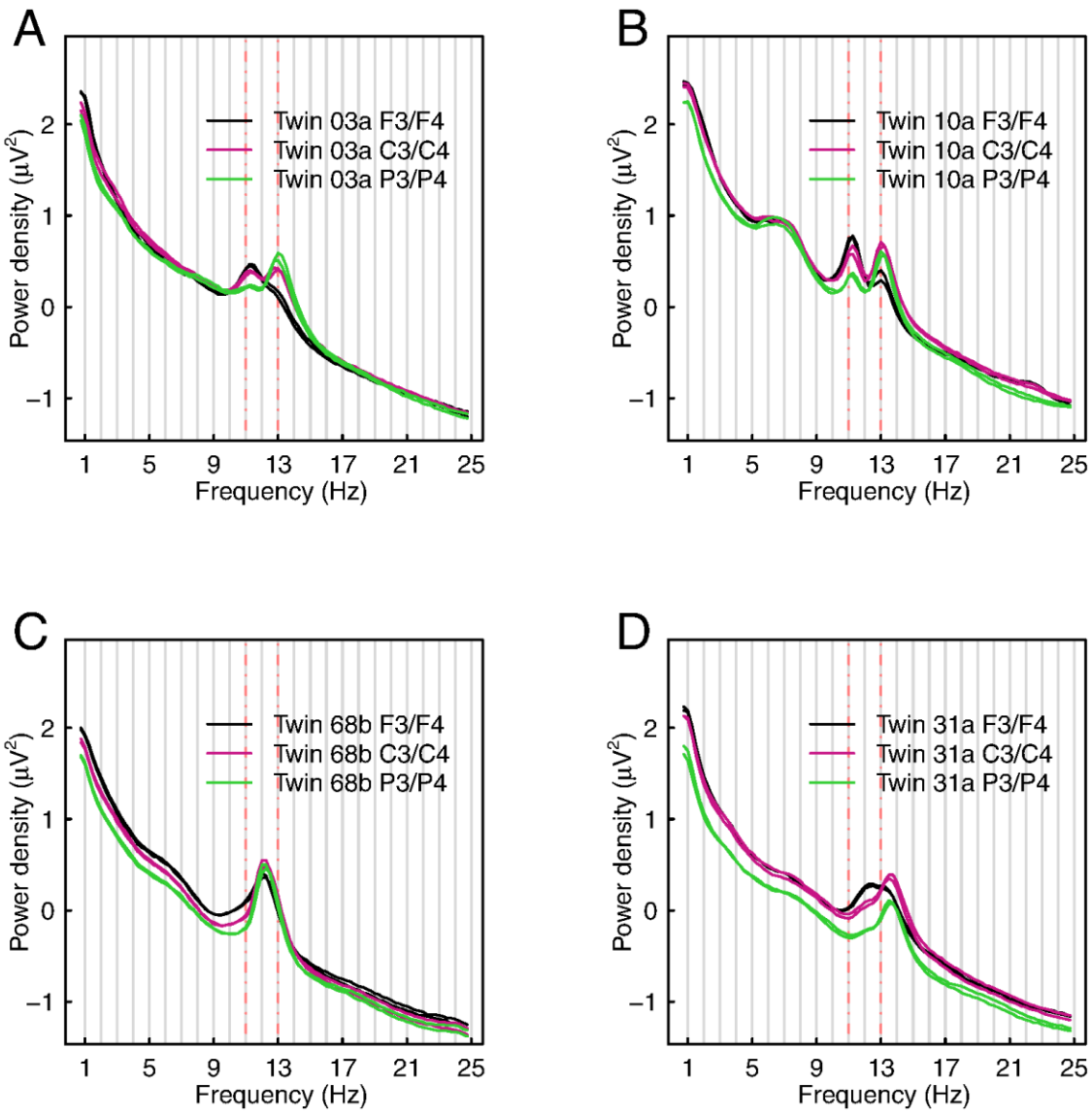

Figure 3.15: Log-10 transformed power spectra of multiple subjects showing diversity of possible slow and fast spindle frequency ranges as well as their distribution over the scalp. Each plot consists of six power spectra from one subject: two nights from the mean of frontal derivations are shown in black, two nights from the mean of central derivations are shown in magenta and two nights from the mean of parietal derivations are shown in green. EEG recordings from twin study were used, therefore subject id consists of a number (defines twin pair) and a character (defines a twin within the pair). Red dashed vertical lines in 11 and 13 Hz are placed to easier distinguish differences in spindle peaks between the subjects. (**A**, **B**) subjects with slow spindle frequency peak at 11 Hz and fast spindle frequency peak at 13 Hz; (**C**) subject with only one spindle frequency peak visible at 12 Hz; (**D**) subject with slow spindle frequency peak at 12 Hz and fast spindle frequency peak at 14 Hz.

3.3.1.4.1 *NREM sleep amplitude spectrum*

Amplitude spectrum in NREM sleep was computed for both frontal derivations (F3A2 and F4A1) and both parietal derivations (P3A2 and P4A1). EEG signal from each derivation was high-pass filtered (-3dB at 1.5 Hz) and Fast Fourier Transform was applied using a 4 seconds sliding window (1 sec shift). Fragments with artifacts were excluded prior to spectral analysis. Artifact detection was performed as described in section 3.3.1.1. Resulting amplitude spectra were used to investigate the 10–16 Hz frequency range. 10–16 Hz frequency range in the amplitude spectrum will be referred to as σR. For each channel (F3A2, F4A1, P3A2 and P4A1) σR was normalized (dividing σR values by the sum over σR) and the linear trend from σR was removed. In order to localize spindle activity, mean σR of both frontal amplitude spectra (σRF) as well as mean σR of both parietal amplitude spectra (σRP) were investigated.

3.3.1.4.2 *Spindle activity localization in amplitude spectrum*

Spindle activity localization was performed for σRF and σRP separately, but in the same manner. To localize spindle activity, the 2nd derivative of σR was computed (Dr2σR). The second derivative of the function measures its curvature. The stronger the curve, the higher is absolute 2nd derivative value. The sign of the 2nd derivative corresponds to the direction of the curve, in which a positive sign reflects an upward curve and a negative sign reflects a downward curve. Since the most prominent positive peaks in σR were of interest (local maxima of the σR with the strongest downwards curve), the algorithm focused on minima of Dr2σR.

The curve of a positive peak in σR must be prominent to avoid misclassification. Therefore, two thresholds were defined in order to control for sufficient curvature of peak candidates in σR. The curve of a positive peak in σR was considered to be

prominent if Dr2σR was lower than the threshold pC=-0.0005, and was considered sufficient if Dr2σR was lower than the threshold sC=pC*0.65. Threshold criteria were established on the basis of visual inspection of σR from multiple subjects. Following rules were applied to find a first spindle frequency peak in σR:

Abbreviations	
σR	10–16 Hz frequency range in the amplitude spectrum
Dr2σR	2nd derivative of σR
pC	the threshold defining prominent peak candidate
sC	the threshold defining sufficient peak candidate

Localization of activity peaks in σR

(Step 1) Select the frequency bin with the most negative value in Dr2σR. It is a peak candidate frequency bin called pkCn.

IF Dr2σR(pkCn) < pC

(Step 2) Investigate the left and right pkCn neighbor values in σR.

IF σR(pkCn) < σR(pkCn + 0.25 Hz)

OR σR(pkCn) < σR(pkCn - 0.25 Hz)

NEWpkCn = the neighbor with higher value in σR.

(Step 3) **IF** Dr2σR(NEWpkCn) < sC

pkCn = NEWpkCn

Go to (2)

ELSE

This pkCn is not valid, go to (1) and take the next minimal place in the Dr2σR, which was not analyzed yet, as pkCn.

END

ELSE

pkCn is accepted as an activity peak in σR.

END

ELSE

No valid peaks.

END

In the first step (1), the algorithm selected the candidate frequency bin (pkCn) in σR with the strongest downwards curve. The curvature in this place must be stronger than the threshold (pC) in order to be further analyzed. If there were no places with prominent downward curvatures available in σR, the procedure was over without localization of the spindle frequency peak.

If pkCn was selected, the region of this place was further analyzed (2) in order to localize the local maximum in σR. If the σR value on the left or right side of pkCn was higher than the σR value in pkCn, the place with a higher σR value was marked as a new pkCn. The curvature in the new pkCn must be stronger than the sufficient threshold (sC) in order to be further analyzed (3). The curvature threshold criterion for the new pkCn was lower since pC has been already fulfilled for this local maximum. Step (2) was repeated as long as pkCn was not a local maximum in σR. (Please refer to Figure 3.16 illustrating this stepwise selection process of the pkCn)

Step (2) assured that the spindle frequency peak was localized in the local maximum of the amplitude spectrum. Step (3) was introduced to avoid any case when a strong downwards curve localized in (1) existed on a side of the continuous slope rather than on a peak.

The above procedure, with two modifications, was applied to find a second spindle frequency peak in σR. First, all the places in σR investigated during the localization of the first spindle frequency peak were excluded from the pkCn selection in step (1). Second, between the first and second localized peak, there had to be positive values in Dr2σR. The second condition assured that localized spindle frequency peaks were distinct to each other. Peak detection in amplitude spectra is illustrated in Figure 3.16.

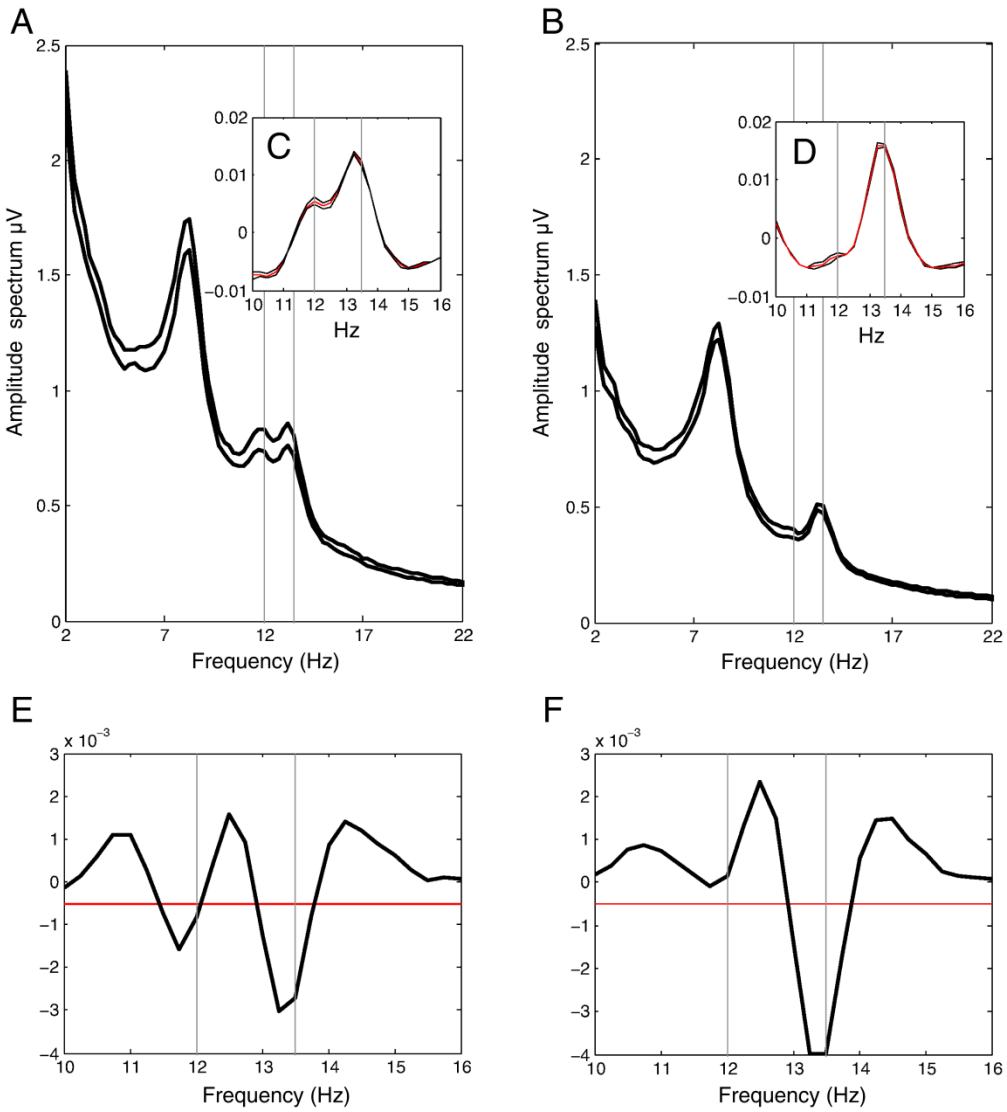

Figure 3.16: The scheme of spindle frequency peak detection in NREM sleep amplitude spectra computed for (**A**) frontal and (**B**) parietal derivations. 10–16 Hz frequency range for each amplitude spectrum was normalized, linear trend was removed and the mean of two frontal (**C**) and two parietal (**D**) derivations was investigated (in **C** and **D** black color represents amplitude spectrum of each derivation and red color the mean of them). In order to identify slow spindle frequency peak in (**C**), the 2nd derivative was computed (**E**) and two peaks crossing the threshold (red line) were identified (all additional requirements described in section: 3.3.1.4.2 and 3.3.1.4.3). After localizing a slower negative peak in (**E**), slow spindle frequency peak was set as local maximum for this place in (**C**). In order to identify fast spindle frequency peak in (**D**), the 2nd derivative was computed (**F**). This time only one peak in (**F**) exceeded the threshold. However, in parietal amplitude spectrum one localized peak was assumed to be sufficient to find fast spindle frequency peak. After the peak localization in (**F**), fast spindle frequency peak was set as local maximum for this place in (**D**). Vertical gray lines present localized spindle peaks.

3.3.1.4.3 *Spindle activity localization: merging information from frontal and parietal brain areas*

With spindle frequency peaks localized in both, amplitude spectrum (σR) from frontal channels (σRF) and amplitude spectrum from parietal channels (σRP), algorithm combined this information to obtain fast and slow spindle frequency peak. The outcome of spindle activity localization in the amplitude spectrum depended on the individual EEG spectral composition. Two, one or zero spindle frequency peaks could be identified in σR. Fast spindle activity is always strong in amplitude spectrum from parietal derivations (σRP) during NREM sleep, and as a result this activity was always localized in the parietal amplitude spectrum. Therefore, there was always at least one frequency peak localized in parietal σR. If only one frequency peak was detected in parietal σR, it was accepted as a fast spindle frequency peak (fsP). If two spindle frequency peaks were localized in parietal σR, the faster of the two frequency peaks was accepted as fsP.

Localization of the slow spindle frequency peak (ssP) in amplitude spectrum from frontal derivations (σRF) must be evaluated with more caution. Therefore, σRP was subtracted from σRF, which resulted in continuous information about amplitude spectrum differences (σDf). σDf is illustrated in Figure 3.17G. The σDf values were assigned a positive value in frequencies where the activity was stronger in frontal EEG, and negative in frequencies where the activity was stronger in parietal EEG. The σDf was expected to be negative in fsP and positive in ssP with a continuous shift between slow and fast spindle activity.

If two frequency peaks were localized in σRF, a slower frequency peak was considered as a possible ssP and an additional test was applied in order to accept it:

Abbreviations	
σR	10–16 Hz frequency range in the amplitude spectrum
σRF	σR from frontal derivations
σRP	σR from parietal derivations
σDf	σRP subtracted from σRF
fsP	fast spindle frequency peak
ssP	slow spindle frequency peak

Localization of slow spindle peak in σDf

(Step 1) Investigate σDf with starting point in fsP: move towards slower frequencies and find the first local maximum (localMx) in σDf with a positive value.

(Step 2) **IF** ssP >= localMx – 0.25 Hz

(Step 3) **AND** fsP – ssP >= 1 Hz

ssP is a valid slow spindle peak

ELSE

ssP must be re-examined

END

localMx identified in step (1) does not have to be in the same place as a slow spindle frequency peak. However, in most cases a slow spindle peak and localMx should overlap. If the frequency of localized ssP is much lower than LocalMx (2), there is a high probability that the alpha frequency peak was wrongly classified as ssP. In this scenario, ssP had to be re-examined. Furthermore, the ssP had to be re-examined (3) when it was identified very close to fsP, since this is a very unlikely situation.

When fewer than two frequency peaks were identified in the σRF or when ssP had to be re-examined, σDf was used to localize ssP. ssP was chosen as the first local maximum in σDf on the left side of fsP (search started at a frequency 0.75 Hz slower

than fsP). Localization of slow spindle frequency peak in σDf is illustrated in Figure 3.17. Spindle frequency localization in σDf was less exact than using frontal σR, but it was more robust, so it was used in case of any uncertainty with ssP localization in frontal σR.

3.3.1.4.4 *Individual spindle range*

Besides the spindle frequency peaks the algorithm has to localize a)the start of the spindle frequency range, b)the separation place between slow and fast spindle ranges and c) the end of the spindle range. For this purpose the amplitude spectra were used.. The start of the spindle frequency range was the closest place in amplitude spectrum to the slow spindle frequency peak, which was in a slower frequency and had a positive value found in second derivative of σRF corresponding to the curve going upwards in σRF. The separation frequency bin between the slow and fast spindle ranges was a zero crossing point in σDf between the slow spindle frequency peak and the fast spindle frequency peak. The end of the spindle frequency range was the closest frequency bin in the amplitude spectrum to the fast spindle frequency peak, which was in a faster frequency and had a positive value found in second derivative of σRP.

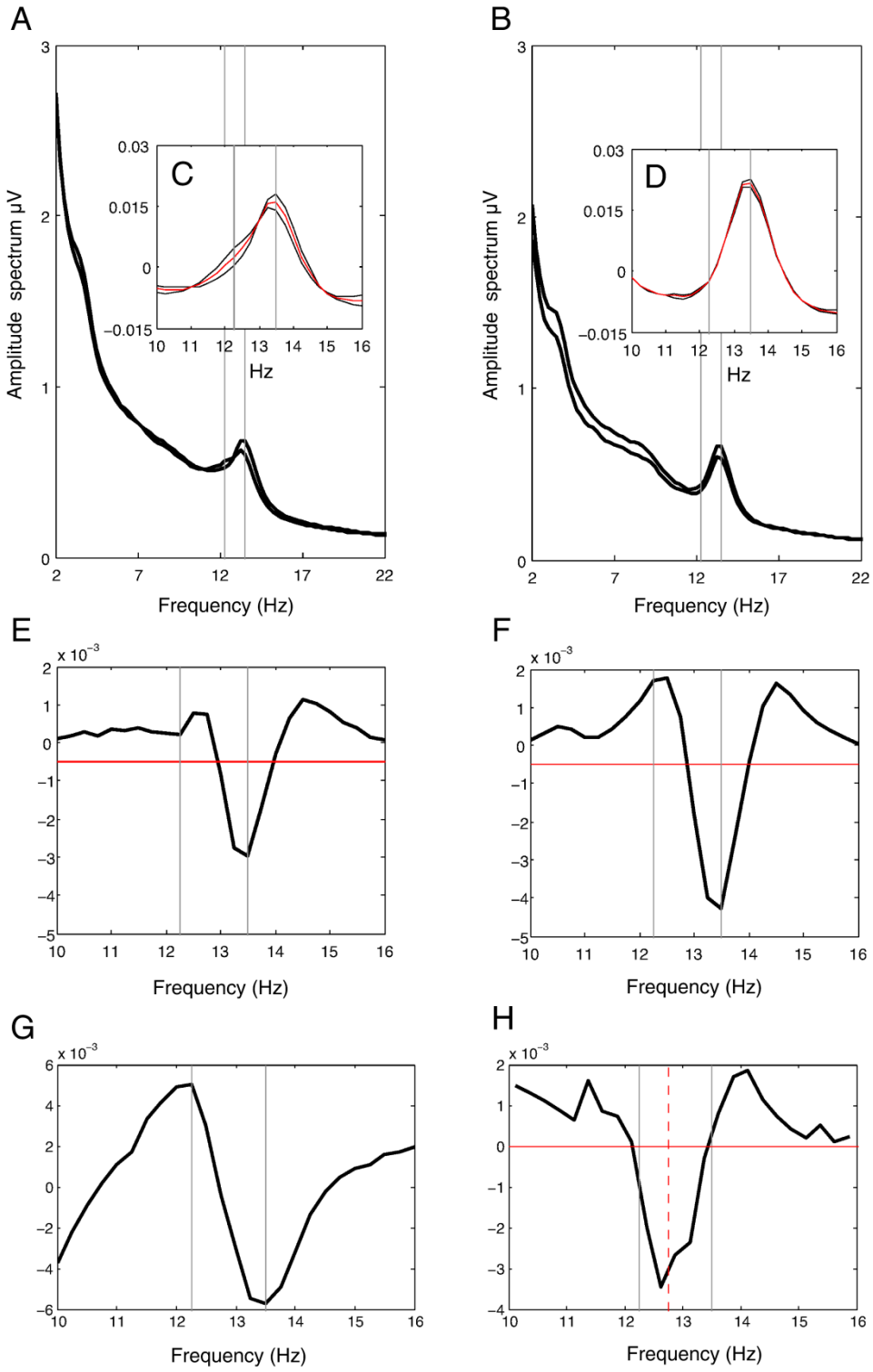

Figure 3.17: The scheme of spindle frequency peak detection in NREM sleep amplitude spectra. First steps (**A**, **B**, **C**, **D**, **E**, **F**) have been described in Figure 3.16. In the illustrated case slow spindle peak in frontal derivations is not visible and algorithm failed to find there two peaks (**E**). In this situation algorithm subtracted parietal sigma range (**D**) from frontal sigma range (**C**) resulting in (**G**). Slow spindles are more prominent in frontal derivations and fast spindles are more prominent in parietal derivations, therefore (**G**) was negative in fast spindle range and positive in slow spindle range with continuous transition between the peaks. In order to find slow spindle peak a first derivative from (**G**) was investigated (**H**) starting at the frequency 0.75 Hz slower (dashed red line) than the localized fast spindle frequency peak. A shift in investigation (dashed red line) was introduced because of possible

small instabilities in fast spindle frequency peaks between the derivations (possible slower fast spindle peak in frontal derivations). Slow spindle peak was localized in a bin, where 1st derivative (**H**) first time crossed zero (red line), which responded to the first local maximum in (**G**). Vertical gray lines present localized spindle peaks.

3.3.1.4.5 *Spindle detection with localized slow and fast spindle peaks*

Spindle detection was performed in the same way as described in section 3.3.1.2. However, for this purpose the examined frequency range depended on a) the localized start and end of the spindle frequency range, b)the slow and fast spindle frequency peaks, as well as c) the separation place between slow and fast spindle ranges.

In a first scenario when the detection of all sleep spindles was of interest without the separation between the slow and fast ones, the frequency range of the wavelet used for spindle detection started at a frequency 1 Hz higher than the localized start of the spindle range and stopped at a frequency 1 Hz lower than the end of the spindle range.

Secondly, when the detection of slow spindles was of interest, the frequency range of the wavelet used for spindle detection started at a frequency 1 Hz higher than the localized start of the spindle range and stopped at a frequency 1 Hz lower than the separation place between the slow and fast spindle ranges. To assure a proper separation between slow and fast spindles, a wavelet with frequency corresponding exactly to fast spindle frequency peak (fast spindle wavelet: fsW) was constructed. Spindle activity detected with the slow spindle detection wavelets was considered only if it was higher than the spindle activity detected using fsW. Similar logic was applied for fast spindle detection.

3.3.2 *Heritability of sleep spindles*

3.3.2.1 *Genetic variance analysis and intraclass correlation coefficients*

MANCOVA analysis (covariates: sex, age, cohabitation) showed that none of the covariates significantly affected the investigated sleep spindle parameters. However, genetic variance analysis (GVA) was not applicable for all slow spindle parameters computed for NREM sleep besides slow spindle amplitude (all values were significantly higher for DZ twins). GVA was also not applicable for slow spindle length in stage 2 as well as for slow spindle number and length in slow wave sleep (SWS), since sample means of averaged over-pairs measures revealed significant differences between the twin samples (in all cases mean values were significantly higher in DZ twins).

Table 3.4: Genetic variance analysis, type of estimate applied (GCT: combined among- and within-twin pair component estimate, GWT: within-pair estimate) and intraclass correlation coefficients (ICCs) for sleep spindle localization in frequency range. ICC MZ: ICCs of monozygotic (MZ) twins, ICC DZ: ICCs of dizygotic (DZ) twins, ICC MZ cn: ICCs of consecutive nights for each subject in MZ group, ICC DZ cn: ICCs of consecutive nights for each subject in DZ group. ICC results include: original sample ICC (upper percentile of bootstrapped data, median of bootstrapped data).

Variable	*p*	GWT *vs.* GCT	ICC MZ	ICC DZ	ICC MZ cn	ICC DZ cn
Begin of spindle range	.0324	GWT	0.77(0.41, 0.12)	0.63(0.63, 0.19)	0.88(0.32, 0.08)	0.82(0.47, 0.14)
Slow spindle peak	.0016	GWT	0.80(0.43, 0.12)	0.57(0.64, 0.18)	0.91(0.34, 0.09)	0.94(0.48, 0.13)
Fast spindle peak	<.0001	GWT	0.93(0.44, 0.12)	0.63(0.60, 0.18)	0.94(0.34, 0.09)	0.96(0.49, 0.13)
End of spindle range	<.0001	GWT	0.92(0.41, 0.12)	0.65(0.64, 0.19)	0.95(0.31, 0.08)	0.96(0.49, 0.13)

The results of GVA and ICC with respect to spindle localization in frequency range are shown in Table 3.4. Significant genetic control was found for all parameters defining localization of spindles in the frequency range. According to Landis and Koch (1977) benchmark, ICCs for consecutive nights were always *almost perfect*. Slightly higher within-twin pair similarity and night stability ICC estimations were found for parameters based on fast spindles localization.

Table 3.5: Genetic variance analysis, type of estimate applied (GCT: combined among- and within-twin pair component estimate, GWT: within-pair estimate) and intraclass correlation coefficients (ICCs) for NREM sleep spindle parameters.
Variables abbreviations as in Table 3.4.
* Analysis of variance not applicable (significant differences between the means in DZ and MZ twin set).

Variable	*type*	*p*	GWT *vs.* GCT	ICC MZ	ICC DZ	ICC MZ cn	ICC DZ cn
Number of spindles	slow*	-	-	0.96(0.43, 0.12)	0.62(0.64, 0.18)	0.96(0.32, 0.09)	0.89(0.48, 0.14)
	fast	.0759	GWT	0.67(0.45, 0.12)	0.49(0.64, 0.19)	0.88(0.33, 0.09)	0.88(0.44, 0.14)
	all	.0125	GWT	0.88(0.40, 0.12)	0.54(0.66, 0.18)	0.95(0.33, 0.08)	0.86(0.44, 0.12)
Spindle length	slow*	-	-	0.97(0.41, 0.11)	0.79(0.66, 0.19)	0.96(0.31, 0.09)	0.95(0.48, 0.14)
	fast	.0062	GWT	0.69(0.44, 0.12)	0.44(0.64, 0.17)	0.91(0.32, 0.08)	0.94(0.47, 0.12)
	all	.0010	GWT	0.86(0.44, 0.12)	0.47(0.66, 0.18)	0.94(0.30, 0.08)	0.96(0.48, 0.13)
Spindle amplitude	slow	.0011	GCT	0.85(0.46, 0.12)	0.19(0.64, 0.18)	0.88(0.31, 0.09)	0.84(0.46, 0.13)
	fast	.0354	GWT	0.82(0.46, 0.12)	0.53(0.61, 0.18)	0.86(0.30, 0.08)	0.64(0.47, 0.13)
	all	.0007	GCT	0.89(0.44, 0.12)	0.30(0.64, 0.19)	0.90(0.34, 0.09)	0.87(0.47, 0.13)
Spindle density	slow*	-	-	0.96(0.44, 0.12)	0.64(0.64, 0.20)	0.96(0.31, 0.08)	0.93(0.48, 0.14)
	fast	.1203	GWT	0.68(0.44, 0.12)	0.50(0.63, 0.18)	0.87(0.31, 0.08)	0.90(0.46, 0.13)
	all	.0068	GWT	0.90(0.43, 0.12)	0.57(0.65, 0.18)	0.96(0.32, 0.09)	0.90(0.46, 0.13)
Integrated spindle activity	slow*	-	-	0.95(0.44, 0.12)	0.68(0.67, 0.19)	0.96(0.34, 0.08)	0.94(0.48, 0.12)
	fast	.0325	GWT	0.72(0.45, 0.13)	0.51(0.65, 0.19)	0.84(0.31, 0.09)	0.82(0.46, 0.13)
	all	.0269	GWT	0.88(0.44, 0.11)	0.64(0.63, 0.18)	0.94(0.31, 0.09)	0.90(0.47, 0.14)

GVA and ICC estimates of spindle parameters in NREM sleep are shown in Table 3.5. A significant genetic effect was identified in all investigated spindle parameters besides fast spindle quantity (marginal effect for number of spindles and just a trend in spindle density). Lower night stability was observed for fast spindle amplitude in DZ twins compared to MZ twins, therefore GVA estimation in these cases should be treated with caution. Mean ICCs for spindle parameters were 0.84 and 0.52 in the MZ twins and DZ twins, respectively. Mean ICCs for night-to-night stability were 0.91 in the MZ group and 0.88 in the DZ group.

Table 3.6: Genetic variance analysis, type of estimate applied (GCT: combined among- and within-twin pair component estimate, GWT: within-pair estimate) and intraclass correlation coefficients (ICCs) for stage 2 sleep spindle parameters.
Variables abbreviations as in Table 3.4.
* Analysis of variance not applicable (significant differences between the means in DZ and MZ twin set).

Variable	*type*	*p*	GWT *vs.* GCT	ICC MZ	ICC DZ	ICC MZ cn	ICC DZ cn
Number of spindles	slow	.0048	GWT	0.91(0.42, 0.12)	0.71(0.68, 0.18)	0.94(0.31, 0.09)	0.91(0.49, 0.13)
	fast	.1898	GWT	0.71(0.42, 0.12)	0.59(0.63, 0.18)	0.86(0.33, 0.09)	0.90(0.48, 0.13)
	all	.1747	GWT	0.85(0.45, 0.12)	0.66(0.63, 0.18)	0.93(0.30, 0.09)	0.90(0.47, 0.13)
Spindle length	slow*	-	-	0.96(0.42, 0.12)	0.83(0.62, 0.19)	0.95(0.33, 0.09)	0.95(0.45, 0.13)
	fast	.0073	GWT	0.68(0.41, 0.11)	0.40(0.63, 0.18)	0.91(0.32, 0.09)	0.92(0.48, 0.13)
	all	.0006	GWT	0.86(0.45, 0.11)	0.45(0.66, 0.18)	0.95(0.31, 0.08)	0.97(0.49, 0.12)
Spindle amplitude	slow	.0030	GCT	0.85(0.43, 0.12)	0.21(0.69, 0.17)	0.88(0.31, 0.08)	0.85(0.45, 0.12)
	fast	.0411	GWT	0.82(0.43, 0.12)	0.54(0.62, 0.18)	0.87(0.33, 0.09)	0.63(0.46, 0.12)
	all	.0009	GCT	0.89(0.45, 0.12)	0.31(0.60, 0.17)	0.90(0.33, 0.08)	0.86(0.47, 0.12)
Spindle density	slow	<.0001	GWT	0.96(0.44, 0.13)	0.74(0.61, 0.19)	0.96(0.34, 0.09)	0.93(0.49, 0.13)
	fast	.1725	GWT	0.70(0.47, 0.12)	0.56(0.66, 0.18)	0.88(0.30, 0.09)	0.91(0.45, 0.13)
	all	.0247	GWT	0.91(0.47, 0.12)	0.67(0.65, 0.18)	0.96(0.31, 0.08)	0.91(0.49, 0.13)
Integrated spindle activity	slow	<.0001	GWT	0.94(0.43, 0.12)	0.71(0.63, 0.19)	0.96(0.33, 0.09)	0.94(0.45, 0.12)
	fast	.0390	GWT	0.74(0.43, 0.13)	0.55(0.65, 0.18)	0.85(0.32, 0.08)	0.84(0.48, 0.13)
	all	.0200	GWT	0.89(0.44, 0.12)	0.67(0.64, 0.18)	0.94(0.33, 0.08)	0.92(0.43, 0.13)

The results of GVA and ICC with respect to sleep stage 2 are shown in Table 3.6. Significant genetic control was identified for all parameters besides fast spindle number and density as well as all spindle number. ICC results showed that, in the case of fast spindles, the reason for the lack of a significant genetic control effect was on account of the relatively low within-pair similarity in MZ set, whereas in the case of all spindles, the reason was due to a higher than usual within-pair similarity within the DZ set. According to Landis and Koch (1977) benchmark, ICCs for night stability were *almost perfect* for all parameters except for fast spindle amplitude in the DZ set. Therefore the GVA result for fast spindle amplitude should be treated with caution. Mean ICCs for spindle parameters in stage 2 were 0.84 in the MZ twins and 0.57 in the DZ twins. Mean ICCs for night-to-night stability were 0.91 in the MZ group and 0.88 in the DZ group.

Table 3.7: Genetic variance analysis, type of estimate applied (GCT: combined among- and within-twin pair component estimate, GWT: within-pair estimate) and intraclass correlation coefficients (ICCs) for slow wave sleep spindle parameters.
Variables abbreviations as in Table 3.4.
* Analysis of variance not applicable (significant differences between the means in DZ and MZ twin set).

Variable	*type*	*p*	GWT *vs.* GCT	ICC MZ	ICC DZ	ICC MZ cn	ICC DZ cn
Number of spindles	slow*	-	-	0.91(0.45, 0.12)	0.55(0.63, 0.19)	0.92(0.33, 0.08)	0.77(0.44, 0.12)
	fast	.0166	GWT	0.44(0.50, 0.11)	0.14(0.62, 0.19)	0.88(0.33, 0.08)	0.82(0.47, 0.13)
	all	.0007	GWT	0.83(0.44, 0.11)	0.46(0.64, 0.19)	0.90(0.30, 0.09)	0.75(0.44, 0.14)
Spindle length	slow*	-	-	0.95(0.42, 0.12)	0.62(0.62, 0.19)	0.91(0.35, 0.09)	0.94(0.46, 0.13)
	fast	.0099	GWT	0.71(0.45, 0.12)	0.45(0.64, 0.19)	0.74(0.31, 0.08)	0.85(0.45, 0.13)
	all	.0020	GWT	0.84(0.46, 0.12)	0.48(0.68, 0.18)	0.87(0.31, 0.09)	0.89(0.49, 0.13)
Spindle amplitude	slow	.0002	GCT	0.86(0.42, 0.12)	0.19(0.64, 0.19)	0.88(0.33, 0.09)	0.81(0.47, 0.13)
	fast	.0051	GCT	0.81(0.42, 0.12)	0.32(0.60, 0.17)	0.86(0.33, 0.08)	0.63(0.47, 0.14)
	all	<.0001	GCT	0.87(0.46, 0.13)	0.14(0.65, 0.19)	0.88(0.32, 0.09)	0.79(0.47, 0.13)
Spindle Density	slow	<.0001	GWT	0.95(0.44, 0.12)	0.38(0.63, 0.18)	0.94(0.29, 0.08)	0.92(0.48, 0.13)
	fast	.0220	GWT	0.55(0.44, 0.12)	0.13(0.66, 0.18)	0.85(0.31, 0.09)	0.81(0.47, 0.13)
	all	.0024	GCT	0.88(0.45, 0.12)	0.27(0.69, 0.19)	0.95(0.32, 0.09)	0.85(0.49, 0.13)
Integrated spindle activity	slow	<.0001	GWT	0.96(0.48, 0.11)	0.44(0.63, 0.18)	0.92(0.34, 0.08)	0.92(0.48, 0.13)
	fast	.0073	GWT	0.58(0.46, 0.12)	0.14(0.66, 0.18)	0.84(0.33, 0.09)	0.71(0.50, 0.13)
	all	.0071	GCT	0.86(0.44, 0.12)	0.39(0.63, 0.19)	0.93(0.33, 0.08)	0.83(0.48, 0.13)

The results of GVA and ICC with respect to SWS are shown in Table 3.7. Genetic control of all investigated parameters was found, although relatively low ICC results for within-pair similarity in the MZ set were observed. The mean ICC value computed for all spindle parameters in SWS was 0.80 in the MZ twins and 0.34 in the DZ twins. Mean ICCs for night-to-night stability were 0.88 in the MZ group and 0.81 in the DZ group.

Considering all periods of sleep combined, the mean value of ICCs computed for slow spindle parameters (excluding frequency parameters: onset of the spindle frequency range and the slow spindle frequency peak) was 0.92 in the MZ twins and 0.55 in the DZ twins, whereas night stability was 0.93 in the MZ group and 0.89 in the DZ group. The mean value of ICCs computed for fast spindle parameters (excluding frequency parameters: the fast spindle frequency peak and the end of the spindle frequency range) was 0.68 in the MZ twins and 0.41 in the DZ twins, whereas night

stability was 0.86 in the MZ group and 0.81 in the DZ group. The mean value of ICCs computed for parameters of all spindles detected in the central derivation, was 0.87 in the MZ twins and 0.46 in the DZ twins, whereas night stability was 0.92 in the MZ group and 0.87 in the DZ group.

3.3.2.2 *Cluster analysis*

Figure 3.18 illustrates the distribution of standardized Euclidean (seuclidean) distance values between sleep spindle parameters computed for each night EEG recording within different groups. Spindle parameters consisted of: the onset of the spindle frequency range, the slow spindle frequency peak, the fast spindle frequency peak and the end of the spindle frequency range as well as parameters of detected spindles: amplitude, length and density in stage 2 as well as in SWS for slow, fast and all spindles. The mean of seuclidean distance values was 1.80 ± 0.82 (mean ± SD) between consecutive nights, 2.21 ± 1.18 between MZ twins, 4.64 ± 1.72 between DZ twins and 6.32 ± 2.13 between unrelated subjects. Pairwise comparisons of similarity distributions between these groups revealed only a marginal difference between intra-individual similarity and MZ twins similarity (p=.0781, Wilcoxon rank-sum test). Means of all other groups were significantly different when compared pairwise (p=.0083 when comparing DZ twins with inter-individual similarity and p<.0001 for all other comparisons).

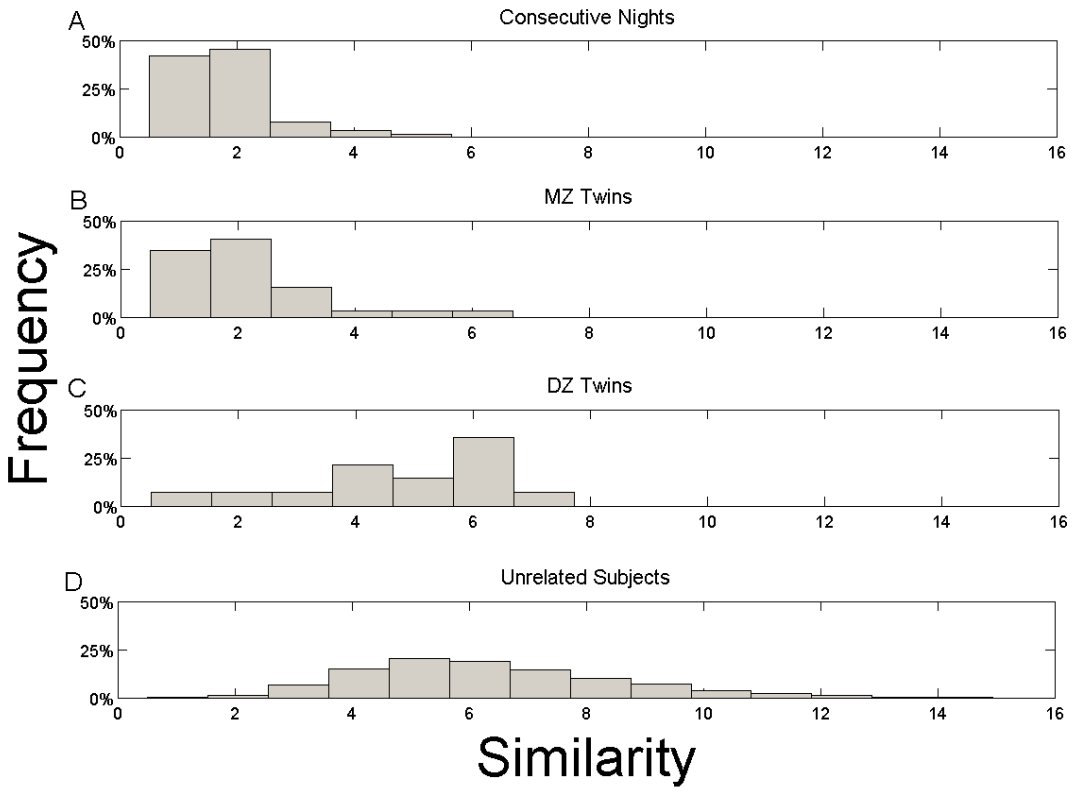

Figure 3.18: Distribution of standardized Euclidean distances. Each subject was represented by a vector of 22 spindle parameters: amplitudes, lengths and densities during stage 2 and slow wave sleep for slow, fast and all spindles, plus begin of spindle range, slow spindle peak, fast spindle peak and end of spindle range. (**A**) consecutive nights of each subject (n=92); (**B**) pairs of monozygotic (MZ) twins (each subject represented by two nights mean, n=32); (**C**) pairs of dizygotic (DZ) twins (each subject represented by a two nights mean, n=14); (**D**) unrelated subjects (n=16560). If there is no similarity *z*=0; if there is perfect similarity *z*=infinity.

Cluster analysis was performed on mean spindle parameters of 2 recording nights as well as on each night represented separately. In the case when each night was treated separately, it was assumed that the two nights for the same subject clustered, if the distance between them was closer than to any unrelated subject. It was assumed that a twin pair clustered if the distance between twins for any combination of their nights was closer than to any unrelated subject. Analysis of mean spindle parameters of two nights revealed that 23 of 32 twin pairs clustered within MZ set (Figure 3.19), whereas 2 of 14 twin pairs clustered within DZ set.

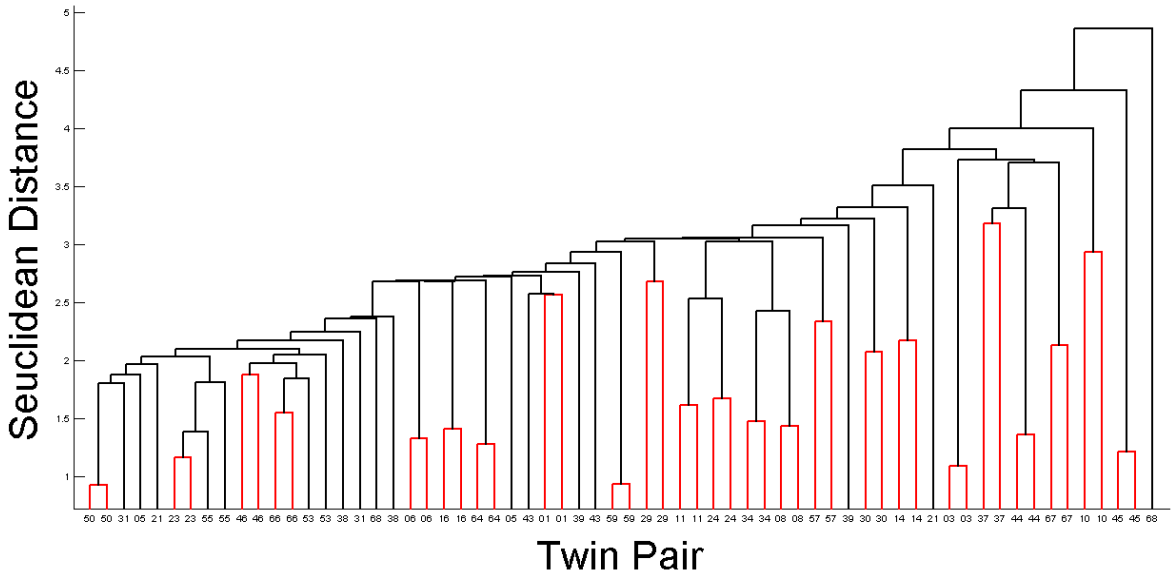

Figure 3.19: Dendrogram of cluster analysis in monozygotic (MZ) twins based on distances between vectors of 22 spindle parameters: amplitudes, lengths and densities during stage 2 and slow wave sleep for slow, fast and all spindles, plus begin of spindle range, slow spindle peak, fast spindle peak and end of spindle range. Each subject is represented by two nights spindle parameters mean. Metric was standardized Euclidean distance between vectors. Subjects with the same number represent the same MZ pair on *x* axis, distance between clusters is on *y* axis. Red clusters depict MZ pairs which clustered together.

When clustering was performed on separated nights, 3 more pairs clustered within the MZ set and the same pairs clustered within DZ set (Figure 3.20). With respect to consecutive nights, 55 of 64 subjects clustered within the MZ set and 22 of 28 within the DZ set. When cluster analysis was repeated on all 184 nights from the combined MZ and DZ sets, 83.7% of consecutive nights, 75.0% of MZ pairs and 14.3% of DZ pairs clustered.

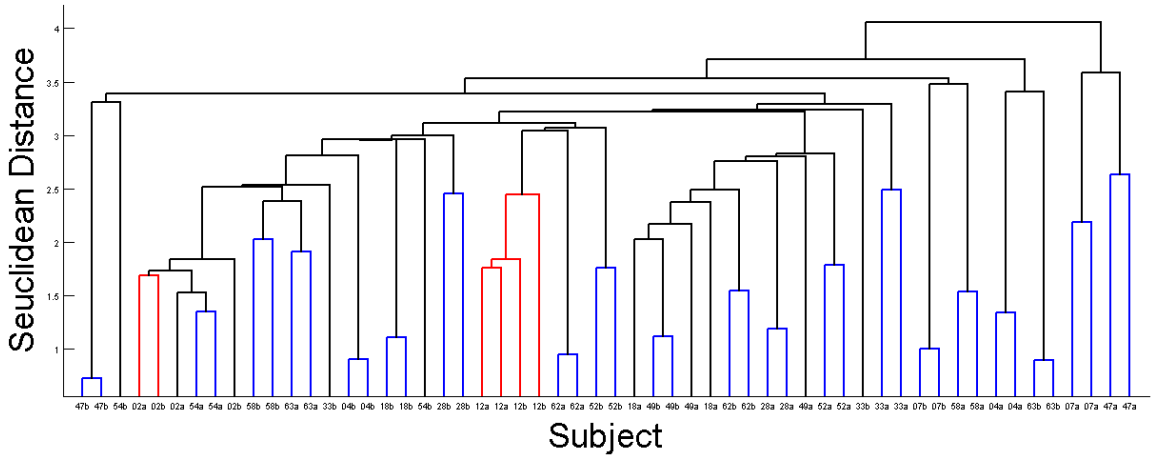

Figure 3.20: Dendrogram of cluster analysis in dizygotic (DZ) twins based on distances between vectors of 22 spindle parameters: amplitudes, lengths and densities during stage 2 and slow wave sleep for slow, fast and all spindles, plus begin of spindle range, slow spindle peak, fast spindle peak and end of spindle range. Metric was standardized Euclidean distance between vectors. Subject id consists of a number (defines DZ pair) and a character (defines a twin within the pair). Subjects id's are on *x* axis, distance between clusters is on *y* axis. Blue clusters depict those subjects whose consecutive nights clustered together but not with related DZ twin. Red clusters depict DZ pairs which clustered together.

3.3.3 *Summary of sleep spindle analysis*

The new spindle detector based on Continuous Wavelet Transform was in satisfactory agreement with visual scoring and the automatic SIESTA algorithm. It offers an individualized detection threshold for each EEG derivation as well as localization of slow and fast spindle frequency peaks and ranges.

The analysis of sleep spindle parameters revealed a significant genetic influence on their localization within a frequency range as well as on their amplitude, length, quantity and integrated activity, with the exception of fast spindle quantity in stage 2 and whole NREM sleep as well as all spindle number in stage 2. GVA could not be performed on multiple slow spindle parameters, since their values were significantly different when comparing the DZ set with the MZ set. However, when analysis was repeated in a subgroup of MZ twins closely matched to DZ twins for age, gender and

cohabitation, significant differences between MZ and DZ twins were not observed, and in all cases a significant genetic effect was identified (see Supplement).

ICC computed for slow sleep spindle parameters revealed a better night-to-night stability as well as a higher similarity within twin pairs when compared to fast spindles.

Clustering experiments performed on basic spindle features revealed their individual profile, with similarity between MZ twins in the range of night-to-night stability and similarity between DZ twins close to unrelated subjects (Figure 3.18).

3.4 *Rapid eye movement analysis*

3.4.1 *Automatic detection of REMs: description of algorithm*

3.4.1.1 *Preprocessing before REMs detection*

The first part of the algorithm checks the properties of the signal and rejects periods of signal with EMG, EEG or other artifacts or segments without rapid eye movements.

Artifact rejection: There are different types of artifacts in an EOG signal, which can lead to false REM detection. Amplitude and frequency thresholds were used to exclude fragments with movement, high muscle and EEG contamination.

Amplitude: If the signal in the EOG channels exceeds 850 μV, a 15 sec fragment is eliminated from REM detection. Such a high amplitude is usually caused by voluntary subject movement. A 5 sec fragment is rejected before detection of a high amplitude, because signal changes usually start a few seconds before it reaches high amplitude. A 10 sec fragment is eliminated after high amplitude detection, which was found to be a reasonable amount of time for the signal to return back to baseline, and for the subject to calm down.

Frequencies: In order to identify high frequency muscle artifacts, EOG data are filtered using a digital high-pass finite input response (FIR) filter (-3 dB at 19.8 Hz, < -80 dB at 19 Hz) and a low-pass FIR filter (-3 dB at 45.5 Hz, < -80 dB at 48 Hz). The standard deviation of the signal is computed in a 1 sec sliding window (step: 0.5 sec); if it exceeds 6 μV, a window of 3 sec is excluded from REM detection.

Rejection of segments without eye movements: Horizontal and vertical eye movements in EOG channels produce coincident, out-of-phase waveforms. During REMs, the correlation of EOG channels is highly negative; in the absence of eye movements, pearson correlation is expected to be low; in the case of

technical or physiological artifacts (e.g. delta waves), the correlation should be highly positive. A positive correlation is used to exclude fragments, where REMs are not probable. Considering sweating artifacts lead to slow oscillatory baseline drifts, they may produce a high positive correlation but should not affect REMs detection. Therefore, in order to avoid false rejection of these fragments, EOG data are first filtered using a digital high-pass FIR filter (-3 dB at 0.47 Hz, < -80 dB at 0.3 Hz). Pearson correlation coefficients are computed for 5 sec sliding windows (step: 0.5 sec), and a segment is excluded if the correlation coefficient between EOG signals is above a threshold *p*. Since correlation coefficients are influenced by the amplitude of REMs, two different thresholds were used depending on the variance in the signal. If the standard deviation of the signal exceeds 15 µV in both EOG channels, the threshold was set at *p*=0.15 and otherwise at *p*=0.6.

3.4.1.2 *Detection of REMs*

A. <u>Data preprocessing</u>

1) Signal filtering: The duration of most REMs have been described to range from 1 Hz to 5 Hz (Boukadoum and Ktonas, 1986). Therefore, in order to minimize higher frequency noise and artifacts, the signal is filtered using a digital low-pass FIR filter (-3 dB at 5.2 Hz, < -80 dB at 6 Hz). Furthermore, to exclude slow eye movements, the signal would have to be high-pass filtered. The algorithm, however, is based on amplitude changes of EOG. Thus, high-pass filtering would attenuate slow waves but may produce additional fast amplitude changes in the signal, which would lead to false detections. In order to establish slow eye movement exclusion without high-pass filtering and to avoid false detections in the high-pass filtered EOG, the algorithm analyses two versions of the signal in

order to determine the number of REMs. One version is low-pass filtered (EOG) and the second is additionally filtered using a digital high-pass FIR filter (-3 dB at 0.47 Hz, < -80 dB at 0.3 Hz) (EOGfilt).

2) Computation of the first derivative: REM detection is based on the first derivative of the EOG signal which shows deflections in the signal. The derivative (DR) was computed for the low-pass filtered EOG (DRleft and DRright) as well as for the EOG with an additional high-pass filtering (filtDRleft and filtDRright).

B. Detection method

1) Identification of REM candidate points: REM candidate points were identified in both EOG channels. Two thresholds were used: a) a basic threshold (bT), where the derivative exceeds 261μV/sec and b) a relaxed threshold (rT), where the derivative exceeds 165 μV/sec. The threshold criteria were established on the basis of visual inspection of the EOG in the training set. Two thresholds were used in order to account for the observed differences in the amplitude of detected REMs between the two EOG channels. The relaxed threshold (rT), ensures detection of REMs that are clearly visible in one EOG channel but attenuated in the other. In the particular case when signal in the left EOG exceeds the threshold in the upward direction, the following rules were applied:

(1) **If** DRleft(*i*) > bT **and** filtDRleft(*i*) > bT **and** DRright(*i*) < bT – rT

EOGleft(*i*) valid candidate point

(2) **Elseif** DRleft(*i*) > rT **and** filtDRleft(*i*) > rT **and** DRright(*i*) < 0 **and**

DRleft(i) > 0 for >= 100 msec **and** EOGleft(*i*) > -100 μV

EOGleft(*i*) valid candidate point

(3) **Else**

the point is not valid; reject detection

End

The first part (1) demands that the basic threshold is always crossed by both EOG signals (EOG and EOGfilt) in order to avoid scoring slow eye movements. If the basic threshold is crossed, a third condition is examined to verify that there is no strong deflection of the other EOG signal in the same direction as the first. Although no absolute synchronicity between the two EOG channels is demanded, it is also requested that a deflection in the same direction as the first channel is low (< bT-rT). The second part (2) of the rules states that if the increase in the EOG signal is lower but still above the relaxed threshold, the deflection in the other channel must be in the opposite direction (DRright(*i*) < 0). Additionally, the duration of the increase has to be equal to or longer than 100 msec and the value of the EOG signal should have the same sign as the derivative value or be close to the baseline (EOGleft(*i*) > -100 μV). The first additional criterion for the relaxed threshold was introduced to mark REM candidate points only in time points where movement is clear although it is attenuated. The second criterion was introduced to minimize marking REM candidate points in time points, where a signal with high amplitude comes back to baseline. Similar rules were applied when the signal decreased and when the other EOG channel (i.e.in this case, EOG of the right eye) is analyzed.

2) Identification of binocular conjugate synchrony: After identifying all possible REM candidate points in each EOG channel, the algorithm evaluates whether there is a binocular conjugate synchrony between the marked REM candidate points in both channels. As stated above, the algorithm does not request absolute synchronicity. This is in line with previously published REM detection algorithms where binocular conjugate synchrony between 20 and 100 msec is usually required (Boukadoum and Ktonas, 1986). A cut-off value of 70 msec was used to identify synchronous REM. For each REM candidate point in one channel, a corresponding REM candidate point in the other channel within ±70 msec and a deflection in the opposite direction is sought. Additionally, the deflection of at least one of the candidate points must be above the basic threshold (261 μV/sec). Pairs of candidate points that satisfy all criteria are taken as candidate pairs. An additional condition ensured that only REMs clearly visible in comparison to the noise of the EOG channels were considered (noise is defined here as everything affecting the signal which is not caused by rapid eye movements). It also prevented false classification of pairs within the peaks of in-phase deflections, which could happen due to the non-synchronicity which was allowed (<= 70 msec). For each pair of candidate points, a signal fragment is evaluated which starts 100 msec before the first candidate point and ends 100 msec after second candidate point (= pair neighborhood). For both candidate points, the deflections had to be prominent when compared to signal within pair neighborhood range, which means the maximum/minimum value of the local neighborhood (candidate point ± 20 msec) should be 1.35-fold higher than the absolute of the minimum/maximum value of the pair neighborhood. The empirical threshold of T = 1.35 was derived from the training set, and was found to be sufficient to provide a good signal to noise ratio. Each pair of candidate

points that satisfied all criteria listed above was accepted as a candidate pair and it was marked at the midway time point between the left and right EOG candidate point ([left candidate point + right candidate point] / 2).

3) REMs scoring: REMs were scored when the string of consecutive candidate pairs exceeded 30ms. Additionally, if it was shorter than 70ms, REMs were classified as short. Short REMs should be clearly visible in both EOG channels in order to minimize false detections. Therefore, it was required that the median values for short REMs in the two derivative functions (left and right) should be above the basic threshold. There had to be a minimum interval of 110 msec between two detected REMs (see Figure 3.21 for illustration of the algorithm).

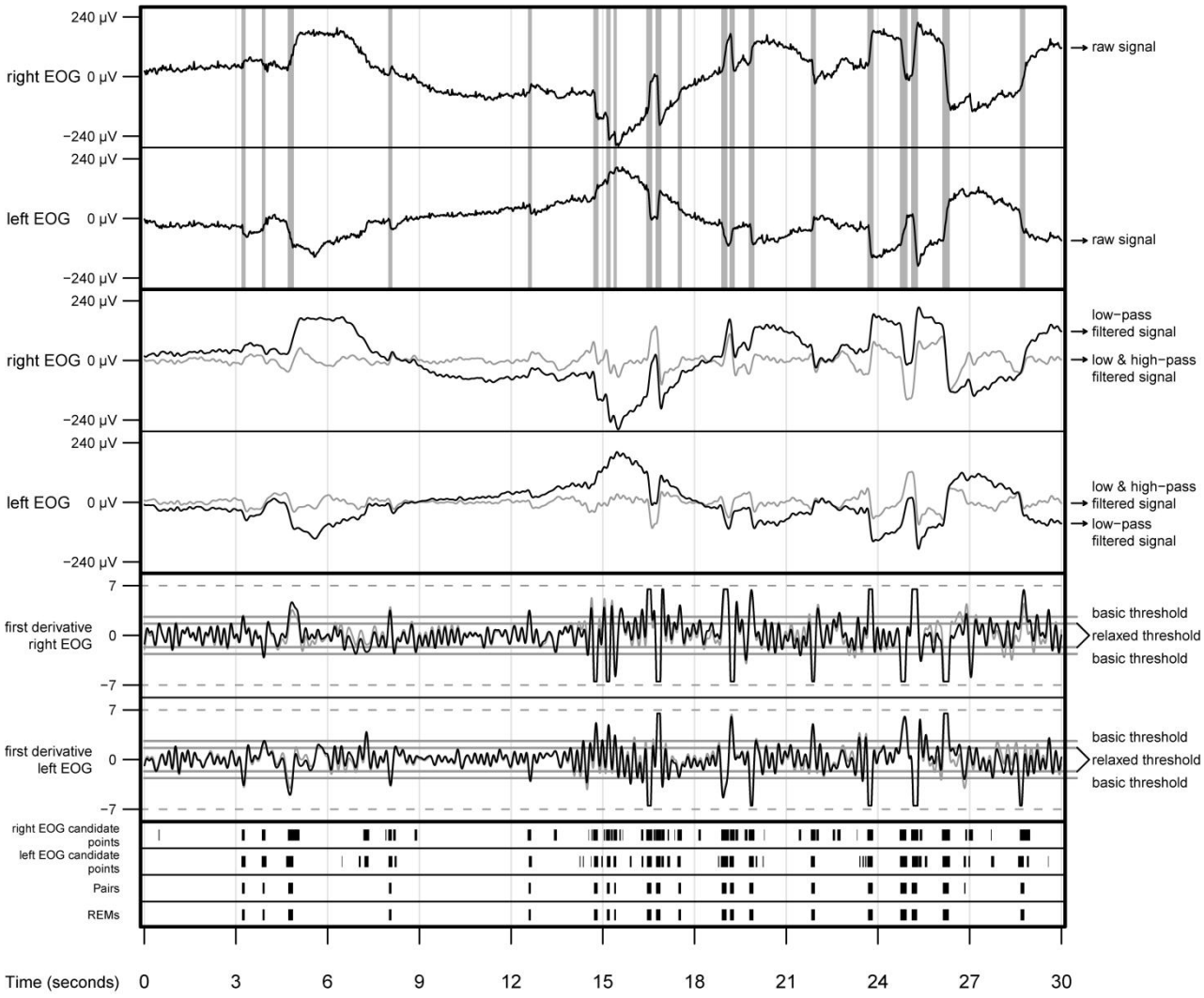

Figure 3.21: Scheme of REM detection. (a) Right and left EOG signals with detected REMs (grey vertical lines). (b) Filtered signals from (a) used for REM detection. (c) Derivatives of filtered signals in (b). (d) and (e) REM candidate points identified in right and left EOG. (f) Candidate pairs created from REM candidate points. (g) REMs created from strings of candidate pairs which fulfill all the criteria described in methods part.

3.4.1.3 *REM detector validation*

The agreement between all scorings of the validation data set (expert scorers, automated algorithm) is illustrated in Figure 3.22. The epoch-wise correlation of REM density across the night between the conditions (two experts and algorithm) showed an overall high similarity disregarding systematic shifts in the scoring. The correlation values are given in the upper panel of Figure 3.22. For the two experts, correlation

ranged between 0.83 and 0.97 with an average correlation of 0.91. The correlation between expert 1 and the algorithm ranged between 0.87 and 0.97 with an average correlation of 0.94. Similarly, the average correlation between expert 2 and the algorithm was 0.90 (0.79 to 0.97).

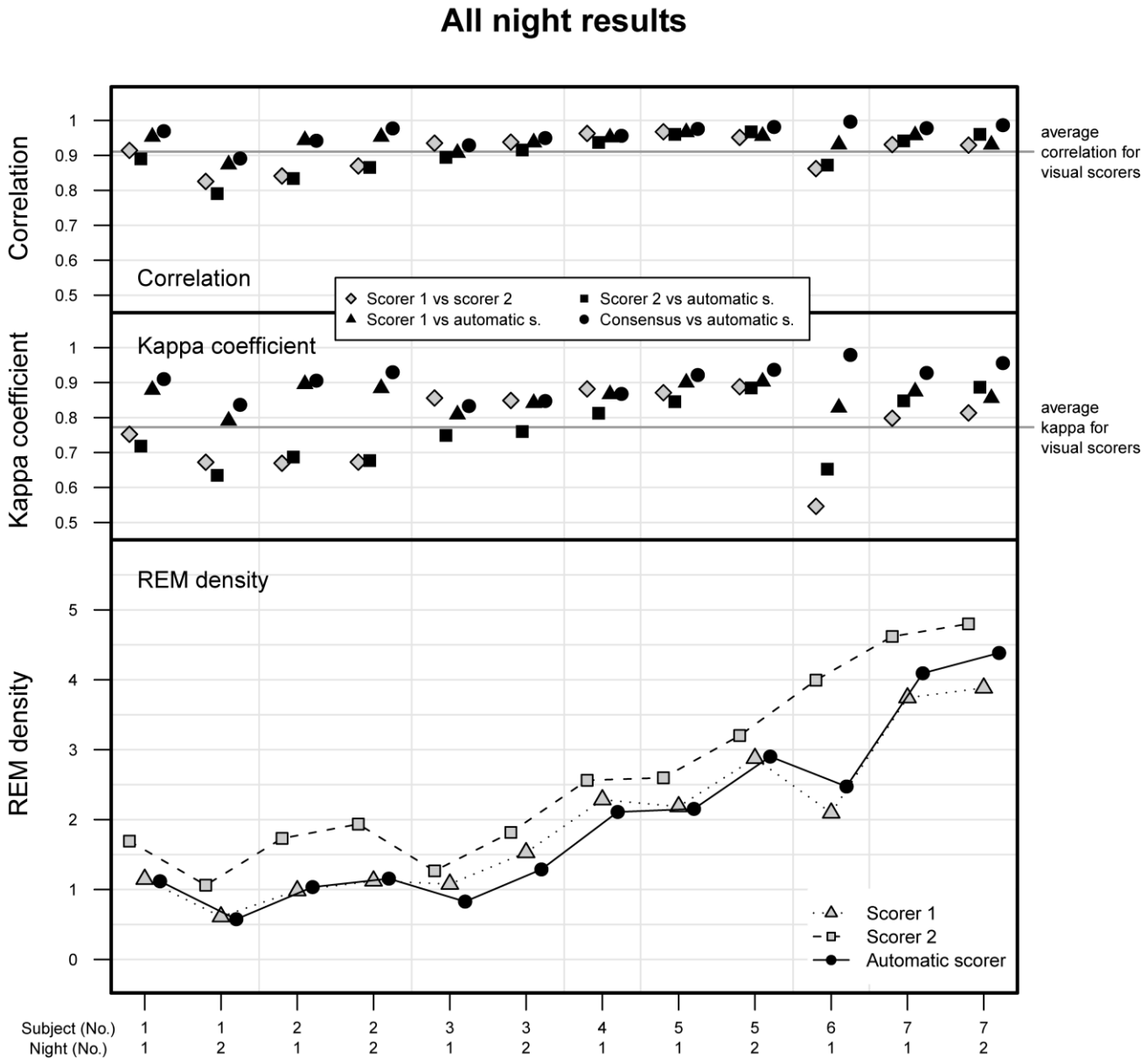

Figure 3.22: Validation set. (a) The epoch-wise correlation of REM density across the night. (b) The kappa coefficient of REM density for each night. (c) Average REM density result for each night.

Since some differences were observed between the experts scorings, the correlation between the algorithm and the expert scorings was additionally computed for those epochs where both experts scored equally for REM density (consensus scoring). This constitutes a third evaluation set derived from the consensus subset where both scorers agree and the algorithm could be tested against. The correlation between the algorithm and the consensus scoring ranged from 0.89 to 0.99 with an average correlation of 0.96.

The kappa coefficient for each night of the validation set is given in the middle panel of Figure 3.22. Kappa for the agreement between the two expert scorers was lower than the correlation coefficients and ranged from 0.56 to 0.89 with an average kappa of 0.77. Agreement between scorer 1 and the algorithm was 0.86 (0.79 to 0.90), between scorer 2 and the algorithm 0.76 (0.64 to 0.89), and between the consensus scoring and the algorithm 0.90 (0.83 to 0.98). Upon classifying kappa values per night according to published benchmarks (Landis and Koch, 1977), the agreement between the two expert scorers was only moderate for one night, but substantial for five nights and almost perfect for six nights. The agreement between expert 1 and the algorithm was substantial for one night and almost perfect for 11 nights, whereas the agreement with scorer 2 was substantial for seven nights and almost perfect for five nights. The agreement between the consensus scoring and the algorithm was almost perfect, as defined by Landis and Koch benchmark, for all nights.

With respect to the development data set of 59 recordings (scored by scorer 1), the correlation between expert scorer and the algorithm ranged between 0.89 and 0.97, with an average correlation of 0.94 (see Figure 3.23). The kappa coefficient ranged from 0.72 to 0.91 with average kappa of 0.85. The agreement between the expert scorer and the algorithm was substantial for nine nights and almost perfect for 50

nights. As described in the methods section, the development data set was used to establish the basic features of the algorithm. The specific thresholds however, derived from two different nights, were not included in this sample. The present analysis of similarities between expert and the algorithm in the development data set shows that results from the algorithm are in the range of visual scoring for any night (Figure 3.23 lower panel).

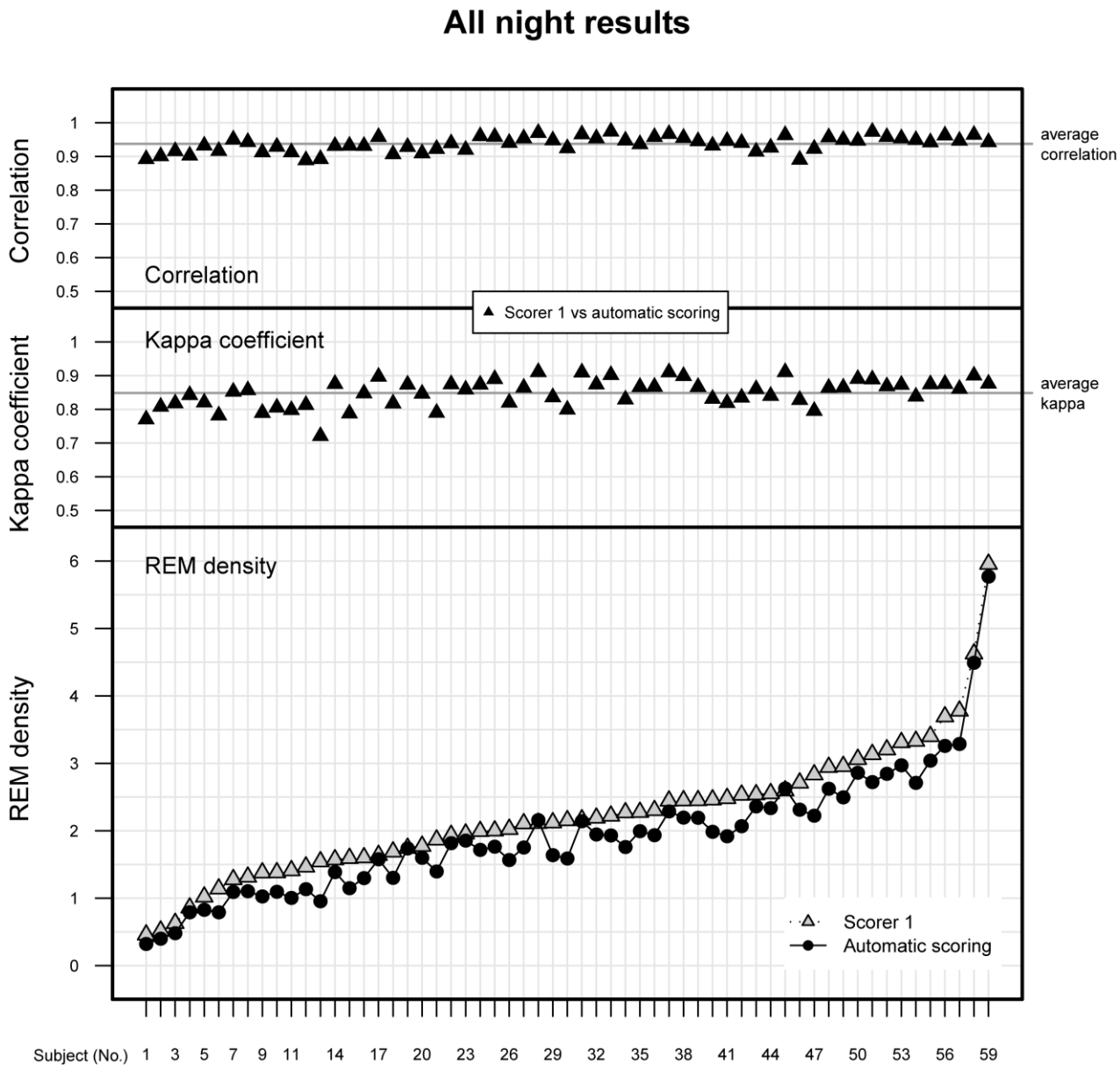

Figure 3.23: Development set. (a) The epoch-wise correlation of REM density across the night. (b) The kappa coefficient of REM density for each night. (c) Average REM density result for each night.

3.4.2 *Heritability of phasic REM sleep parameters*

3.4.2.1 *Genetic variance analysis and intraclass correlation coefficients*

The criterion of normal distribution was not fulfilled for the number of all detected REMs inside REM bursts (RinB), and therefore it was log transformed prior to any analysis. Sample means of averaged over-pairs measures revealed no significant night effects as well as no significant differences between the twin samples. None of the covariates significantly affected the results. The results of GVA and ICC with respect to phasic REM sleep parameters are shown in Table 3.8.

Table 3.8: Genetic variance analysis and intraclass correlation coefficients for phasic REM parameters. Results of genetic variance analysis, type of estimate applied (GCT: combined among- and within-twin pair component estimate, GWT: within-pair estimate) and intraclass correlation coefficients (ICCs). REM: rapid eye movement, ICC MZ: ICCs of monozygotic (MZ) twins, ICC DZ: ICCs of dizygotic (DZ) twins, ICC MZ cn: ICCs of consecutive nights for each subject in MZ group, ICC DZ cn: ICCs of consecutive nights for each subject in DZ group. RA: REM activity, RD: REM density, allRA: the number of all detected REMs, 3sRA: the number of 3-sec mini-epochs containing at least one REM, allRD: allRA / number of REM sleep epochs, 3sRD: 3sRA / number of REM sleep epochs, RinB: the number of all detected REMs inside REM bursts, RoutB: the number of all detected REMs outside REM bursts, RinB%: percentage of REMs in burst state. ICC results include: original sample ICC (upper percentile of bootstrapped data, median of bootstrapped data).

* Logarithm transformed data.

Variable	*p*	GWT *vs.* GCT	ICC MZ	ICC DZ	ICC MZ cn	ICC DZ cn
allRD all night	.0051	GWT	0.84(0.49, 0.11)	0.33(0.63, 0.19)	0.89(0.37, 0.08)	0.66(0.45, 0.13)
3sRD all night	.0027	GWT	0.83(0.45, 0.11)	0.31(0.60, 0.19)	0.85(0.33, 0.08)	0.74(0.50, 0.12)
3sRD 1st cycle	.0036	GCT	0.58(0.44, 0.11)	-0.16(0.64, 0.18)	0.49(0.31, 0.08)	0.07(0.44, 0.12)
3sRD 2nd cycle	.0096	GWT	0.70(0.44, 0.12)	0.04(0.66, 0.19)	0.41(0.28, 0.08)	0.59(0.47, 0.12)
3sRD 3rd cycle	.0774	GWT	0.68(0.41, 0.12)	0.22(0.64, 0.17)	0.70(0.35, 0.08)	0.38(0.45, 0.12)
3sRD 1st third	.0965	GWT	0.60(0.42, 0.11)	0.21(0.67, 0.18)	0.46(0.33, 0.08)	0.32(0.50, 0.13)
3sRD 2nd third	.0041	GCT	0.80(0.43, 0.11)	0.19(0.64, 0.18)	0.73(0.31, 0.08)	0.68(0.46, 0.13)
3sRD 3rd third	.0762	GWT	0.70(0.42, 0.11)	0.31(0.61, 0.19)	0.67(0.31, 0.08)	0.43(0.44, 0.13)
allRA all night	.0020	GWT	0.88(0.47, 0.10)	0.44(0.61, 0.18)	0.90(0.33, 0.08)	0.71(0.50, 0.13)
3sRA all night	.0054	GWT	0.85(0.46, 0.10)	0.49(0.64, 0.18)	0.88(0.31, 0.07)	0.78(0.47, 0.12)
RinB all night*	.0002	GWT	0.74(0.42, 0.11)	0.25(0.64, 0.17)	0.79(0.29, 0.08)	0.87(0.43, 0.12)
RoutB all night	.2467	GWT	0.70(0.43, 0.13)	0.66(0.68, 0.19)	0.80(0.34, 0.08)	0.69(0.47, 0.13)
RinB% all night	.0002	GWT	0.70(0.42, 0.12)	0.13(0.62, 0.18)	0.64(0.32, 0.08)	0.80(0.46, 0.13)

Significant genetic control was found for mean REM density throughout whole night sleep (both allRD and 3sRD), the 1st and 2nd sleep cycle as well as the second third of the night. Genetic effects on REM density for the 3rd sleep cycle and the other two thirds of the night sleep (1st and 3rd) were marginally significant. Furthermore, the analysis identified a significant genetic influence on whole night REM activity (both allRA and 3sRA), RinB and RinB% but not for RoutB.

According to Landis and Koch (1977), benchmark ICCs for consecutive nights of all phasic REM parameters considered over whole night sleep were at least *substantial*. However, when analyzing REM density in smaller fragments of night sleep, night-to-night stability was low in general (*substantial* stability only for the 2nd third of the night in the DZ set and for 3 fragments of night in MZ set) and showed considerable variation between MZ and DZ sets. Stability of REM density for the 1st and 3rd cycle as well as for the 3rd third of the night in the DZ set was strongly lower compared to the MZ set, and therefore GVA estimations, in such cases, should be treated with caution.

RoutB was the only phasic parameter measured over the whole night, where no genetic effects were observed. ICC results show, that the reason was a substantial within-pair similarity in DZ twins rather than a similarity drop in MZ twins compared to other phasic REM parameters.

3.4.3 *Summary of rapid eye movement analysis*

The agreement between the new automatic REM detection and human scorers was within or above the range of agreement between the two human scorers for the validation data set. Highest rates of agreement (almost perfect agreement for all nights) were obtained when the automatic detection was compared to human scoring for those epochs where both human scorers agreed on REM density values (consensus scoring). Because automatic REM detection marks each event in time, the analysis of additional phasic REM parameters, besides basic REM density, was possible (based on REMs clustering or so called REM bursts). Significant genetic variance was observed in all phasic REM parameters throughout the whole night with the exception of the REMs occurring outside REM bursts (RoutB).

Discussion

The first aim of the present work was to develop a robust automated detection procedure of sleep spindles and rapid eye movements (REMs), since previous research identified these EEG components as putative biomarkers in psychiatric diseases, and further research in this field will require large study samples, which can be analyzed more quickly and reliably with an automatic system.

A large data set was used for the development of the REM detection algorithm, which was then validated in a second independent data set against two experts. The agreement between the automated detection and human scorers was within or above the range of agreement between the two human scorers for the validation data set. Highest rates of agreement (*almost perfect* agreement for all nights) were obtained when the automated detection was compared to human scoring for those epochs where both human scorers agreed on REM density values (consensus scoring). Therefore, the developed automated detection algorithm seems well suited for application in large clinical and epidemiological studies. (Please refer to section 4.1 for a more detailed discussion)

In developing automatic sleep spindle detection we took into consideration the existence of two types of spindles, the inter-individual differences in slow and fast spindle frequency ranges, and inter-individual as well as inter-channel differences in the amplitude of EEG signal. Sleep spindles are of interest because of their possible role in memory consolidation as well as existing evidence for an abnormal spindle

activity in patients with schizophrenia. The algorithm was validated on EEG recordings obtained during naps against two scorers, a human scorer and the SIESTA algorithm, an already established commercial automatic spindle detector. The pairwise comparisons between the scorers revealed a high correlation regarding the amounts of spindles, and satisfactory agreement regarding the amount of overlapping signal marked by both scorers. The highest congruence was observed when the two automatic algorithms were compared. Concerning precise distinction between slow and fast spindles as well as flexible detection thresholds based on signal amplitude in each channel, the developed spindle detector of the present work may offer more detailed and more exact spindle information than previous solutions. (Please refer to section 4.2 for a more detailed discussion)

In the twin study, prior knowledge about the heritability of background EEG in NREM sleep was complemented with the comparison of tonic and phasic REM parameters. This includes absolute EEG spectral power, amount and structural organization of REMs as well as NREM sleep spindle characteristics and NREM / REM sleep power spectra morphology. EEG data were compared between a group of n=32 healthy monozygotic (MZ) and n=14 dizygotic (DZ) same-gender twins. EEG data of two recording nights were analyzed; in addition to estimating the genetic effects, the differences were illustrated in within-pair similarity and night-to-night stability of given parameters by intraclass correlation coefficients (ICC) and cluster analysis. A substantial genetic influence was observed on both the spectral composition and phasic REM sleep parameters. Regarding sleep spindles, a substantial genetic influence was observed on slow as well as fast spindles in both stage 2 and slow wave sleep (SWS). “Fingerprint” properties of REM and NREM EEG spectra morphology were confirmed. In addition, cluster analysis performed on vectors of

basic sleep spindle characteristics showed a highly individual character of spindle activity, although the results of clustering were less impressive than those of EEG spectra. Significant differences were observed in within-pair similarity between the twin groups in each clustering experiment. (Please refer to section 4.3 for a more detailed discussion)

4.1 *Rapid eye movements detection*

To provide an overview of previously published REM detection methods, the major studies including the results of their validation are summarized in Table 4.1. Early studies on REM detection algorithms were based mainly on the EOG signal amplitude of filtered signals. More recent papers combined the amplitude and signal velocity criteria by analyzing half-waves or peak angles. Other methods included matched filtering, wavelet transform and analyses of the spectral content of EOG signals. Minard and Krausman (1971) developed a similar REM detection procedure as the one presented here. The validation results of their algorithm against human scorers have not been reported. The authors defined REMs as an abrupt out-of-phase signal change and allowed a 50 msec lag between the EOG channels. Their detection method was designed for analog electronic circuits. The algorithm presented here shares this approach to the automatic detection of REMs. However, due to the technical evolution it was now possible to introduce signal processing features in order to identify and reject both physiological (e.g. muscle artifacts or slow eye movements) and technical (coming from high-pass filtering) artifacts. In addition, two deflection thresholds allowed for the detection of REMs with differing amplitudes in both EOG channels. Furthermore, procedures to distinguish REMs from the noise of the EOG channels were included.

Table 4.1: Overview of previous studies on REM detection algorithms that include validation result. ↔: referenced to, AA: automatic algorithm, cC: correct classifications, D: depressed subjects, LC: left canthus, M1: left mastoid, M2: right mastoid, n.a.: information not available, RC: right canthus, Sens: sensitivity, Spec: specificity.

Study	EOG montage	Algorithm main features	Validation set	Comparison	Accuracy results
Smith *et al.*, 1971	LC, RC ↔ supernasion	Filter, amplitude threshold, synchrony	3 nights	1 scorer *vs.* AA	Sens: 99-100% % cC: 98-100%
Ktonas and Smith, 1978	LC, RC ↔ supernasion	modified Smith *et al.*, 1971 plus high-frequency artifact detector	6 nights	1 scorer *vs.* AA	Sens: 100%
			random sample with 97 REMs	1 scorer *vs.* AA	Sens: 94% % cC: 88%
McPartland *et al.*, 1978	LC ↔ M1; RC ↔ M2	amplitude threshold, synchrony evaluation	245 nights (D)	REM activity rating (9 point scale) *vs.* AA	correlation of whole night REM activity rating *vs.* automated REM counts: 0.91
Kupfer *et al.*, 1984	see McPartland *et al.*, 1978		23 nights		0.90
			41 nights (D)		0.83
Kupfer *et al.*, 1986	see McPartland *et al.*, 1978		26 nights (D)		0.88
Othmer *et al.*, 1979	n.a.	Amplitude/duration/slope thresholds, synchrony	?	1 scorer *vs.* AA	Agreement: 97.7%
Martinerie *et al.*, 1980	n.a.	Amplitude/duration thresholds for half-waves	4 nights with 1000 REMs	1 scorer *vs.* AA	Sens: 80% % cC: 71%
Gopal and Haddad 1981	LC, RC ↔ forehead	Filter, smoothing, amplitude/slope thresholds for half-waves	3x5 min REM sleep (3 infants)	average of 2 scorers *vs.* AA	Epoch-wise (10 sec) correlation of REM count: 0.91
Hatzilabrou *et al.*, 1994	LC, RC ↔ n.a.	Matched filtering with REM templates	18x10 min REM (9 infants)	1 scorer *vs.* AA	Concordance: 73-90%
Doman *et al.*, 1995	LC, RC ↔ (M1+M2)/2	Filter, slope/angle thresholds, synchrony	240 min REM (12 healthy, 12 D)	consensus count of 4 scorers *vs.* AA	Epoch-wise correlation of visual and automatic REM count: 0.96
			10 min REM		Sens: 90% Spec: 93%
Takahashi and Atsumi, 1997	LC, RC ↔ n.a.	Signal smoothing, 2nd derivative, amplitude/ slope/duration thresholds	93 min REM (3 subjects)	2 independent scorers (A and B) *vs.* AA	Concordance: A and AA:87.0% B and AA: 84.2% epoch-wise correlation: A and AA: 0.942 B and AA: 0.955
Tsuji *et al.*, 2000	n.a. (horizontal EOG)	Discrete wavelet transform	30 min REM	1 scorer *vs.* AA	Sens: 96% % cC: 78%
Tan *et al.*, 2001	LC ↔ forehead	Integrated amplitude from period-amplitude analysis	16 subjects, 2 nights each (baseline and temazepan administration)	1 scorer *vs.* AA	Correlation of whole night of REM density vs AA: baseline night: 0.90 drug night: 0.97
Agarwal *et al.*, 2005	LC↔M1, RC↔M2	Filter, amplitude, correlation, synchrony, angle thresholds	5x30 min of REM (5 subjects)	1 scorer *vs.* AA	Sens: 67.2% Spec: 77.5%

The results of the presented algorithm, however, may be limited by the fact that sleep EOG montage was done according to Rechtschaffen and Kales (1968). In this two-channel montage, all eye movements produce coincidental out-of-phase waveforms. As a result, it is easy to distinguish eye movements from artifacts, but it is impossible to determine the direction of eye movement. EOG montages described by Padovan

and Pansini (1972) and Schneider (1978) included more channels and offer the advantage of determining the direction of eye movements. The present work, however, focused on the practical usability of the algorithm in clinical studies using the standard recommended EOG montage (Iber *et al*., 2007).

In addition, it is open to discussion whether REM density is the parameter best suited to reflect phasic components of REM sleep. In order to evaluate a REM detector, the comparison of exclusively marked single REMs could be a more precise alternative. However, since REM density assessment was the main focus of previous studies in psychiatric patients and healthy human subjects, the present work chose REM density as a comparison parameter. This decision was based also on the availability of a large development and validation data set where REM density was already scored.

The algorithm was validated in n=12 polysomnographic recordings from n=7 healthy young subjects which is a relatively large validation set compared to previous studies (see Table 4.1). There are two studies on REM algorithms that have been validated in even larger data sets (McPartland *et al*., 1978; Tan *et al*., 2001). These papers, however, reported only night-wise comparison results. Future studies are required to test the robustness of the presented detection method in data sets with subjects from different age groups and with different disorders of sleep regulation or psychiatric disorders.

It is important to take into account that relevant differences in REM density scoring might develop between human scorers, even if they have been trained in the same laboratory and have scored REMs according to the same criteria. Interestingly, all differences observed in REM density scoring between the experts and the algorithm

were stable on both nights for any given subject (see Figure 3.22). This may result from different sensitivity thresholds combined with individual REM features of the subjects. Thus, small differences in applying the scoring rules may add up to large overall differences in REM density scorings for some individuals. The average correlation coefficient between human experts (0.91) was within the range reported by other groups where correlations of 0.90, 0.85–0.90 and 0.983 were reported between visual scorers by Minard and Krausman (1971), Gopal and Haddad (1981) and Takahashi and Atsumi (1997), respectively. However, prior studies did not report whether a disagreement between expert scorers influenced the absolute values of REM density. In order to obtain a more reliable set of data, the algorithm was compared to a subset of epochs where both experts agreed on the same REM density score (consensus scoring), which resulted in increased agreement. Next to inter-scorer variability the aspect of intra-scorer variability may also be of relevance. Agarwal *et al.* (2005) reported significant changes in the identification of individual REM events when the recordings were re-scored after one year. This phenomenon was also observed in present studies. When comparing the results of automatic detector and scorer 1 between validation and development set (see Figure 3.22 lower panel and Figure 3.23 lower panel), the observed differences in absolute REM density values were not of the same pattern: absolute REM density values scored by scorer 1 in the development set exceeded values scored by the algorithm in most cases. This was not observed in the validation set and may be due to the time lag of more than two years between the REM density scoring done by scorer 1 in the two data sets. This observation clearly underscores the need for an automatic detection of REMs.

In summary, this part of the present work presents a robust automatic REM detection algorithm that is easily applicable in larger sleep EEG studies with electrode montages according to standard guidelines. Establishing automatic REM detection ensures complete reproducibility, excludes method drifts across time, and allows reliable long term evaluation of REM density as a putative biomarker in patients with affective disorders. Thus, a reliable automatic REM detection is a crucial prerequisite for translating results from biomarker research to the clinical context.

4.2 *Sleep spindle detection*

Previously published sleep spindle detection methods proposed a number of approaches. Proposed solutions to detect spindle activity were based on fast Fourier transform (Huuponen *et al.*, 2007), band-pass filtering (Schimicek *et al.*, 1994; Ferrarelli *et al.*, 2007; Bódizs *et al.*, 2009; Mölle *et al.*, 2011), wavelet transform (Latka *et al.*, 2005; Wamsley *et al.*, 2012) and its generalization, a matching pursuit algorithm which deconstructs signal into waveforms (Zygierewicz *et al.*, 1999). Continuous wavelet transform (CWT) offers a good time and frequency resolution and provides a number of wavelets which capture well the sleep spindle characteristics. CWT was chosen for the presented detection algorithm, because its outcome depends not only on the power in a given frequency, but also on the shape of graphoelements in the signal (Addison, 2002) and therefore may be more specific than a band-pass filtering.

Thresholds for spindle detection based on the amplitude of the analyzed EEG signal are widely applied in recent algorithms (Latka *et al.*, 2005; Huuponen *et al.*, 2007; Ferrarelli *et al.*, 2007; Bódizs *et al.*, 2009; Mölle *et al.*, 2011 and Wamsley *et al.*, 2012). A first reason may be age-related changes in EEG power spectrum. It has

been reported that the EEG power in delta (1–4 Hz), theta (1–8 Hz) as well as sigma (10–16 Hz) frequency is lower in middle aged males in comparison to young males (Dijk *et al.*, 1989b). Second, it has been reported that the EEG power in females is higher than in males (Dijk *et al.*, 1989c), which could be due to differences in skull thickness. In addition, even during the same recording, the measured EEG amplitude may vary across channels due to electrode placement. In recordings performed using high-density EEG caps, the differences in signal amplitude between the electrodes are clearly visible (Ferrarelli *et al.*, 2007) and probably higher than in standard EEG recordings, since it is much more difficult to fix the high numbers of electrodes properly.

Studies on the EEG power spectrum in 8–16 Hz frequency range during NREM sleep showed high inter-individual variability and intra-individual stability (de Gennaro *et al.*, 2005). Since slow as well as fast sleep spindle activity is present in this frequency range, the differences in slow and fast spindle frequencies strongly account for the observed inter-individual variability in EEG power spectrum. This aspect becomes important when a separation between slow and fast sleep spindles is of interest. Assuming that there is an inter-individual variability in spindle peak frequencies, a separation between slow and fast spindles based on the predefined threshold, which is the same for all subjects, would lead to a number of misclassifications in some of them. Interestingly, there is no agreement up to now on the value of such a predefined threshold. The average spindle frequency peak was reported at 11.5 Hz in frontal brain areas and at 13 Hz in parietal brain areas by Werth *et al.* (1997). However, Ferrarelli *et al.* (2010) set the division threshold between fast and slow spindles at 14 Hz (slow spindle 12–14 Hz, fast spindle 14–16 Hz), whereas Schonwald *et al.* (2012) set it at 13 Hz. Therefore, it is interesting that until now only

the spindle detection solutions described by Bódizs *et al.* (2009) and Mölle *et al.* (2011) have considered variabilities in spindle frequencies between the subjects. The spindle detection proposed by Bódizs *et al.* (2009) was the first method where the localization of slow and fast spindle frequencies was based on the frequency spectra in NREM sleep, and the band-pass filters for spindle detection were constructed accordingly to detected spindle activities.

The presented algorithm searches for slow and fast spindles activity according to the idea proposed by Bódizs. In addition, the presented procedure is fully automated and localizes the exact spindle frequency peaks. Instead of band-pass filters, wavelets are constructed in order to detect slow and fast spindles according to detected activities. The detection threshold setup presented here has not been proposed in previous algorithms. It is based on the median of band-pass filtered stage 2 signal activity in the 3.5–20 Hz range with each condition thought to provide a maximum robustness across subjects. Only stage 2 from NREM sleep was considered for threshold setup, since the EEG spectral characteristics during slow wave sleep (SWS) are significantly different than during stage 2 sleep and the amount of SWS varies between nights. Band-pass filtering in 3.5–20 Hz range should minimize the influence of high amplitude vertex waves and K-complexes. The median of signal root mean square should provide higher robustness than the mean against temporary events. Both detection methods which localize slow and fast spindle frequency prior to detection (Bódizs *et al.*, 2009 and Mölle *et al.*, 2011) use the spindle detection thresholds based on signal properties exactly in spindle frequency ranges. Therefore, there is the risk that a strong spindle activity could significantly affect these thresholds, resulting in decreased detection sensitivity.

The presented method uses two thresholds, a higher one for spindle detection and a lower one for spindle length estimation. A similar solution was proposed by Ferrarelli *et al.* (2007). The lower threshold helps to estimate the spindle length properly, including waning spindle parts.

The algorithm was validated in n=18 polysomnographic nap recordings from n=10 healthy subjects. The size of a validation set seems to be sufficient when compared to the previous studies. For example, in the study of Wamsley *et al.* (2012) a spindle detector was validated on n=20 visually scored EEG recordings, while Huuponen *et al.* (2007) reported n=12 visually scored recordings, and Bódizs *et al.* (2009) used up to 20 min of visually scored NREM sleep from n=12 subjects. Ferrarelli *et al.* (2007) did not report the size of the validation set. Only the development of the SIESTA spindle detector (Anderer *et al.*, 2005) was based on a large dataset of almost 11,000 visually marked episodes with sleep spindles used for thresholds setup, training and method validation.

The presented spindle detector was compared to one visual scorer as well as to the SIESTA spindle detector (Anderer *et al.*, 2005). The correlations of detected spindles between scorers were satisfactory, however, the pairwise comparisons of signals, marked as sleep spindle episodes revealed ratios of concordance below 0.7. Automatic algorithms had better concordance with each other than each of them with the visual scorer. The reason for the lower agreement between visual scoring and either algorithms was the lower sensitivity of visual scoring in comparison to automatic detectors. This is not surprising since visual scorers may have difficulties to identify spindles intermingled with other dominating EEG oscillations, i.e. theta or delta waves. When comparing two algorithms it seemed that the SIESTA algorithm

marked longer signal fragments than the presented detector, in case the same sleep spindle was found by both. This difference could result from the construction of the SIESTA algorithm. In this solution, spindle candidates are identified with the algorithm proposed by Schimicek *et al.* (1994). This detector uses the band-pass filter in order to remove all the activity in EEG besides the sigma frequency band, where sleep spindles are present. A constant predefined amplitude threshold is then applied in order to detect sleep spindles. In the SESTA algorithm this fixed threshold was lowered in order to maximize the detection sensitivity. In order to increase the specificity, the marked signal is then evaluated by a trained classifier, where the classification is based on spindle duration and the mean amplitudes in four frequency bands: spindle, theta, alpha, and fast beta. As a result the accepted spindle ranges are either long, due to detection with very low activity thresholds, or the whole fragment is rejected since it did not pass the classification criteria. In this respect, it seems that the presented algorithm has an advantage, since the threshold criteria were established to detect bursts of spindle activity and not to detect each slight increase in sigma power.

Regarding the agreement between scorers, an interesting suggestion was made by Bódizs *et al.* (2009). He proposed that in view of the growing knowledge about sleep spindles and available signal processing tools, the algorithms should be constructed to follow the scientific findings instead of visual detection. The relevance of the differences between the visual and the automatic spindle detection clearly arises from contradictory findings on spindle abnormalities in psychiatric disorders. The studies in schizophrenia patients, where sleep spindles were detected visually, showed either no differences in spindle activity between patients and controls (Van Cauter *et al.*, 1991; Poulin *et al.*, 2003), or increased spindle activity in patients (Hiatt

et al., 1985). In contrast, recent studies which were based on automatic spindle detection reported a significantly decreased spindle activity in patients with schizophrenia (Ferrarelli *et al.*, 2007 and 2010; Wamsley *et al.*, 2012). Also, studies in patients with depression reported inconsistent results. As an example, Lopez *et al.* (2010) found a decrease in frontal spindle activity, especially in females, whereas Plante *et al.* (2012) reported an increase in frontal and parietal spindle parameters in females and no differences or decreases in males. In these studies different automatic spindle detectors were used. It is an open question how differences in spindle detection methods could affect these contrary results.

In summary, this part of study presented an automatic sleep spindle detection algorithm which carefully localizes fast and slow spindles frequency for each individual and estimates the signal amplitude for each investigated channel. In view of inconsistent findings on spindle activity in depression as well as in schizophrenia, it seems that reproducing these studies in a large study sample would be worth following up, using a more exact detection method and considering differences in gender as well as medication.

4.3 *Heritability of sleep EEG*

4.3.1 *Genetic variance analysis*

A substantial genetic influence was observed on both the spectral composition and the phasic REM sleep parameters. A significant genetic variance in spectral power was observed in delta to sigma, and high beta to gamma frequencies as well as in all phasic REM parameters throughout the whole night, except for the REMs occurring outside REM bursts (RoutB). All estimates of genetic variance in spectral power for the derivation C3A2 were similar when the analysis was repeated for the derivation

C4A1 (see Supplement). In order to minimize the effects of possible covariates, the analysis was repeated in a subgroup of MZ twins closely matched for age, cohabitation and gender to the group of DZ twins (see Supplement). The comparison of REM EEG parameters between matched MZ and DZ twins confirmed the findings in the whole twin sample. In addition, a significant genetic influence was found for the remaining 7 frequency bins (1 Hz, 16–21 Hz) and low beta frequency band of REM sleep EEG. The current findings complement previous studies of Ambrosious *et al.* (2008), which were performed on the same data set and reported the heritability of background NREM EEG in the range of 2–18 Hz and in some sleep architecture parameters: the duration of stage 3 and REM sleep as well as marginal effects were observed for the duration of stage 4.

The present study demonstrates a strong genetic determination of both the absolute and the relative amount as well as structural organization of REMs. This finding clearly promotes the relevance of these sleep characteristics for psychiatric research, since Lauer *et al.* (1995) identified REM density as a promising endophenotype for affective disorders. Genetic effects on REM density and REM activity were stable and independent of the definition of the given parameters (expected improvement in sensitivity when counting single REMs did not influence estimations of genetic regulation), lending further support to a study by Linkowski, who first reported a genetic influence on REM density (1989 and 1991). In addition, when considering sleep cycles and night thirds, a high night-to-night variance was found in REM density results, especially in the DZ set. Therefore, genetic variance assessed for parts of the night should be treated with caution. However, analyzing the mean of two consecutive nights of each parameter should provide some control of intra-subject variability.

Regarding sleep spindles in NREM sleep, a substantial genetic influence was observed on slow as well as fast spindles in both, stage 2 and slow wave sleep (SWS). A significant genetic effect was observed on all parameters focused on spindle frequency. Slow spindles detected in frontal derivations showed significant genetic variance in all parameters, which could be analyzed. Unfortunately, genetic variance analysis (GVA) could not be performed for a number of slow spindle parameters due to significantly higher values in DZ twins. However, when DZ twins were compared to a subgroup of closely matched MZ twins, a significant genetic influence was found for all remaining parameters and, moreover, all findings in the whole twin sample were confirmed. Fast spindles detected in the parietal derivation showed a significant genetic variance in length, amplitude, as well as in integrated activity during sleep stage 2, and a significant genetic effect on all parameters during SWS. However, GVA repeated on MZ twins matched to DZ twins did not confirm the results for spindle amplitude in stage 2 and showed only marginal effects on the integrated spindle activity in stage 2 and SWS.

4.3.2 *Intraclass correlation coefficients*

In REM sleep, high overall differences were observed in within-pair resemblance between MZ and DZ twins. When comparing intraclass correlation coefficients (ICCs) of intra-individual stability and within-pair similarity between both twin groups it became apparent that data from MZ twins closely resembled their intra-individual stability, sometimes exceeding it. In contrast, DZ twins showed a clearly lower within-pair similarity when compared to their night-to-night stability of REM sleep characteristics. When focusing on all REM sleep parameters with good night-to-night stability (corresponding ICCs crossed significance threshold and were at least *substantial* according to Landis and Koch (1977) benchmark), the observed within-

pair resemblance in the MZ group was always significant. In contrast, significant within-pair similarity in DZ twins was only observed for two frequency bins (31–32 Hz). Thus, similarity differences between MZ and DZ twins were highest for parameters with good night-to-night stability, leading to the estimation of strong genetic effects. A previous twin study in a smaller sample by Linkowski *et al.* (1989 and 1991) already reported that sleep parameters showing best night-to-night stability have the strongest genetic component. This phenomenon was observed in all investigated tonic and phasic REM sleep parameters.

The clear dependence of night-to-night stability and within-pair resemblance in the MZ group was not always observed in NREM sleep spindle parameters. Intra-individual stability translated into similar results in the MZ group for slow spindle parameters, but not for fast spindles. A drop in the MZ twins within-pair similarity was already observed in stage 2 sleep, which was even more pronounced in SWS. *Almost perfect* ICC estimates (according to Landis and Koch, 1977) for intra-individual stability considering fast spindle quantities (spindle count as well as spindle density) for the MZ as well as the DZ group were only *moderate* when comparing MZ twins. A significant genetic effect on fast spindle quantities in SWS was obtained because there was almost no similarity between DZ twins (*slight* according to benchmark). Conversely, a*lmost perfect* ICC estimates for slow spindle quantities were observed in MZ twin set for both night-to-night stability and within-pair resemblance during stage 2 as well as SWS. Cox *et al.* (2012) found that spindle density in SWS, but not in light sleep, significantly correlated with declarative memory retention without distinguishing between fast and slow spindles. Mölle *et al.* (2009) observed that spindles focus into the depolarizing slow oscillations up-state after a learning episode. These spindles were later recognized as fast spindles by Mölle *et*

al. (2011). The present work shows that, although there is a genetic influence, the environmental influence on the occurrence of fast spindles is higher, especially in SWS. This observation suggests that fast spindles could be involved in the consolidation of new memories in SWS and that the mentioned result by Cox (association of sleep spindles in SWS with declarative memory) was probably due to increased density in fast spindles.

Intra-individual stability and within-MZ-pair similarity ICC estimates for the localization of spindle oscillations in their respective frequency range were higher for fast (always *almost perfect*) than for slow ones, and conversely, the mean of ICC estimates for all other spindle parameters were higher for slow spindles (*almost perfect* mean stability in MZ and DZ group and *almost perfect* within-MZ-pair similarity). These results point to relevant issues in the localization of slow spindles in the frequency range as already reported by De Gennaro *et al.* (2005), Bódizs *et al.* (2009) and Mölle *et al.* (2011). Furthermore, the presented results also show that these issues do not affect the detection of slow spindles, and conversely, that fast spindles show less consistency in activity, although it is easier to point them in the frequency range.

4.3.3 *Cluster analysis*

The human sleep EEG frequency spectrum is characterized by high inter-individual differences, as well as high night-to-night stability resulting in good clustering results for multiple recording nights of the same subject in both NREM and REM sleep (Buckelmüller *et al.*, 2006). Cluster analysis performed in children and across adolescent development also shows trait-like characteristics of sleep EEG power spectra (Tarokh *et al.*, 2011). In the present study, strong differences were demonstrated for both NREM and REM sleep EEG spectra clustering properties

between MZ and DZ twins. In addition, a first attempt was made to separate individuals and twin pairs in a clustering experiment, where basic spindle characteristics were used (amplitude, length and density of slow, fast and all spindles in stage 2 and SWS plus their localization in the frequency range). Again, significant differences were observed between the twin groups. The similarity distribution of MZ twins was only marginally lower when compared to intra-individual similarity.

The clustering results in the NREM sleep frequency spectrum up to 20 Hz were comparable to the clustering results of REM sleep frequency spectrum up to 45 Hz. This is an improvement in REM sleep clustering results on previous findings. Tarokh *et al.* (2011) reported lower clustering properties of REM sleep EEG. As a possible reason, the authors suggested a decreased individual character of REM sleep in some subjects (lack of characteristic frequency peaks, which in NREM sleep are always present at least in the range of spindle activity) and lower amounts of REM sleep periods, which result in less reliable measures. The present analyses revealed high genetic influence and night-to-night stability of REM power spectrum also in high EEG frequency bands. When restricting the frequency range to 20 Hz, there was an evident drop in clustering results for consecutive nights, however, the overall high rate of clustering between MZ twins was not affected by this phenomenon. The results show that high frequencies provide additional information about the REM power spectrum morphology.

The clustering results of the REM power spectrum restricted to 20 Hz were comparable to the clustering results of sleep spindle parameters. Lower clustering properties of sleep spindles are not surprising given the described lower stability of fast spindles (see section 4.3.2). However, removing fast spindle parameters from

the analysis further decreased the clustering results, showing their considerable inter-subject variations.

Figures 3.2, 3.6 and 3.18 illustrate that the distribution of similarities between MZ twins is close to intra-individual stability in NREM and REM sleep, as well as in sleep spindles. In DZ twins, on the other hand, the distribution of similarities is always close to unrelated subjects. Figure 3.4 illustrates that differences in the morphology of REM sleep EEG spectra for the most dissimilar MZ twins who failed to cluster are small, whereas the most dissimilar DZ twins show high variance in the distribution of spectrum power peaks across the whole investigated frequency range.

4.3.4 *Summary*

Steriade (2000) proposed common neuronal mechanisms generating EEG oscillations independent of vigilance state. Ambrosious *et al.* (2008) suggested that heritability findings in wake and NREM sleep background EEG indicate that there might be a common genetically driven neuronal mechanism generating these oscillations. Furthermore, Smit *et al.* (2005) reported that a significant proportion of the heritable variance in all wake EEG frequency bands might be attributed to a common genetic source. Figures 3.9 and 3.10 illustrate EEG spectra in REM and NREM sleep of the most dissimilar MZ twins detected by cluster analysis either in REM or NREM sleep. Comparison between these two sleep phases suggests that differences between the twins are preserved in both NREM and REM sleep as long as they do not arise from spindle activity in NREM sleep, which is not present in REM sleep. This finding further supports the idea that oscillations in different vigilance stages derive from common neuronal mechanisms.

All estimations of genetic effects considered absolute EEG power. Smit *et al.* (2005) analyzed the heritability of background wake EEG in detail and suggested that part of the observed genetic variance could be an outcome of skull and scalp thickness. Both variables influence EEG power and are most likely heritable. This is indeed a possible shortcoming of investigating genetic variance in the absolute EEG power. However, cluster analysis based on EEG morphology that is independent of absolute signal amplitude confirmed strong heritability of EEG in REM sleep.

In summary, the present results support a substantial genetic determination of tonic and phasic REM sleep, as well as spindle parameters, and complement previous findings of the high genetic determination of NREM power spectrum (Ambrosius *et al.*, 2008; De Gennaro *et al.*, 2008).

The present analysis on the two types of EEG sleep spindles revealed a strong genetic determination of slow spindles in particular, and weaker effects in fast ones, especially considering their quantities expressed in overall number or density. These results support the previous hypothesis of different sleep spindle generators (Anderer *et al.*, 2001) and distinct roles of low and fast spindles in memory consolidation (Mölle *et al.*, 2011).

Strong genetic effects were demonstrated on REM EEG frequencies up to 45 Hz. The observed genetic variance in higher REM EEG frequencies is of interest since Knott *et al.* (2001) reported differences in the absolute and relative power of wake EEG in the range of 12.5–25 Hz between patients with depression and healthy controls. In view of the given interference of muscle artifacts with EEG analysis, investigating REM sleep, which is characterized by muscle atonia, may offer a better opportunity to identify disease specific differences in higher EEG frequencies. The results support the exploitation of REM sleep abnormalities with respect to clinically

relevant biomarkers in patients with affective disorders (Lauer, 1991 and 1995). Specifically, basic and clinical studies support the notion that REM EEG measures help to identify patients that respond to certain antidepressant treatment (Griebel and Holsboer, 2012).

4.4 *Perspectives*

Up to now, the striking difference between investigations on human wake and sleep EEG lies in the size of the investigated samples. Twin studies on heritability of wake EEG included around ten times more MZ and DZ twin pairs (Van Baal *et al.*, 1996; Van Beijsterveldt *et al.*, 1996; Smit *et al.*, 2005) in comparison to studies on sleep EEG (Linkowski *et al.*, 1989; 1991; Ambrosius *et al.*, 2008; De Gennaro *et al.*, 2008). The study presented in this work is unfortunately not an exception. The sample size of n=35 MZ twin pairs and only n=14 DZ twin pairs made it challenging to analyze precise heritability estimates. De Gennaro *et al.* (2008) reported heritability estimates on NREM sleep EEG, although the investigations were performed on even smaller sample sizes. In the case of the current study, jackknife as well as bootstrapping simulations showed instability of within-pair similarities in the DZ sample. Although a substantial genetic determination of reported parameters was clear, more precise heritability reports might include large errors. “Fingerprint” characteristics of topographical power distributions reported by Finelli *et al.* (2001) could also not be investigated in this twin sample since the limited number of electrodes resulted in insufficient spatial distributions. Further studies including a higher number of participants, more electrodes and EEG recordings from wake, as well as sleep are needed to answer questions concerning the hypothesized common genetic source of neuronal mechanisms generating EEG oscillations (Steriade 2000).

The detectors for rapid eye movements and for sleep spindles were developed to facilitate future biomarker research on these parameters in psychiatric disorders. Biomarkers could provide a possibility to decrease the complexity of the phenotype in complex psychiatric disorders, providing a better chance to detect genes and discover the mechanism of the disease. Moreover, clinically relevant biomarkers could improve the therapy by providing a predictive value of the outcome. For future studies of predictive biomarkers in sleep EEG, large sample sizes including patients of different age, gender and medication type will be crucial. Strong evidence for the importance of medication type arises from the investigated possible predictive biomarker in quantitative wake EEG, the so called Antidepressant Treatment Response (ATR) index (Leuchter *et al.*, 2009). These studies included almost 400 participants and reported that ATR showed a predictive value in patients treated with escitalopram, but not with bupropion, two antidepressants with different function. The inconsistent findings regarding spindle activity in schizophrenia (Poulin *et al.*, 2003; Ferrarelli *et al.*, 2010) and depression (Lopez *et al.*, 2010; Plante *et al.*, 2012) as well as the mentioned results of Leuchter show that EEG related biomarkers may have a clinically relevant predictive value only under standardized conditions (detection method, drugs, age, gender of patients).

References

Achermann P (2004): The two-process model of sleep regulation revisited. Aviat Space Environ Med; 75(3):A37–43.

Addison PS (2002): The illustrated wavelet transform handbook: Introductory theory and applications in science, engineering, medicine and finance. Institute of Physics Publishing, Bristol, Philadelphia.

Agarwal R, Takeuchi T, Laroche S, Gotman J (2005): Detection of rapid-eye movements in sleep studies. IEEE Trans Biomed Eng; 52:1390–1396.

Åkerstedt T and Fröberg JE (1977): Psychophysiological circadian rhythms in women during 72 h of sleep deprivation. Waking Sleeping; 1:387–394.

Åkerstedt T, Folkard S, Portin C (2004): Predictions from the threeprocess model of alertness. Aviat Space Environ Med; 75(3):A75–83.

Ambrosius U, Lietzenmaier S, Wehrle R, Wichniak A, Kalus S, Winkelmann J, Bettecken T, Holsboer F, Yassouridis A, Friess E (2008): Heritability of sleep electroencephalogram. Biol Psychiatry; 64:344–348.

Anderer P, Klösch G, Gruber G, Trenker E, Pascual-Marqui RD, Zeitlhofer J, Barbanoj MJ, Rappelsberger P, Saletu B (2001): Low-resolution brain electromagnetic tomography revealed simultaneously active frontal and parietal sleep spindle sources in the human cortex. Neuroscience; 103(3):581–592.

Anderer P, Gruber G, Parapatics S, Woertz M, Miazhynskaia T, Klosch G, Saletu B, Zeitlhofer J, Barbanoj MJ, Danker-Hopfe H, Himanen SL, Kemp B, Penzel T, Grozinger M, Kunz D, Rappelsberger P, Schlogl A, Dorffner G (2005): An E-health solution for automatic sleep classification according to Rechtschaffen and Kales: validation study of the Somnolyzer 24 x 7 utilizing the Siesta database. Neuropsychobiology; 51(3):115–133.

Anokhin A, Steinlein O, Fischer C, Mao Y, Vogt P, Schalt E, Vogel F (1992): A genetic study of the human low voltage electroencephalogram. Hum Genet; 90:99–112.

Armitage R (2007): Sleep and circadian rhythms in mood disorders. Acta Psychiatr Scand; 115(433):S104–115.

Aserinsky E (1971): Rapid eye movement density and pattern in the sleep of normal young adults. Psychophysiology; 8(3):361–375.

Becker PT and Thoman EB (1981): Rapid eye movement storms in infants: rate of occurrence at 6 months predicts mental development at 1 year. Science; 212:1415–1416.

Becker A, Busjahn A, Faulhaber HD, Bähring S, Robertson J, Schuster H, Luft FC (1997): Twin zygosity. Automated determination with microsatellites. J Reprod Med; 42:260–266.

Billiard M. (2003): Normal Sleep In: Billiard M, ed. Sleep: Physiology Investigations and Medicine. New York, NY: Kluwer Academic/Plenum Publishers.

Bódizs R, Körmendi J, Rigó P, Lázár AS (2009): The individual adjustment method of sleep spindle analysis: methodological improvements and roots in the fingerprint paradigm. J Neurosci Methods; 178(1):205–213.

Borbély AA (1980): Sleep: circadian rhythm versus recovery process. In: Functional states of the brain: their determinants. Eds: Koukkou M, Lehmann D, Angst J. Elsevier, Amsterdam, The Netherlands, 151–161.

Borbély AA, Baumann F, Brandeis D, Strauch I, Lehmann D (1981): Sleep deprivation: effect on sleep stages and EEG power density in man. Electroencephalogr Clin Neurophysiol; 51:483–493.

Borbély, AA (1982): A two process model of sleep regulation. Hum Neurobiol; 1:195–204.

Boukadoum, AM and Ktonas PY (1986): EOG-based recording and automated detection of sleep rapid eye movements: a critical review, and some recommendations. Psychophysiology; 23:598–611.

Buckelmüller J, Landolt HP, Stassen HH, Achermann P (2006): Trait-like individual differences in the human sleep electroencephalogram. Neuroscience; 138:351–356.

Cash SS, Halgren E, Dehghani N, Rossetti AO, Thesen T, Wang C, Devinsky O, Kuzniecky R, Doyle W, Madsen JR, Bromfield E, Eross L, Halász P, Karmos G, Csercsa R, Wittner L, Ulbert I (2009): The human K-complex represents an isolated cortical down-state. Science; 324(5930):1084–1087.

Chou TC, Bjorkum AA, Gaus SE, Lu J, Scammell TE, Saper CB (2002): Afferents to the ventrolateral preoptic nucleus. J Neurosci; 22(3):977–990.

Christian JC, Kang KW, Norton JJ Jr (1974): Choice of an estimate of genetic variance from twin data. Am J Hum Genet; 26:154–161.

Christian JC, Borhani NO, Castelli WP, Fabsitz R, Norton JA Jr, Reed T, Rosenman R, Wood PD, Yu PL (1987): Plasma cholesterol variation in the National Heart, Lung and Blood Institute Twin Study. Genet Epidemiol; 4:433–446.

Clark C, Dupont R, Golshan S, Gillin JC, Rapaport MH, Kelsoe JR (2000): Preliminary evidence of an association between increased REM density and poor antidepressant response to partial sleep deprivation. J Affect Disord; 59:77–83.

Clemens Z, Fabó D, Halász P (2005): Neuroscience; 132:529–535.

Clemens Z, Mölle M, Eröss L, Jakus R, Rasonyi G, Halasz P, Born J (2011): Fine-tuned coupling between human parahippocampal ripples and sleep spindles. Eur J Neurosci; 33:511–520.

Contreras D, Destexhe A, Sejnowski TJ, Steriade M (1997): Spatiotemporal patterns of spindle oscillations in cortex and thalamus. J Neurosci; 17(3):1179–1196.

Cohen J (1960): A coefficient of agreement for nominal scales. Educ Psychol Meas; 20:37–46.

Cohrs S (2008): Sleep disturbances in patients with schizophrenia: impact and effect of antipsychotics. CNS Drugs; 22(11):939–962.

Cox R, Hofman WF, Talamini LM (2012): Involvement of spindles in memory consolidation is slow wave sleep-specific. Learn Mem; 19:264–267.

Curró Dossi R, Paré D, Steriade M (1991): Short-lasting nicotinic and long-lasting muscarinic depolarizing responses of thalamocortical neurons to stimulation of mesopontine cholinergic nuclei. J Neurophysiol; 65:393–406.

Czeisler CA, Duffy JF, Shanahan TL, Brown EN, Mitchell JF, Rimmer DW, Ronda JM, Silva EJ, Allan JS, Emens JS, Dijk DJ, Kronauer RE (1999): Stability, precision, and near-24-hour period of the human circadian pacemaker. Science; 284:2177–2181.

Datta S, Siwek DF, Stack EC (2009): Identification of cholinergic and non-cholinergic neurons in the pons expressing phosphorylated cyclic adenosine monophosphate response element-binding protein as a function of rapid eye movement sleep. Neuroscience; 163(1):397–414.

Dauvilliers Y, Maret S, Tafti M (2005): Genetics of normal and pathological sleep in humans. Sleep Med Rev; 9:91–100.

Dauvilliers Y, Rompre S, Gagnon JF, Vendette M, Petit D, Montplaisir J (2007): REM sleep characteristics in narcolepsy and REM sleep behavior disorder. Sleep; 30:844–849.

De Gennaro L, Ferrara M, Vecchio F, Curcio, G, Bertini M (2005): An electroencephalographic fingerprint of human sleep. NeuroImage; 26:114–122.

De Gennaro L, Marzano C, Fratello F, Moroni F, Pellicciari MC, Ferlazzo F, Costa S, Couyoumdjian A, Curcio G, Sforza E, Malafosse A, Finelli LA, Pasqualetti P, Ferrara M, Bertini M, Rossini PM

(2008): The electroencephalographic fingerprint of sleep is genetically determined: a twin study. Ann Neurol; 64:455–460.

Diekelmann S and Born J (2010): The memory function of sleep. Nat Rev Neurosci; 11:114–126.

Dijk DJ, Beersma DG, Daan S, Lewy AJ (1989): Bright morning light advances the human circadian system without affecting NREM sleep homeostasis. Am J Physiol; 256:106–111.

Dijk DJ, Beersma DG, van den Hoofdakker RH (1989): All night spectral analysis of EEG sleep in young adult and middle-aged male subjects. Neurobiol Aging; 10(6):677–682.

Dijk DJ, Beersma DG, Bloem GM (1989): Sex differences in the sleep EEG of young adults: visual scoring and spectral analysis. Sleep; 12(6):500–507.

Dinges DF, Douglas SD, Zaugg L, Campbell DE, McMann JM, Whitehouse WG, Orne EC, Kapoor SC, Icaza E, Orne MT (1994): Leukocytosis and natural killer cell function parallel neurobehavioral fatigue induced by 64 hours of sleep deprivation. J Clin Invest; 93(5):1930–1939.

Doman J, Detka C, Hoffman T, Kesicki D, Monahan JP, Buysse DJ, Reynolds CF, Coble PA, Matzzie J, Kupfer DJ (1995): Automating the sleep laboratory: implementation and validation of digital recording and analysis. Int J Biomed Comput; 38:277–290.

Doran SM (2003): The dynamic topography of individual sleep spindles. Sleep Res Online; 5:133–139.

Drake CL, Roehrs TA, Royer H, Koshorek G, Turner RB, Roth T (2000): Effects of an experimentally induced rhinovirus cold on sleep, performance, and daytime alertness. Physiol Behav; 71:75–81.

Dugovic C, Maccari S, Weibel L, Turek FW, Van Reeth O (1999): High corticosterone levels in prenatally stressed rats predict persistent paradoxical sleep alterations. J Neurosci; 19:8656–8664.

Ferrarelli F, Huber R, Peterson MJ, Massimini M, Murphy M, Riedner BA, Watson A, Bria P, Tononi G (2007): Reduced sleep spindle activity in schizophrenia patients. Am J Psychiatry; 164(3):483–492.

Ferrarelli F, Peterson MJ, Sarasso S, Riedner BA, Murphy MJ, Benca RM, Bria P, Kalin NH, Tononi G (2010): Thalamic dysfunction in schizophrenia suggested by whole-night deficits in slow and fast spindles. Am J Psychiatry; 167(11):1339–1348.

Ficca G, Gori S, Ktonas P, Quattrini C, Trammell J, Salzarulo P (1999): The organization of rapid eye movement activity during rapid eye movement sleep is impaired in the elderly. Neurosci Lett; 275:219–221.

Finelli LA, Achermann P, Borbély AA (2001): Individual 'fingerprints' in human sleep EEG topography. Neuropsychopharmacology; 25:57–62.

Fleiss JL (1981): Statistical Methods for Rates and Proportions. Wiley, New York (second edition).

Friess E, Schmid D, Modell S, Brunner H, Lauer CJ, Holsboer F, Ising M (2008): Dex/CRH-test response and sleep in depressed patients and healthy controls with and without vulnerability for affective disorders. J Psychiatr Res; 42:1154–1162.

Gais S, Molle M, Helms K, Born J (2002): Learning-dependent increases in sleep spindle density. J Neurosci; 22:6830–6834.

Gais S, Albouy G, Boly M, Dang-Vu TT, Darsaud A, Desseilles M, Rauchs G, Schabus M, Sterpenich V, Vandewalle G, Maquet P, Peigneux P (2007): Sleep transforms the cerebral trace of declarative memories. Proc Natl Acad Sci; 104:18778–18783.

Geyer H (1937): Ueber den Schlaf von Zwillingen. Z Indukt Abstamm Verebungsl; 78:524–527.

Girardeau G, Benchenane K, Wiener SI, Buzsaki G, Zugaro MB (2009): Selective suppression of hippocampal ripples impairs spatial memory. Nature Neurosci; 12:1222–1223.

Gong H, Szymusiak R, King J, Steininger T, McGinty D (2000): Sleep-related c-Fos protein expression in the preoptic hypothalamus: effects of ambient warming. Am J Physiol; 279:R2079–2088.

Gopal IS and Haddad GG (1981): Automatic detection of eye movements in REM sleep using the electrooculogram. Am J Physiol; 241:R217–221.

Greene RW, Gerber U, McCarley RW (1989): Cholinergic activation of medial pontine reticular formation neurons in vitro. Brain Research; 476(1):154–159.

Gvilia I, Xu F, McGinty D, Szymusiak R (2006): Homeostatic regulation of sleep: a role for preoptic area neurons. J Neurosci; 26:9426–9433.

Haseman JK and Elston RC (1970): The estimation of genetic variance from twin data. Behav Genet; 1(1):11–19.

Hatzilabrou GM, Greenberg N, Sclabassi RJ, Carroll T, Guthrie RD, Scher MS (1994): A comparison of conventional and matched filtering techniques for rapid eye movement detection of the newborn. IEEE Trans Biomed Eng; 41:990–995.

Hatzinger M, Hemmeter UM, Brand S, Ising M, Holsboer-Trachsler E (2004): Electroencephalographic sleep profiles in treatment course and longterm outcome of major depression: association with DEX/CRH-test response. J Psychiatr Res; 38:453–465.

Hiatt JF, Floyd TC, Katz PH, Feinberg I (1985): Further evidence of abnormal non-rapid-eye-movement sleep in schizophrenia. Arch Gen Psychiatry; 42:797–802.

Hobson JA, McCarley RW, Wyzinski PW (1975): Sleep cycle oscillation: reciprocal discharge by two brainstem neuronal groups. Science; 189(4196):55–58.

Hobson JA (2009): REM sleep and dreaming: towards a theory of protoconsciousness. Nat Rev Neurosci; 10:803–862.

Hori A (1986): Sleep characteristics in twins. Jap J Psych Neurol; 40:35–46.

Hu B, Steriade M, Deschênes (1989): The effects of peribrachial stimulation on reticular thalamic neurons: the blockage of spindle waves. Neuroscience; 31:1–12.

Huupponen E, Gomez-Herrero G, Saastamoinen A, Varri A, Hasan J, Himanen SL (2007): Development and comparison of four sleep spindle detection methods. Artif Intell Med; 40:157–170.

Imeri L and Opp MR (2009): How (and why) the immune system makes us sleep. Nat Rev Neurosci; 10:199–210.

Iber C, Ancoli-Israel S, Chesson A, Quan SF (2007): The AASM Manual for the Scoring of Sleep and Associated Events: Rules, Terminology and Technical Specifications. The American Academy of Sleep Medicine, Westchester, Illinois.

John J, Wu MF, Boehmer LN, Siegel JM (2004): Cataplexy-active neurons in the hypothalamus: implications for the role of histamine in sleep and waking behavior. Neuron; 42:619–634.

Jouvet, M (1962): Research on the neural structures and responsible mechanisms in different phases of physiological sleep. Arch Ital Biol; 100:125–206.

Keshavan MS, Reynolds CF III, Miewald MJ, Montrose DM, Sweeney JA, Vasko RC Jr, Kupfer DJ (1998): Delta sleep deficits in schizophrenia: evidence from automated analyses of sleep data. Arch Gen Psychiatry; 55:443–448.

Killgore WD (2010): Effects of sleep deprivation on cognition. Prog Brain Res; 185:105–129.

Kloepfer C, Riemann D, Nofzinger EA, Feige B, Unterrainer J, O'Hara R, Sorichter S, Nissen C (2009): Memory before and after sleep in patients with moderate obstructive sleep apnea. J Clin Sleep Med; 5:540–548.

Kraeplin E (1883): Compendium der Psychiatrie zum Gebrauch fuer Studierende und Aerzte. Abel Verlag, Leipzig.

Ktonas PY and Smith JR (1978): Automatic REM detection: modifications on an existing system and preliminary normative data. Int J Biomed Comput; 9:445–464.

Ktonas PY, Bes FW, Rigoard MT, Wong C, Mallart R, Salzarulo P (1990): Developmental changes in the clustering pattern of sleep rapid eye movement activity during the first year of life: a Markov-process approach. Electroencephalogr Clin Neurophysiol; 75:136–140.

Kupfer DJ, Ulrich RF, Coble PA, Jarrett DB, Grochocinski V, Doman J, Matthews G, Borbély AA (1984): Application of automated REM and slow wave sleep analysis: I. Normal and depressed subjects. Psychiatry Res; 13:325–334.

Kupfer DJ, Reynolds CF, Ulrich RF, Grochocinski VJ (1986): Comparison of automated REM and slow-wave sleep analysis in young and middle-aged depressed subjects. Biol Psychiatry; 21:189–200.

Landis JR and Koch GG (1977): The measurement of observer agreement for categorical data. Biometrics; 33:159–174.

Larsen LH, Moe KE, Vitiello MV, Prinz PN (1995): Age trends in the sleep EEG of healthy older men and women, J Sleep Res; 4:160–172.

Latka M, Kozik A, Jernajczyk J, West BJ, Jernajczyk W (2005): Wavelet mapping of sleep spindles in young patients with epilepsy. J Physiol Pharmacol; 56(4):15–20.

Lauer CJ, Riemann D, Wiegand M, Berger M (1991): From early to late adulthood. Changes in EEG sleep of depressed patients and healthy volunteers. Biol Psychiatry; 29:979–993.

Lauer CJ, Krieg JC, Garcia-Borreguero D, Ozdaglar A, Holsboer F (1992): Panic disorder and major depression: a comparative electroencephalographic sleep study. Psychiatry Res; 44:41–54.

Lauer CJ, Schreiber W, Holsboer F, Krieg JC (1995): In quest of identifying vulnerability markers for psychiatric disorders by all-night polysomnography. Arch Gen Psychiatry; 52:145–153.

Leuchter AF, Cook IA, Gilmer WS, Marangell LB, Burgoyne KS, Howland RH, Trivedi MH, Zisook S, Jain R, Fava M, Iosifescu D, Greenwald S (2009): Effectiveness of a quantitative electroencephalographic biomarker for predicting differential response or remission with escitalopram and bupropion in major depressive disorder. Psychiatry Res; 169(2):132–138.

Lim J and Dinges DF (2010): A meta-analysis of the impact of short-term sleep deprivation on cognitive variables. Psychol Bull; 136(3):375–389.

Linkowski P, Kerkhofs M, Hauspie R, Susanne C, Mendlewicz J (1989): EEG sleep patterns in man: a twin study. Electroencephalogr Clin Neurophysiol; 73:279–284.

Linkowski P, Kerkhofs M, Hauspie R, Mendlewicz J (1991): Genetic determinants of EEG sleep: A study in twins living apart. Electroencephalogr Clin Neurophysiol; 79:114–118.

Linkowski P (1999): EEG sleep patterns in twins. J Sleep Res; 8:S11–13.

Lopes Aguiar C, Romcy-Pereira RN, Escorsim Szawka R, Galvis-Alonso OY, Anselmo-Franci JA, Pereira Leite J (2008): Muscarinic acetylcholine neurotransmission enhances the late-phase of longterm potentiation in the hippocampal-prefrontal cortex pathway of rats in vivo: a possible involvement of monoaminergic systems. Neuroscience; 153:1309–1319.

Lopez J, Hoffmann R, Armitage R (2010): Reduced sleep spindle activity in early-onset and elevated risk for depression. J Am Acad Child Adolesc Psychiatry; 49(9):934–943.

De Maertelaer V, Hoffman G, Lemaire M, Mendlewicz J (1987): Sleep spindle activity changes in patients with affective disorders. Sleep; 10(5):443–451.

Martinerie J, Joseph JP, Naillon M (1980): Computerized detection of rapid eye movements during paradoxical sleep. Int J Biomed Comput; 11:163–171.

Matsuzaki M (1969): Differential effects of sodium butyrate and physostigmine upon the activities of para-sleep in acute brain stem preparations. Brain Research; 13(2):247–265.

McGinty D and Szymusiak R (2008): Hypothalamic regulation of sleep and arousal. Ann N Y Acad Sci; 1129:275–286.

McPartland RJ, Kupfer DJ, Coble P, Spiker D, Matthews G (1978): REM sleep in primary depression: a computerized analysis. Electroenceph Clin Neurophysiol; 44:513–517.

Mednick S, Nakayama K, Stickgold R (2003): Sleep-dependent learning: a nap is as good as a night. Nat Neurosci; 6(7):697–698.

Mileykovskiy BY, Kiyashchenko LI, Kodama T, Lai YY, Siegel JM (2000): Activation of pontine and medullary motor inhibitory regions reduces discharge in neurons located in the locus coeruleus and the anatomical equivalent of the midbrain locomotor region. J Neurosci; 20(22):8551–8558.

Minard JG and Krausman D (1971): Rapid eye movement definition and count: an on-line detector. Electroenceph Clin Neurophysiol; 31:99–102.

Modell S, Ising M, Holsboer F, Lauer CJ (2002): The Munich vulnerability study on affective disorders: stability of polysomnographic findings over time. Biol Psychiatry; 52(5):430–437.

Modell S, Ising M, Holsboer F, Lauer CJ (2005): The Munich vulnerability study on affective disorders: premorbid polysomnographic profile of affected high-risk probands. Biol Psychiatry; 58(9):694–699.

Morin A, Doyon J, Dostie V, Barakat M, Hadj Tahar A, Korman M, Benali H, Karni A, Ungerleider LG, Carrier J (2008): Motor sequence learning increases sleep spindles and fast frequencies in post-training sleep. Sleep; 31:1149–1156.

Mölle M, Eschenko O, Gais S, Sara SJ, Born J (2009): The influence of learning on sleep slow oscillations and associated spindles and ripples in humans and rats. Eur J Neurosci; 29:1071–1081.

Mölle M, Bergmann T, Marshall L, Born J (2011): Fast and slow spindles during the sleep slow oscillation – disparate coalescence and engagement in memory processing. Sleep; 34(10):1411–1421.

Nelson JP, McCarley RW, Hobson JA (1983): REM sleep burst neurons, PGO waves, and eye movement information. J Neurophysiol; 50:784–797.

Niedermeyer E and DaSilva FL (1999): Electroencephalography: Basic Principles, Clinical Applications, and Related Fields. Baltimore, MD: Lippincott Williams & Wilkins.

Nishida M and Walker MP (2007): Daytime naps, motor memory consolidation and regionally specific sleep spindles. PLoS ONE; 2:e341.

Oppenheim AV (2006): Discrete-Time Signal Processing, 2/E. India: Pearson Education.

Othmer SC, Othmer E, Fishman PM, Vannier MW (1979): Digital detection of rapid eye movements in sleep [Abstract]. Sleep Res; 8:270.

O'Neill J, Pleydell-Bouverie B, Dupret D, Csicsvari J (2010): Play it again: reactivation of waking experience and memory. Trends Neurosci; 33:220–229.

Pace-Schott EF and Hobson JA (2002): The neurobiology of sleep: genetics, cellular physiology and subcortical networks. Nat Rev Neurosci; 3(8):591–605.

Padovan I and Pansini M (1972): New possibilities of analysis in electronystagmography. Acta Otolaryngol; 73:121–125.

Parmeggiani PL (2003): Thermoregulation and sleep. Front Biosci; 8:557–567.

Plante DT, Goldstein MR, Landsness EC, Peterson MJ, Riedner BA, Ferrarelli F, Wanger T, Guokas JJ, Tononi G, Benca RM (2012): Topographic and sex-related differences in sleep spindles in major depressive disorder: A high-density EEG investigation. J Affect Disord; 12:S0165–0327.

Plihal W and Born J (1997): Effects of early and late nocturnal sleep on declarative and procedural memory. J Cogn Neurosci; 9:534–547.

Poulin J, Daoust AM, Forest G, Stip E, Godbout R (2003): Sleep architecture and its clinical correlates in first episode and neurolepticnaive patients with schizophrenia. Schizophr Res; 62:147–153.

Rao U, Dahl RE, Ryan ND, Birmaher B, Williamson DE, Rao R, Kaufman J (2002): Heterogeneity in EEG sleep findings in adolescent depression: unipolar versus bipolar clinical course. J Affect Disord; 70(3):273–280.

Ribeiro S, Mello CV, Velho T, Gardner TJ, Jarvis ED, Pavlides C (2002): Induction of hippocampal long-term potentiation during waking leads to increased extrahippocampal zif-268 expression during ensuing rapid-eye-movement sleep. J Neurosci; 22:10914–10923.

Rechtschaffen A and Kales A (1968): A Manual of Standardized Terminology, Techniques and Scoring System for Sleep Stages of Human Subjects. Los Angeles: UCLA Brain Information Service.

Rechtschaffen A, Bergmann BM, Everson CA, Kushida CA, Gilliland MA (1989): Sleep deprivation in the rat: X. Integration and discussion of the findings. Sleep; 12:68–87.

Rechtschaffen A and Bergmann BM (1995): Sleep deprivation in the rat by the disk-over-water method. Behavioural Brain Research; 69:55–63.

Reynolds CF and Kupfer DJ (1987): Sleep research in affective illness: state of the art circa 1987. Sleep; 10:199–215.

Robertson EM (2009): From creation to consolidation: a novel framework for memory processing. PLoS Biol; 7:e19.

Rosanova M and Ulrich D (2005): Pattern-specific associative long-term potentiation induced by a sleep spindle-related spike train. J Neurosci; 25:9398–9405.

Saper CB, Scammell TE, Lu J (2005): Hypothalamic regulation of sleep and circadian rhythms. Nature; 437(7063):1257–1264.

Schimicek P, Zeitlhofer J, Anderer P, Saletu B (1994): Automatic sleep-spindle detection procedure: Aspects of reliability and validity. Clin Electroencephalogr; 25:26–29.

Schneider D (1978): Spatio-temporal properties of rapid eye movements in human REM sleep: I. Qualitative analysis. Waking Sleeping; 2:63–67.

Schonwald SV, Carvalho DZ, de Santa-Helena EL, Lemke N, Gerhardt G (2012): Topography-specific spindle frequency changes in Obstructive Sleep Apnea. BMC Neurosci; 13:89.

Sherin JE, Shiromani PJ, McCarley RW, Saper CB (1996): Activation of ventrolateral preoptic neurons during sleep. Science; 271(5246):216–219.

Shrout PE, Fleiss JL (1979): Intraclass correlations: uses in assessing rater reliability. Psychol Bull; 86(2):420–428.

Siegel JM, Tomaszewski KS (1983): Behavioral organization of reticular formation: studies in the unrestrained cat. I. Cells related to axial, limb, eye, and other movements. J Neurophysiol; 50(3):696–716.

Siegel JM (2005): Clues to the functions of mammalian sleep. Nature; 437(7063):1264–1271.

Siegel JM (2009a): The Neurobiology of Sleep. Semin Neurol; 29(4):277–296.

Siegel JM (2009b): Sleep viewed as a state of adaptive inactivity. Nat Rev Neurosci; 10(10):747–753.

Simonova O, Roth B, Stein J (1967): EEG studies of healthy population-normal rhythms of resting recording. Acta Univ Carol Med (Praha); 13(7):543–551.

Smit DJ, Posthuma D, Boomsma DI, Geus EJ (2005): Heritability of background EEG across the power spectrum. Psychophysiology; 42:691–697.

Smith H (1936): The problem of comparing the results of two experiments with unequal errors. J Counc Sci Ind Res; 9:211–212.

Smith JR, Cronin MJ, Karacan I (1971): A multichannel hybrid system for rapid eye movement detection (REM detection). Comput Biomed Res; 4:275–290.

Steiger A and Kimura M (2010): Wake and sleep EEG provide biomarkers in depression. J Psychiatr Res; 44:242–245.

Steinlein O, Anokhin A, Yping M, Schalt E, Vogel F (1992): Localization of a gene for the human low-voltage EEG on 20q and genetic heterogeneity. Genomics; 12:69–73.

Steriade M, Dossi RC, Nuñez A (1991): Network modulation of a slow intrinsic oscillation of cat thalamocortical neurons implicated in sleep delta waves: cortically induced synchronization and brainstem cholinergic suppression. J Neurosci; 11(10):3200–3217.

Steriade M (2000): Corticothalamic resonance, states of vigilance and mentation. Neuroscience; 101(2):243–276.

Stickgold R, Hobson JA, Fosse R, Fosse M (2001): Sleep, learning, and dreams: off-line memory reprocessing. Science; 294:1052–1057.

Szymusiak R, Gvilia I, McGinty D (2007): Hypothalamic control of sleep. Sleep Med; 8(4):291–301.

Tafti M, Petit B, Chollet D, Neidhart E, de Bilbao F, Kiss JZ, Wood PA, Franken P (2003): Deficiency in short-chain fatty acid beta-oxidation affects theta oscillations during sleep. Nat Genet; 34(3):320–325.

Takahashi K and Atsumi Y (1997): Precise measurement of individual rapid eye movements in REM sleep of humans. Sleep; 20:743–752.

Talairach J and Tournoux P (1988): Co-Planar Stereotaxic Atlas of the Human Brain. Thieme, Stuttgart.

Tan X, Campbell IG, Feinberg I (2001): A simple method for computer quantification of stage REM eye movement potentials. Psychophysiology; 38:512–516.

Tarokh L, Carskadon MA, Achermann P (2011): Trait-like characteristics of the sleep EEG across adolescent development. J Neurosci; 31:6371–6378.

Taheri S and Mignot E (2002): The genetics of sleep disorders. Lancet Neurol; 1:242–250.

Teber I, Kohling R, Speckmann EJ, Barnekow A, Kremerskothen J (2004): Muscarinic acetylcholine receptor stimulation induces expression of the activity regulated cytoskeleton-associated gene (ARC). Brain Res Mol Brain Res; 121:131–136.

Tinguely G, Finelli LA, Landolt HP, Borbély AA, Achermann P (2006): Functional EEG topography in sleep and waking: state-dependent and state-independent features. NeuroImage; 32:283–292.

Touma C, Bunck M, Glasl L, Nussbaumer M, Palme R, Stein H, Wolferstätter M, Zeh R, Zimbelmann M, Holsboer F, Landgraf R (2008): Mice selected for high versus low stress reactivity: a new animal model for affective disorders. Psychoneuroendocrinology; 33(6):839–862.

Tsuji Y, Satoh H, Itoh N, Sekiguchi Y, Nagasawa K (2000): Automatic detection of rapid eye movements by discrete wavelet transform. Psychiatry Clin Neurosci; 54:276–277.

Tucker AM, Dinges DF, Van Dongen HP (2007): Trait interindividual differences in the sleep physiology of healthy young adults. J Sleep Res; 16:170–180.

Van Baal GC, De Geus EJ, Boomsma DI (1996): Genetic architecture of EEG power spectra in early life. Electroencephalogr Clin Neurophysiol; 98:502–514.

Van Beijsterveldt CE, Molenaar PC, de Geus EJ, Boomsma DI (1996): Heritability of human brain functioning as assessed by electroencephalography. Am J Hum Genet; 58:562–573.

Van Cauter E, Linkowski P, Kerkhofs M, Hubain P, L'Hermite- Baleriaux M, Leclercq R, Brasseur M, Copinski G, Mendlewicz J (1991): Circadian and sleep-related endocrine rhythms in schizophrenia. Arch Gen Psychiatry; 48:348–356.

Van Dongen HPA, Vitellaro KM, Dinges DF (2005): Individual differences in adult human sleep and wakefulness: Leitmotif for a research agenda. Sleep; 28:479–496.

Von Economo C (1930): Sleep as a problem of localization. J Nerv Ment Dis; 71:249–259.

Walker MP and Van der Helm E (2009): Overnight therapy? The role of sleep in emotional brain processing. Psychol Bull; 135(5):731–748.

Wamsley EJ, Tucker MA, Shinn AK, Ono KE, McKinley SK, Ely AV, Goff DC, Stickgold R, Manoach DS (2012): Reduced sleep spindles and spindle coherence in schizophrenia: mechanisms of impaired memory consolidation? Biol Psychiatry; 71(2):154–161.

Webb WB and Campbell SS (1983): Relationship in sleep characteristics of identical and fraternal twins. Arch Gen Psychiat; 40:1093–1095.

Wilson MA and McNaughton BL (1994): Reactivation of hippocampal ensemble memories during sleep. Science; 265:676–679.

Wulff K, Gatti S, Wettstein JG, Foster RG (2010): Sleep and circadian rhythm disruption in psychiatric and neurodegenerative disease. Nat Rev Neurosci; 11(8):589–599.

Werth E, Achermann P, Dijk DJ, Borbély AA (1997): Spindle frequency activity in the sleep EEG: individual differences and topographic distribution. Electroencephalogr Clin Neurophysiol; 103(5):535–542.

Zardetto-Smith AM and Johnson AK (1995): Chemical topography of efferent projections from the median preoptic nucleus to pontine monoaminergic cell groups in the rat. Neurosci Lett; 199(3):215–219.

Zygierewicz J, Blinowska KJ, Durka PJ, Szelenberger W, Niemcewicz S, Androsiuk W (1999): High resolution study of sleep spindles. Clin Neurophysiol; 110(12):2136–2147.

Heritability of REM Sleep EEG: Supplementary Material

MZ_{match}: a subgroup of n=14 MZ twin pairs who were closely matched for age, gender and cohabitation to the group of DZ twins (mean ± SD: MZ_{match}: 22.2±2.8yr, 18–27yr, 7m:7f, 10 pairs lived together; DZ: 22.1±2.7yr, 18–26yr, 7m:7f, 10 pairs lived together).

Matched MZ set, derivation C3A2:

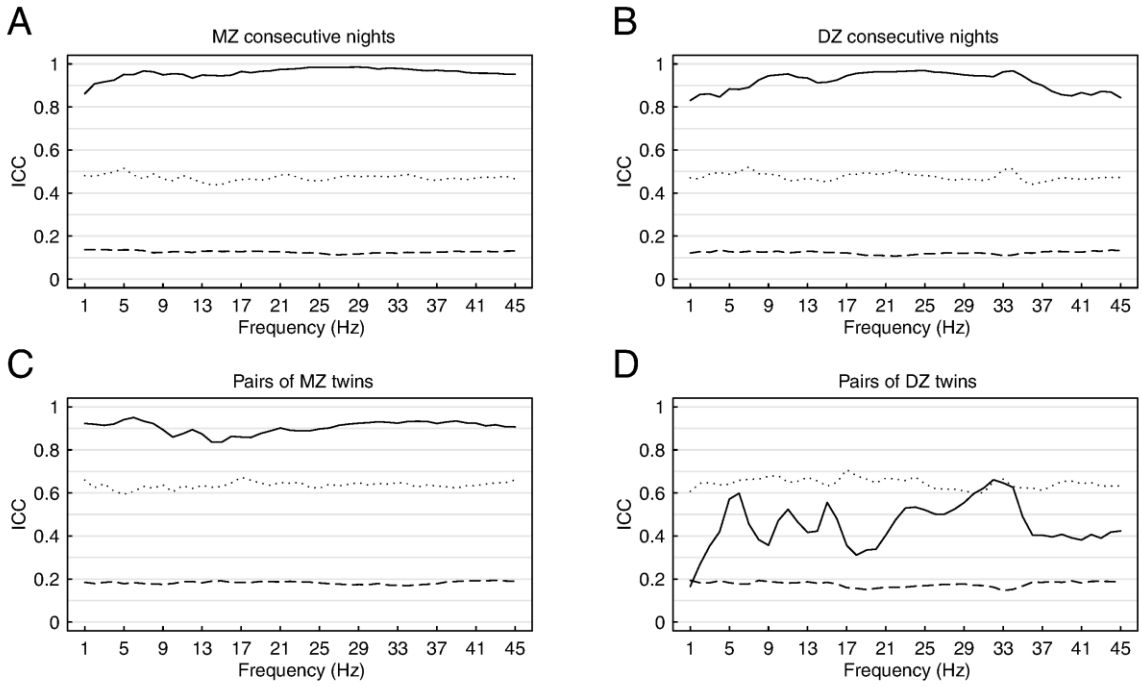

Supplementary Figure S1: Matched MZ sample. Derivation C3A2. Intraclass correlation coefficients (ICCs) of rapid eye movement (REM) sleep frequency bins. On each plot solid line represents the observed real data, dotted line represents the upper percentile of bootstrapped values and dashed line represents the median of bootstrapped values. (**A**) consecutive nights of each subject in matched monozygotic (MZ_{match}) set (n=28); (**B**) consecutive nights of each subject in dizygotic (DZ) set (n=28); (**C**) pairs of MZ_{match} twins (each subject represented by a two nights mean, n=14); (**D**) pairs of DZ twins (each subject represented by a two nights mean, n=14). On the average, the upper percentile and the median of bootstrapped values differ between groups, which is the outcome of different sample sizes.

Supplementary Table S2: EEG frequency bands in REM sleep. Matched MZ sample. Derivation C3A2. Results of genetic variance analysis, type of estimate applied (GCT: combined among- and within-twin pair component estimate, GWT: within-pair estimate) and intraclass correlation coefficients (ICCs). REM: rapid eye movement, ICC MZ: ICCs of matched monozygotic (MZ_{match}) twins, ICC DZ: ICCs of dizygotic (DZ) twins, ICC MZ_{match} cn: ICCs of consecutive nights for each subject in MZ_{match} group, ICC DZ cn: ICCs of consecutive nights for each subject in DZ group. ICC results include: original sample ICC (upper percentile of bootstrapped data, median of bootstrapped data).

Variable	*p*	GWT vs GCT	ICC MZ_{match}	ICC DZ	ICC MZ_{match} cn	ICC DZ cn
δ	.0072	GCT	0.92(0.67, 0.19)	0.27(0.63, 0.18)	0.93(0.47, 0.13)	0.87(0.45, 0.12)
θ	.0059	GCT	0.94(0.64, 0.19)	0.51(0.64, 0.19)	0.96(0.46, 0.13)	0.90(0.46, 0.12)
α	.0019	GWT	0.88(0.67, 0.19)	0.40(0.71, 0.18)	0.95(0.48, 0.12)	0.95(0.43, 0.12)
σ	.0186	GWT	0.86(0.68, 0.18)	0.45(0.61, 0.18)	0.94(0.49, 0.13)	0.92(0.46, 0.11)
α/σ	.0052	GWT	0.88(0.65, 0.18)	0.52(0.67, 0.19)	0.94(0.48, 0.13)	0.95(0.42, 0.12)
low σ	.0097	GWT	0.87(0.62, 0.19)	0.41(0.64, 0.18)	0.94(0.49, 0.12)	0.93(0.45, 0.11)
high σ	.0409	GWT	0.84(0.64, 0.19)	0.53(0.64, 0.19)	0.94(0.47, 0.13)	0.92(0.46, 0.11)
β1	.0016	GWT	0.88(0.64, 0.18)	0.41(0.66, 0.16)	0.97(0.48, 0.12)	0.97(0.58, 0.08)
β2	.0307	GWT	0.92(0.64, 0.18)	0.62(0.65, 0.17)	0.98(0.47, 0.13)	0.96(0.56, 0.11)
φ	.0067	GCT	0.93(0.62, 0.19)	0.40(0.64, 0.19)	0.96(0.47, 0.12)	0.87(0.49, 0.12)

Supplementary Table S3: EEG 1-Hz frequency bins in REM sleep. Matched MZ sample. Derivation C3A2. Results of genetic variance analysis and type of estimate applied (GCT: combined among- and within-twin pair component estimate, GWT: within-pair estimate). REM: rapid eye movement.

Variable	*p*	GWT vs GCT
1 Hz	<.0001	GWT
2 Hz	.0063	GCT
3 Hz	.0114	GCT
4 Hz	.0066	GCT
5 Hz	.0109	GCT
6 Hz	.0101	GCT
7 Hz	.0042	GCT
8 Hz	.0017	GWT
9 Hz	.0004	GWT
10 Hz	.0023	GWT
11 Hz	.0060	GWT
12 Hz	.0030	GWT
13 Hz	.0079	GWT
14 Hz	.0323	GWT
15 Hz	.0563	GWT
16 Hz	.0152	GWT
17 Hz	.0044	GWT
18 Hz	.0019	GWT
19 Hz	.0006	GWT
20 Hz	.0003	GWT
21 Hz	.0004	GWT
22 Hz	.0019	GWT
23 Hz	.0062	GWT
24 Hz	.0137	GWT
25 Hz	.0194	GWT
26 Hz	.0206	GCT
27 Hz	.0123	GCT
28 Hz	.0083	GCT
29 Hz	.0098	GCT
30 Hz	.0096	GCT
31 Hz	.0123	GCT
32 Hz	.0285	GWT
33 Hz	.0049	GWT
34 Hz	.0013	GWT
35 Hz	.0020	GWT
36 Hz	.0079	GCT
37 Hz	.0058	GCT
38 Hz	.0053	GCT
39 Hz	.0050	GCT
40 Hz	.0064	GCT
41 Hz	.0071	GCT
42 Hz	.0096	GCT
43 Hz	.0109	GCT
44 Hz	.0141	GCT
45 Hz	.0139	GCT

Supplementary Table S4: EEG log transformed frequency bands (given in μV²) in REM sleep averaged over pairs. Matched MZ sample. Derivation C3A2. Group mean ± SEM. EEG: electroencephalogram, REM: rapid eye movement, DZ: dizygotic twins, MZ_{match}: matched monozygotic twins.

	DZ n=14			**MZ_{match} n=14**		
	Night 2	**Night 3**	**2 nights mean**	**Night 2**	**Night 3**	**2 nights mean**
δ	17.27±0.06	17.25±0.06	17.26±0.06	17.11±0.09	17.14±0.09	17.13±0.09
θ	15.84±0.09	15.81±0.08	15.83±0.08	15.83±0.13	15.83±0.13	15.83±0.13
α	15.24±0.09	15.21±0.09	15.22±0.09	15.10±0.10	15.10±0.11	15.10±0.11
σ	14.25±0.07	14.19±0.08	14.22±0.08	14.11±0.09	14.08±0.10	14.09±0.09
α/σ	14.20±0.09	14.16±0.10	14.18±0.10	14.11±0.11	14.10±0.10	14.11±0.10
low σ	13.67±0.07	13.62±0.08	13.65±0.08	13.58±0.10	13.54±0.10	13.56±0.10
high σ	13.42±0.08	13.36±0.08	13.39±0.08	13.22±0.10	13.19±0.09	13.20±0.09
β1	14.30±0.09	14.25±0.10	14.27±0.10	14.02±0.11	14.01±0.11	14.02±0.11
β2	12.96±0.08	12.93±0.09	12.95±0.09	12.84±0.13	12.84±0.12	12.84±0.12
φ	11.86±0.06	11.83±0.06	11.85±0.06	11.77±0.09	11.78±0.09	11.78±0.09

Supplementary Table S5: Phasic REM parameters averaged over pairs. Matched MZ sample. Group mean ± SEM. REM: rapid eye movement, RA: REM activity, RD: REM density, allRA: the number of all detected REMs, 3sRA: the number of 3-sec mini-epochs containing at least one REM, allRD: allRA / number of REM sleep epochs, 3sRD: 3sRA / number of REM sleep epochs, RinB: the number of all detected REMs inside REM bursts, RoutB: the number of all detected REMs outside REM bursts, RinB%: percentage of REMs in burst state, DZ: dizygotic twins, MZ_{match}: matched monozygotic twins.

* Logarithm transformed data.

	DZ n=14			**MZ_{match} n=14**		
	Night 2	**Night 3**	**2 nights mean**	**Night 2**	**Night 3**	**2 nights mean**
allRD all night*	1.55±0.10	1.59±0.08	1.58±0.08	1.45±0.11	1.49±0.11	1.48±0.11
3sRD all night	2.06±0.19	2.11±0.15	2.08±0.16	1.87±0.23	1.97±0.26	1.92±0.24
3sRD 1st cycle	1.07±0.14	1.20±0.15	1.13±0.10	1.21±0.25	1.10±0.18	1.16±0.20
3sRD 2nd cycle	1.85±0.19	1.73±0.17	1.79±0.16	1.45±0.17	1.80±0.35	1.62±0.23
3sRD 3rd cycle	1.92±0.19	2.11±0.22	2.01±0.19	1.80±0.28	1.79± 0.31	1.79±0.28
3sRD 1st third	1.12± 0.20	1.11±0.15	1.11±0.15	1.11±0.23	1.23±0.22	1.17±0.22
3sRD 2nd third	1.90±0.18	2.03±0.19	1.97±0.17	1.77±0.32	1.92±0.32	1.84±0.30
3sRD 3rd third	2.39±0.22	2.34±0.16	2.37±0.17	2.10±0.22	2.23±0.25	2.16±0.22
allRA all night	831.85±118.58	860.03±93.90	845.94±100.30	767.14±192.80	763.78±166.21	765.46±178.34
3sRA all night	402.14±47.36	425.00±39.38	413.57±40.95	370.60±63.69	375.92±55.91	373.26±59.28
RinB all night*	6.06±0.21	6.19±0.17	6.15±0.18	5.97±0.19	6.00±0.18	6.00±0.18
RoutB all night	214.71±18.38	234.67±18.62	224.69±17.44	203.21±18.03	214.67±14.47	208.94±15.95
RinB% all night	0.66±0.02	0.67±0.02	0.67±0.03	0.66±0.02	0.65±0.02	0.65±0.02

Supplementary Table S6: Sleep architecture and phasic REM parameters. Matched MZ sample. Results of genetic variance analysis, type of estimate applied (GCT: combined among- and within-twin pair component estimate, GWT: within-pair estimate) and intraclass correlation coefficients (ICCs). REM: rapid eye movement, ICC MZ: ICCs of matched monozygotic (MZ_{match}) twins, ICC DZ: ICCs of dizygotic (DZ) twins, ICC MZ_{match} cn: ICCs of consecutive nights for each subject in MZ_{match} group, ICC DZ cn: ICCs of consecutive nights for each subject in DZ group. ICC results include: original sample ICC (upper percentile of bootstrapped data, median of bootstrapped data).

Variables abbreviations as in Table S5.

* Logarithm transformed data

Variable	*p*	GWT vs GCT	ICC MZ_{match}	ICC DZ	ICC MZ_{match} cn	ICC DZ cn
REM sleep duration	.2848	GWT	0.45(0.63, 0.19)	0.55(0.63, 0.19)	0.44(0.47, 0.13)	0.56(0.50, 0.12)
REM sleep latency	.5568	GWT	0.54(0.63, 0.18)	0.50(0.69, 0.14)	0.26(0.49, 0.13)	0.57(0.50, 0.11)
allRD all night*	.0021	GWT	0.85(0.67, 0.16)	0.22(0.64, 0.19)	0.83(0.46, 0.12)	0.81(0.42, 0.12)
3sRD all night	.0145	GCT	0.88(0.73, 0.14)	0.31(0.60, 0.19)	0.88(0.49, 0.12)	0.74(0.50, 0.12)
3sRD 1st cycle	.0022	GCT	0.70(0.67, 0.18)	-0.16(0.64, 0.18)	0.63(0.44, 0.14)	0.07(0.44, 0.12)
3sRD 2nd cycle	.0101	GCT	0.81(0.66, 0.19)	0.04(0.66, 0.19)	0.32(0.49, 0.13)	0.59(0.47, 0.12)
3sRD 3rd cycle	.0201	GCT	0.76(0.68, 0.17)	0.22(0.64, 0.17)	0.79(0.46, 0.12)	0.38(0.45, 0.12)
3sRD 1st third	.2366	GWT	0.65(0.67, 0.17)	0.21(0.67, 0.18)	0.55(0.49, 0.12)	0.32(0.50, 0.13)
3sRD 2nd third	.0021	GCT	0.90(0.68, 0.15)	0.19(0.64, 0.18)	0.73(0.46, 0.13)	0.68(0.46, 0.13)
3sRD 3rd third	.1585	GWT	0.67(0.68, 0.17)	0.31(0.61, 0.19)	0.61(0.50, 0.12)	0.43(0.44, 0.13)
allRA all night	.0016	GCT	0.94(0.71, 0.12)	0.44(0.61, 0.18)	0.94(0.61, 0.11)	0.71(0.50, 0.13)
3sRA all night	.0217	GCT	0.91(0.75, 0.13)	0.49(0.64, 0.18)	0.93(0.52, 0.12)	0.78(0.47, 0.12)
RinB all night*	.0010	GWT	0.81(0.65, 0.18)	0.25(0.64, 0.17)	0.82(0.43, 0.13)	0.87(0.43, 0.12)
RoutB all night	.2724	GWT	0.70(0.64, 0.19)	0.66(0.68, 0.19)	0.82(0.49, 0.13)	0.69(0.47, 0.13)
RinB% all night	.0009	GWT	0.75(0.62, 0.18)	0.13(0.62, 0.18)	0.67(0.46, 0.13)	0.80(0.46, 0.13)

Supplementary Table S7: Sleep architecture parameters averaged over pairs. Matched MZ sample. Group mean ± SEM of sleep characteristics in minutes. TST: Total sleep time, SPT: Sleep period time, SEI: *sleep efficiency* index, SOL: sleep onset latency, REM: rapid eye movement, non-REM: non-REM sleep duration, REM: REM sleep duration, RSL: REM sleep latency, DZ: dizygotic twins, MZ_{match}: matched monozygotic twins.

	DZ n=14			**MZ_{match} n=14**		
	Night 2	**Night 3**	**2 nights mean**	**Night 2**	**Night 3**	**2 nights mean**
TST	419.33±6.27	423.64±5.65	421.49±5.73	419.73±6.57	415.57±5.67	417.65±5.51
SPT	462.75±4.31	466.57±3.23	464.66±3.55	469.14±1.47	469.94±2.69	469.54±1.66
SEI	0.94±0.01	0.95±0.01	0.95±0.01	0.94±0.01	0.94±0.01	0.94±0.01
SOL	30.05±4.66	27.23±3.55	28.64±3.94	23.32±2.00	21.85±1.76	22.58±1.57
non-REM	324.21±6.17	324.89±4.50	324.55±5.09	323.91±5.64	320.92±4.94	322.41±5.01
REM	95.12±4.09	98.75±5.07	96.93±4.24	95.82±4.36	94.64±2.57	95.23±3.19
RSL	99.42±9.37	99.08±9.19	99.25±8.81	108.03±9.24	100.14±6.95	104.08±7.35

Whole MZ set, derivation C4A1:

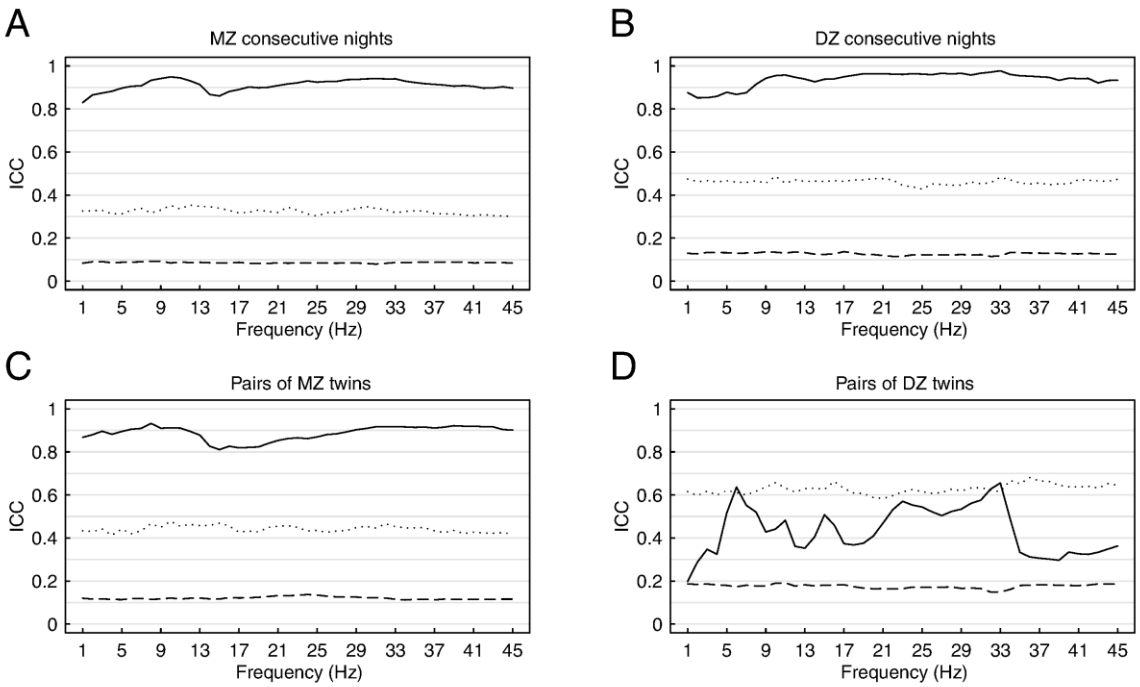

Supplementary Figure S8: Derivation C4A1. Intraclass correlation coefficients (ICCs) of rapid eye movement (REM) sleep frequency bins. On each plot solid line represents the observed real data, dotted line represents the upper percentile of bootstrapped values and dashed line represents the median of bootstrapped values. (**A**) consecutive nights of each subject in monozygotic (MZ) set (n=64); (**B**) consecutive nights of each subject in dizygotic (DZ) set (n=28); (**C**) pairs of MZ twins (each subject represented by a two nights mean, n=32); (**D**) pairs of DZ twins (each subject represented by a two nights mean, n=14). On the average, the upper percentile and the median of bootstrapped values differ between groups, which is the outcome of different sample sizes.

Supplementary Table S9: EEG frequency bands in REM Sleep. Derivation C4A1. Results of genetic variance analysis, type of estimate applied (GCT: combined among- and within-twin pair component estimate, GWT: within-pair estimate) and intraclass correlation coefficients (ICCs). REM: rapid eye movement, ICC MZ: ICCs of monozygotic (MZ) twins, ICC DZ: ICCs of dizygotic (DZ) twins, ICC MZ cn: ICCs of consecutive nights for each subject in MZ group, ICC DZ cn: ICCs of consecutive nights for each subject in DZ group. ICC results include: original sample ICC (upper percentile of bootstrapped data, median of bootstrapped data).

* Analysis of variance not applicable (significant differences between the means in DZ and MZ twin set).

Variable	*p*	GWT vs GCT	ICC MZ	ICC DZ	ICC MZ cn	ICC DZ cn
δ	.0005	GCT	0.89(0.45, 0.12)	0.26(0.65, 0.18)	0.87(0.30, 0.08)	0.87(0.46, 0.13)
θ	.0107	GWT	0.91(0.48, 0.13)	0.61(0.67, 0.19)	0.90(0.32, 0.08)	0.88(0.47, 0.13)
α	<.0001	GWT	0.92(0.43, 0.11)	0.42(0.64, 0.18)	0.94(0.32, 0.09)	0.95(0.50, 0.12)
σ	.0005	GWT	0.85(0.44, 0.12)	0.41(0.62, 0.18)	0.88(0.33, 0.08)	0.93(0.48, 0.12)
α/σ	<.0001	GWT	0.91(0.44, 0.12)	0.45(0.64, 0.19)	0.94(0.32, 0.09)	0.95(0.50, 0.13)
low σ	.0002	GWT	0.87(0.44, 0.13)	0.36(0.63, 0.19)	0.90(0.34, 0.08)	0.93(0.49, 0.12)
high σ	.0028	GWT	0.82(0.41, 0.13)	0.49(0.58, 0.20)	0.86(0.30, 0.08)	0.93(0.48, 0.12)
β1	.0001	GWT	0.84(0.47, 0.11)	0.46(0.61, 0.17)	0.90(0.32, 0.09)	0.96(0.52, 0.12)
β2	.0003	GWT	0.90(0.46, 0.12)	0.57(0.64, 0.18)	0.93(0.31, 0.08)	0.96(0.48, 0.13)
φ	<.0001	GWT	0.92(0.42, 0.12)	0.32(0.62, 0.18)	0.90(0.30, 0.09)	0.94(0.48, 0.13)

Supplementary Table S10: EEG 1-Hz frequency bins in REM sleep. Derivation C4A1. Results of genetic variance analysis and type of estimate applied (GCT GCT: combined among- and within-twin pair component estimate, GWT: within-pair estimate). REM: rapid eye movement.
* Analysis of variance not applicable (significant differences between the means in monozygotic and dizygotic twins).

Variable	*p*	GWT vs GCT
1 Hz	.0014	GCT
2 Hz	.0008	GCT
3 Hz	.0007	GCT
4 Hz	.0005	GCT
5 Hz	.0036	GCT
6 Hz	.0193	GWT
7 Hz	.0033	GWT
8 Hz	.0050	GCT
9 Hz	<.0001	GWT
10 Hz	<.0001	GWT
11 Hz	<.0001	GWT
12 Hz	<.0001	GWT
13 Hz	<.0001	GWT
14 Hz	.0013	GWT
15 Hz	.0049	GWT
16 Hz	.0011	GWT
17 Hz*	-	-
18 Hz*	-	-
19 Hz*	-	-
20 Hz*	-	-
21 Hz*	-	-
22 Hz	.0001	GWT
23 Hz	.0004	GWT
24 Hz	.0006	GWT
25 Hz	.0007	GWT
26 Hz	.0005	GWT
27 Hz	.0005	GWT
28 Hz	.0006	GWT
29 Hz	.0007	GWT
30 Hz	.0006	GWT
31 Hz	.0002	GWT
32 Hz	<.0001	GWT
33 Hz	<.0001	GWT
34 Hz	<.0001	GWT
35 Hz	<.0001	GWT
36 Hz	<.0001	GWT
37 Hz	<.0001	GWT
38 Hz	<.0001	GWT
39 Hz	<.0001	GWT
40 Hz	<.0001	GWT
41 Hz	<.0001	GWT
42 Hz	<.0001	GWT
43 Hz	<.0001	GWT
44 Hz	<.0001	GWT
45 Hz	<.0001	GWT

Matched MZ set, derivation C3A2, sleep spindles:

Supplementary Table S11: Matched MZ sample. Results of genetic variance analysis, type of estimate applied (GCT: combined among- and within-twin pair component estimate, GWT: within-pair estimate) and intraclass correlation coefficients (ICCs) for sleep spindle localization in non-rapid eye movement sleep. ICC MZ: ICCs of matched monozygotic (MZ_{match}) twins, ICC DZ: ICCs of dizygotic (DZ) twins, ICC MZ_{match} cn: ICCs of consecutive nights for each subject in MZ_{match} group, ICC DZ cn: ICCs of consecutive nights for each subject in DZ group. ICC results include: original sample ICC (upper percentile of bootstrapped data, median of bootstrapped data).

Variable	*p*	GWT vs GCT	ICC MZ_{match}	ICC DZ	ICC MZ_{match} cn	ICC DZ cn
Begin of spindle range	.0153	GWT	0.89(0.66, 0.19)	0.63(0.66, 0.19)	0.90(0.48, 0.13)	0.82(0.49, 0.13)
Slow spindle peak	.0006	GWT	0.89(0.66, 0.18)	0.57(0.60, 0.20)	0.93(0.49, 0.13)	0.94(0.48, 0.13)
Fast spindle peak	<.0001	GWT	0.96(0.60, 0.18)	0.63(0.66, 0.19)	0.91(0.48, 0.12)	0.96(0.49, 0.12)
End of spindle range	<.0001	GWT	0.93(0.63, 0.18)	0.65(0.63, 0.19)	0.91(0.47, 0.13)	0.96(0.48, 0.13)

Supplementary Table S12: Matched MZ sample. Derivation C3A2. Genetic variance analysis, type of estimate applied (GCT: combined among- and within-twin pair component estimate, GWT: within-pair estimate) and intraclass correlation coefficients (ICCs) for sleep spindle parameters in non-rapid eye movement sleep.

Variables abbreviations as in Table S11.

Variable	*type*	*p*	GWT vs GCT	ICC MZ_{match}	ICC DZ	ICC MZ_{match} cn	ICC DZ cn
Number of spindles	slow	.0186	GCT	0.98(0.64, 0.20)	0.62(0.64, 0.20)	0.98(0.47, 0.13)	0.89(0.48, 0.13)
	fast	.0389	GWT	0.77(0.64, 0.19)	0.49(0.62, 0.18)	0.94(0.51, 0.13)	0.88(0.45, 0.12)
	all	.0187	GCT	0.92(0.65, 0.19)	0.54(0.63, 0.18)	0.96(0.48, 0.13)	0.86(0.48, 0.13)
Spindle length	slow	.0017	GWT	0.97(0.68, 0.18)	0.79(0.63, 0.20)	0.98(0.47, 0.14)	0.95(0.44, 0.14)
	fast	.0024	GWT	0.86(0.64, 0.18)	0.44(0.66, 0.19)	0.95(0.46, 0.13)	0.94(0.49, 0.13)
	all	.0026	GWT	0.89(0.61, 0.19)	0.47(0.62, 0.18)	0.93(0.49, 0.14)	0.96(0.46, 0.13)
Spindle amplitude	slow	.0027	GCT	0.89(0.63, 0.19)	0.19(0.63, 0.19)	0.88(0.45, 0.13)	0.84(0.45, 0.13)
	fast	.1688	GWT	0.79(0.64, 0.18)	0.53(0.63, 0.18)	0.90(0.46, 0.13)	0.64(0.47, 0.12)
	all	.0031	GCT	0.92(0.67, 0.19)	0.30(0.63, 0.19)	0.95(0.48, 0.14)	0.87(0.47, 0.12)
Spindle density	slow	<.0001	GWT	0.98(0.62, 0.18)	0.64(0.65, 0.19)	0.98(0.46, 0.13)	0.93(0.50, 0.14)
	fast	.0527	GWT	0.76(0.64, 0.20)	0.50(0.62, 0.18)	0.94(0.47, 0.12)	0.90(0.46, 0.13)
	all	.0154	GWT	0.92(0.66, 0.19)	0.57(0.64, 0.19)	0.96(0.46, 0.14)	0.90(0.51, 0.13)
Integrated spindle activity	slow	.0001	GWT	0.97(0.60, 0.18)	0.68(0.60, 0.19)	0.98(0.46, 0.13)	0.94(0.47, 0.13)
	fast	.0316	GWT	0.91(0.62, 0.19)	0.64(0.62, 0.19)	0.96(0.48, 0.12)	0.90(0.49, 0.13)
	all	.0625	GWT	0.73(0.62, 0.19)	0.51(0.70, 0.19)	0.92(0.47, 0.13)	0.82(0.44, 0.13)

Supplementary Table S13: Matched MZ sample. Derivation C3A2. Genetic variance analysis, type of estimate applied (GCT: combined among- and within-twin pair component estimate, GWT: within-pair estimate) and intraclass correlation coefficients (ICCs) for sleep spindle parameters in stage 2 sleep.

Variables abbreviations as in Table S11.

Variable	*type*	*p*	GWT vs GCT	ICC MZ_{match}	ICC DZ	ICC MZ_{match} cn	ICC DZ cn
Number of spindles	slow	.0043	GWT	0.96(0.66, 0.20)	0.71(0.64, 0.19)	0.96(0.49, 0.13)	0.91(0.45, 0.13)
	fast	.0427	GWT	0.80(0.68, 0.18)	0.59(0.66, 0.18)	0.92(0.49, 0.12)	0.90(0.43, 0.12)
	all	.1421	GWT	0.87(0.68, 0.18)	0.66(0.63, 0.18)	0.92(0.47, 0.13)	0.90(0.47, 0.13)
Spindle length	slow	.0032	GWT	0.97(0.64, 0.19)	0.83(0.63, 0.19)	0.98(0.49, 0.13)	0.95(0.48, 0.13)
	fast	.0041	GWT	0.85(0.61, 0.18)	0.40(0.66, 0.20)	0.95(0.46, 0.13)	0.92(0.47, 0.13)
	all	.0021	GWT	0.90(0.66, 0.18)	0.45(0.63, 0.18)	0.95(0.49, 0.13)	0.97(0.46, 0.14)
Spindle amplitude	slow	.0058	GCT	0.90(0.67, 0.18)	0.21(0.65, 0.19)	0.87(0.50, 0.13)	0.85(0.47, 0.13)
	fast	.1816	GWT	0.78(0.63, 0.18)	0.54(0.65, 0.18)	0.90(0.48, 0.13)	0.63(0.45, 0.12)
	all	.0044	GCT	0.92(0.66, 0.18)	0.31(0.65, 0.17)	0.95(0.47, 0.13)	0.86(0.47, 0.12)
Spindle density	slow	.0001	GWT	0.98(0.65, 0.20)	0.74(0.67, 0.20)	0.98(0.49, 0.13)	0.93(0.44, 0.13)
	fast	.0551	GWT	0.80(0.68, 0.19)	0.56(0.64, 0.20)	0.95(0.49, 0.13)	0.91(0.46, 0.13)
	all	.0606	GWT	0.92(0.68, 0.19)	0.67(0.67, 0.18)	0.96(0.48, 0.13)	0.91(0.48, 0.13)
Integrated spindle activity	slow	<.0001	GWT	0.97(0.63, 0.19)	0.71(0.66, 0.19)	0.97(0.48, 0.12)	0.94(0.48, 0.13)
	fast	.0590	GWT	0.76(0.62, 0.19)	0.55(0.69, 0.19)	0.94(0.48, 0.13)	0.84(0.45, 0.14)
	all	.0381	GWT	0.91(0.68, 0.18)	0.67(0.63, 0.19)	0.95(0.45, 0.13)	0.92(0.53, 0.13)

Supplementary Table S14: Matched MZ sample. Derivation C3A2. Genetic variance analysis, type of estimate applied (GCT: combined among- and within-twin pair component estimate, GWT: within-pair estimate) and intraclass correlation coefficients (ICCs) for sleep spindle parameters in slow wave sleep.

Variables abbreviations as in Table S11.

Variable	*type*	*p*	GWT vs GCT	ICC MZ_{match}	ICC DZ	ICC MZ_{match} cn	ICC DZ cn
Number of spindles	slow	.0012	GWT	0.95(0.66, 0.17)	0.55(0.61, 0.19)	0.97(0.47, 0.14)	0.77(0.47, 0.12)
	fast	.1411	GWT	0.50(0.62, 0.17)	0.14(0.65, 0.18)	0.92(0.44, 0.13)	0.82(0.46, 0.14)
	all	.0085	GWT	0.89(0.66, 0.19)	0.46(0.67, 0.19)	0.95(0.49, 0.12)	0.75(0.49, 0.13)
Spindle length	slow	.0001	GWT	0.97(0.63, 0.20)	0.62(0.65, 0.19)	0.93(0.49, 0.12)	0.94(0.49, 0.12)
	fast	.0202	GWT	0.84(0.65, 0.18)	0.45(0.64, 0.18)	0.84(0.47, 0.14)	0.85(0.48, 0.13)
	all	.0022	GWT	0.91(0.63, 0.19)	0.48(0.65, 0.19)	0.90(0.45, 0.13)	0.89(0.48, 0.13)
Spindle amplitude	slow	.0007	GCT	0.89(0.64, 0.19)	0.19(0.66, 0.20)	0.91(0.43, 0.12)	0.81(0.50, 0.13)
	fast	.0148	GCT	0.80(0.66, 0.19)	0.32(0.67, 0.19)	0.92(0.47, 0.13)	0.63(0.45, 0.12)
	all	.0001	GCT	0.92(0.64, 0.19)	0.14(0.62, 0.18)	0.96(0.49, 0.14)	0.79(0.45, 0.13)
Spindle density	slow	<.0001	GWT	0.96(0.69, 0.20)	0.38(0.63, 0.18)	0.98(0.47, 0.13)	0.92(0.45, 0.13)
	fast	.0346	GWT	0.61(0.62, 0.19)	0.13(0.61, 0.18)	0.91(0.46, 0.12)	0.81(0.46, 0.13)
	all	.0005	GWT	0.92(0.62, 0.18)	0.27(0.66, 0.18)	0.97(0.51, 0.13)	0.85(0.47, 0.13)
Integrated spindle activity	slow	<.0001	GWT	0.98(0.64, 0.18)	0.44(0.63, 0.18)	0.98(0.51, 0.13)	0.92(0.46, 0.13)
	fast	.0528	GWT	0.58(0.61, 0.18)	0.14(0.66, 0.17)	0.88(0.47, 0.12)	0.71(0.50, 0.13)
	all	.0032	GWT	0.91(0.63, 0.19)	0.39(0.66, 0.19)	0.96(0.46, 0.13)	0.83(0.45, 0.14)

Whole MZ set, derivation C4A1, sleep spindles:

Supplementary Table S15: Derivation C4A1. Genetic variance analysis, type of estimate applied (GCT: combined among- and within-twin pair component estimate, GWT: within-pair estimate) and intraclass correlation coefficients (ICCs) for sleep spindle parameters in non-rapid eye movement sleep. ICC MZ: ICCs of monozygotic (MZ) twins, ICC DZ: ICCs of dizygotic (DZ) twins, ICC MZ cn: ICCs of consecutive nights for each subject in MZ group, ICC DZ cn: ICCs of consecutive nights for each subject in DZ group. ICC results include: original sample ICC (upper percentile of bootstrapped data, median of bootstrapped data).

* Analysis of variance not applicable (significant differences between the means in DZ and MZ twin set).

Variable	*type*	*p*	GWT vs GCT	ICC MZ	ICC DZ	ICC MZ cn	ICC DZ cn
Number of spindles	slow	-	-	0.93(0.45, 0.12)	0.49(0.64, 0.18)	0.90(0.29, 0.09)	0.91(0.47, 0.13)
	fast	.0350	GWT	0.71(0.45, 0.12)	0.38(0.67, 0.19)	0.86(0.31, 0.09)	0.90(0.47, 0.12)
	all	.0039	GCT	0.92(0.45, 0.13)	0.53(0.64, 0.18)	0.95(0.32, 0.08)	0.91(0.47, 0.13)
Spindle length	slow	-	-	0.91(0.46, 0.12)	0.74(0.63, 0.18)	0.92(0.34, 0.08)	0.94(0.45, 0.14)
	fast	.0187	GWT	0.69(0.42, 0.12)	0.45(0.62, 0.19)	0.89(0.32, 0.09)	0.90(0.44, 0.13)
	all	.0011	GWT	0.88(0.42, 0.12)	0.52(0.62, 0.19)	0.94(0.33, 0.09)	0.95(0.47, 0.13)
Spindle amplitude	slow	.0003	GCT	0.91(0.44, 0.12)	0.18(0.63, 0.18)	0.93(0.33, 0.08)	0.84(0.47, 0.14)
	fast	.0165	GWT	0.82(0.42, 0.12)	0.46(0.59, 0.18)	0.84(0.32, 0.08)	0.76(0.48, 0.12)
	all	.0009	GCT	0.90(0.45, 0.12)	0.30(0.64, 0.18)	0.91(0.31, 0.09)	0.83(0.51, 0.12)
Spindle density	slow	-	-	0.93(0.44, 0.12)	0.52(0.67, 0.18)	0.91(0.32, 0.09)	0.94(0.47, 0.13)
	fast	.0527	GWT	0.72(0.45, 0.12)	0.41(0.64, 0.20)	0.87(0.32, 0.09)	0.92(0.43, 0.13)
	all	.0036	GCT	0.93(0.46, 0.12)	0.56(0.63, 0.17)	0.96(0.32, 0.08)	0.93(0.48, 0.12)
Integrated spindle activity	slow	<.0001	GWT	0.95(0.42, 0.12)	0.61(0.65, 0.18)	0.94(0.33, 0.09)	0.94(0.46, 0.13)
	fast	.0265	GWT	0.74(0.44, 0.12)	0.48(0.67, 0.20)	0.82(0.34, 0.08)	0.88(0.48, 0.13)
	all	.0478	GWT	0.92(0.44, 0.12)	0.75(0.67, 0.17)	0.95(0.32, 0.09)	0.91(0.47, 0.13)

Supplementary Table S16: Derivation C4A1. Genetic variance analysis, type of estimate applied (GCT: combined among- and within-twin pair component estimate, GWT: within-pair estimate) and intraclass correlation coefficients (ICCs) for stage 2 sleep spindle parameters. Variables abbreviations as in Table S15.

* Analysis of variance not applicable (significant differences between the means in DZ and MZ twin set).

Variable	*type*	*p*	GWT vs GCT	ICC MZ	ICC DZ	ICC MZ cn	ICC DZ cn
Number of spindles	slow	.0168	GWT	0.87(0.44, 0.12)	0.55(0.66, 0.19)	0.89(0.34, 0.09)	0.87(0.47, 0.13)
	fast	.1243	GWT	0.72(0.44, 0.13)	0.47(0.66, 0.19)	0.87(0.31, 0.08)	0.91(0.46, 0.13)
	all	.0148	GCT	0.88(0.49, 0.12)	0.65(0.65, 0.18)	0.94(0.31, 0.08)	0.93(0.45, 0.13)
Spindle length	slow	-	-	0.91(0.48, 0.11)	0.74(0.68, 0.18)	0.92(0.33, 0.08)	0.96(0.45, 0.13)
	fast	.0125	GWT	0.69(0.43, 0.13)	0.40(0.64, 0.19)	0.90(0.33, 0.09)	0.90(0.50, 0.14)
	all	.0007	GWT	0.88(0.43, 0.12)	0.49(0.66, 0.18)	0.94(0.36, 0.08)	0.95(0.44, 0.13)
Spindle amplitude	slow	.0006	GCT	0.91(0.45, 0.12)	0.19(0.63, 0.19)	0.93(0.32, 0.09)	0.85(0.49, 0.14)
	fast	.0183	GWT	0.82(0.43, 0.12)	0.46(0.63, 0.18)	0.84(0.30, 0.09)	0.75(0.47, 0.13)
	all	.0012	GCT	0.91(0.44, 0.13)	0.32(0.64, 0.19)	0.91(0.30, 0.08)	0.82(0.46, 0.12)
Spindle density	slow	.0002	GWT	0.93(0.43, 0.12)	0.58(0.60, 0.18)	0.91(0.31, 0.09)	0.93(0.46, 0.13)
	fast	.0844	GWT	0.72(0.46, 0.13)	0.46(0.64, 0.19)	0.87(0.32, 0.08)	0.91(0.45, 0.13)
	all	.0045	GWT	0.93(0.44, 0.12)	0.65(0.66, 0.19)	0.97(0.32, 0.09)	0.94(0.46, 0.14)
Integrated spindle activity	slow	<.0001	GWT	0.95(0.45, 0.12)	0.57(0.62, 0.19)	0.93(0.30, 0.08)	0.96(0.46, 0.13)
	fast	.0366	GWT	0.75(0.44, 0.12)	0.52(0.64, 0.17)	0.83(0.30, 0.08)	0.87(0.49, 0.13)
	all	.0083	GWT	0.93(0.47, 0.12)	0.73(0.63, 0.18)	0.95(0.32, 0.09)	0.93(0.44, 0.13)

Supplementary Table S17: Derivation C4A1. Genetic variance analysis, type of estimate applied (GCT: combined among- and within-twin pair component estimate, GWT: within-pair estimate) and intraclass correlation coefficients (ICCs) for slow wave sleep spindle parameters. Variables abbreviations as in Table S15.

* Analysis of variance not applicable (significant differences between the means in DZ and MZ twin set).

Variable	*type*	*p*	GWT vs GCT	ICC MZ	ICC DZ	ICC MZ cn	ICC DZ cn
Number of spindles	slow	-	-	0.93(0.51, 0.11)	0.56(0.65, 0.20)	0.88(0.35, 0.08)	0.86(0.44, 0.13)
	fast	.0012	GWT	0.57(0.45, 0.12)	0.05(0.63, 0.17)	0.81(0.33, 0.08)	0.87(0.45, 0.12)
	all	.0031	GWT	0.81(0.41, 0.12)	0.37(0.59, 0.19)	0.87(0.31, 0.09)	0.81(0.48, 0.13)
Spindle length	slow	.0013	GWT	0.89(0.44, 0.11)	0.66(0.63, 0.19)	0.83(0.32, 0.08)	0.93(0.47, 0.12)
	fast	.0467	GWT	0.69(0.44, 0.11)	0.41(0.63, 0.19)	0.75(0.32, 0.08)	0.83(0.46, 0.12)
	all	.0005	GWT	0.89(0.46, 0.12)	0.50(0.64, 0.19)	0.87(0.30, 0.08)	0.88(0.49, 0.13)
Spindle amplitude	slow	.0001	GCT	0.91(0.45, 0.12)	0.22(0.68, 0.19)	0.93(0.32, 0.09)	0.79(0.48, 0.13)
	fast	.0061	GCT	0.78(0.44, 0.12)	0.26(0.64, 0.18)	0.73(0.30, 0.08)	0.77(0.47, 0.13)
	all	<.0001	GCT	0.87(0.45, 0.12)	0.16(0.66, 0.18)	0.87(0.30, 0.08)	0.77(0.46, 0.13)
Spindle density	slow	<.0001	GWT	0.94(0.45, 0.11)	0.30(0.63, 0.19)	0.90(0.32, 0.08)	0.95(0.48, 0.13)
	fast	.0025	GWT	0.64(0.43, 0.12)	0.01(0.65, 0.19)	0.83(0.31, 0.09)	0.90(0.47, 0.13)
	all	.0002	GCT	0.92(0.42, 0.12)	0.22(0.62, 0.19)	0.92(0.29, 0.08)	0.89(0.48, 0.13)
Integrated spindle activity	slow	.0011	GCT	0.96(0.47, 0.10)	0.44(0.70, 0.18)	0.91(0.34, 0.08)	0.92(0.48, 0.13)
	fast	.0010	GWT	0.65(0.41, 0.12)	0.08(0.64, 0.18)	0.80(0.31, 0.08)	0.86(0.46, 0.13)
	all	.0005	GCT	0.90(0.44, 0.12)	0.42(0.66, 0.18)	0.90(0.30, 0.09)	0.84(0.47, 0.14)